Wireless and Battery-Free Biosignal Monitoring using Passive RFID Tags

A Thesis

Submitted to the Faculty

of

Drexel University

by

Shrenik Ashwin Vora

in partial fulfillment of the

requirements for the degree

of

Doctor of Philosophy in Electrical Engineering

March 2017

Dedications

I gratefully dedicate this work to my parents, Ashwin and Chetna, who have sacrificed many times over to help me realize my dreams.

Acknowledgments

This thesis has been possible due to the support and efforts of many individuals who had faith in my abilities. I would like to extend my sincere gratitude to my adviser, Dr. Timothy Kurzweg, for his constant support and encouragement. By allowing me to set my own boundaries and work at my own pace, he has truly allowed me to learn and grow as a researcher. Over the past decade, Dr. Kurzweg has taken a genuine interest in my well-being and I couldn't have asked for a better mentor to oversee my academic career. I would also like to thank Dr. Kapil Dandekar who has followed my work closely and has always being available for advise and guidance. I am thankful to Dr. Owen Montgomery and Dr. Adam Fontecchio for having thoughtful discussions that molded my work. A special thanks to Dr. Bruce Eisenstein, who personally encouraged and enabled me to complete my PhD at Drexel. I am grateful for his insightful advise and experienced mentorship.

I appreciate the stimulating discussions I have had with my colleagues; Weston Aenchbacher, Damiano Patron and William Mongan, who have always been generous in sharing their knowledge and resources. I would also like to thank my friends, especially Farnaza, Auritro and Rohit for supporting me when completing my PhD seemed daunting and impossible.

Finally, I would like to thank my family; Nishant, Riddhi and my parents, for being a pillar of support while I maneuvered the ups and downs faced by a PhD candidate. In encouraging me to pursue my dreams, my parents gave me the strength to never give up. To my sister, Riddhi, I am grateful for her kindness, love and companionship. By looking up to me she has always motivated me to do my best.

The work done in this thesis was supported by NSF PFI:BIC subprogram under Grant No. 1430212.

Table of Contents

List of Tables

List of Figures

Abstract

Wireless and Battery-Free Biosignal Monitoring using Passive RFID Tags

Shrenik Ashwin Vora

Advisor: Timothy P. Kurzweg, Ph.D.

Wearable health monitoring devices are becoming increasingly ubiquitous in clinical settings and even in monitoring daily activities. This recent spurt in wearable devices has been made possible through the development of low power electronics, small footprint components and efficient data transmission methods. The next big step in making monitoring devices more 'wearable' is the elimination of batteries. Without the need to replace and recharge batteries, monitoring can be uninterrupted and the monitoring device itself can be seamlessly integrated into garments. However, to achieve this goal, merely reducing sensor power consumption is not enough. There is a need for unconventional methods of health monitoring.

In this work, a novel passive Radio Frequency Identification (RFID) based method for transmitting health parameters wirelessly and without batteries is described. The dissertation proposes an innovative method of transmitting health parameter data by simply turning RFID tags on and off. Technology for RFID based continuous monitoring that include a wireless power harvester and low-power circuits for amplification and health parameter detection are developed in this research. The dissertation includes practical applications of the technology that are demonstrated using heart rate and uterine contraction monitoring as examples. Empirical tests for characterizing the heart rate monitoring system are also conducted. The heart rate monitoring technology is validated with human testing which showed a correlation of over 99% between actual and detected heart rate data.

1. Introduction

1.1 Wireless and Wearable Health Monitoring

Over the last decade we have witnessed an increased movement towards the development of wireless wearable health monitoring devices [95, 96, 134]. Several factors have enabled the current proliferation of wearable devices. These factors include the development of diverse methods of sensing and transmitting health parameters, smaller and unobtrusive monitoring devices and compact and efficient electronic components. These advancements have enabled compact devices capable of continuous monitoring. Monitors that interface easily with hand-held devices and have internet connectivity have enabled remote monitoring and on-demand data access. A number of health parameters, including, heart rate, respiration rate, sleeping patterns, hydration, step counts and many others can now be simultaneously monitored with minimal interruption.

The underlying belief fueling the growth in wearable device research is that such devices will allow for affordable round-the-clock monitoring which will promote early detection and prevention of many diseases. In addition, wearable devices are finding increasing applications in personal fitness tracking. It is believed that ready availability of affordable continuous monitoring devices will translate to a reduction in overall healthcare spending [96]. The healthcare system of the future should be preventive, predictive, preemptive, personalized, pervasive, participatory, patient-centered and precise (p-health system)[134]. Wearable devices have the potential of favorably impacting each of the aforementioned 'p's in the p-health system.

This work proposes a novel RFID based monitoring technology which is battery-free and very suitable for integration into a wearable monitoring platform.

1.2 Wireless Biosignal Monitoring Process

Figure 1.1: Steps involved in Biosignal Monitoring

Biosignals are measurable signals produced by the body that can be monitored and related to the health and status of bodily organs. In spite of the diversity in the electronics used for sensing biosignals and communication platforms employed in transmitting them, almost all wireless wearable monitors have the same building blocks as illustrated in Fig. 1.1. A typical wearable device goes through the following steps to achieve monitoring:

- Sensing: The biosignal of interest is detected and a proportional electrical response is produced
- Amplification: The small electrical response generated by the sensing component is amplified to a level suitable for analysis
- Digitization and Storage: The amplified biosignal is digitized with an analog to digital converter and then stored in a memory device
- Data Transmission: The stored data is transmitted over a wireless communication platform

Readily available small foot-print, ultra-low power microprocessors and other energy efficient electronic components have allowed for optimization of the sensing,

amplification and digitization steps. Low energy communication protocols have further reduced the power requirements for wirelessly transmitting monitored biosignals. These energy savings have allowed the batteries to become smaller, while enabling prolonged continuous monitoring on a single charge.

Figure 1.2: Cardiac monitoring of a new-born baby [44]

Ongoing research in reducing size, improving power efficiency and enhancing wireless connectivity continues to make wearable monitoring more practical. However, this approach cannot solve challenges posed by the needs for all wearable monitors. For example, Fig. 1.2 shows a new-born baby being continuously monitored for its heart rate. A comfortable wireless monitor would definitely be more desirable to the typical scenario presented in the figure. The removal of the wires is possible with existing technology, however this would require the signal amplification, digitization and transmission to all happen from a sensor on the baby's body. These processes

require power, therefore the wireless solution would require a battery. The fact that batteries need to be periodically charged could hinder continuous monitoring. Additionally, devices need to provide access points for batteries. The necessity of such access points presents challenges for integration with the baby's garments. The resultant battery powered device would be cumbersome and uncomfortable for the baby. For applications like these, merely optimizing the steps presented in Fig. 1.1 may not be enough and a different approach to wearable monitoring is warranted.

1.3 Unconventional Biosignal Monitoring

Research on contemporary monitors has been focused on making better wearable sensors [48, 80, 112, 117] and integrating them with a minimal profile[6, 95, 96, 122]. The growth in the wearable devices field has mainly been fueled by reducing component size and power requirements. However, what if the conventional steps in biosignal sensing could be combined or entirely bypassed? In this case, the reduction in system size and power consumption could be considerable. For example, if a passive RFID tag is used for monitoring data transmission, the power required for data transmission can be entirely eliminated. However, the power drains of the digitization and data storage steps still exist. Therefore, in order to truly realize the battery free data transmission potential of RFID technology, the digitization and data storage steps need to be eliminated or rethought. To this end, unconventional biosignal sensing needs to be achieved such that no analog to digital converters or local data storage are required for biosignal transmission.

In this dissertation, a novel way to transmit biosignal parameters without the need for local data storage is developed. The biosignal monitor discussed here employs passive RFID technology and can be used to extract rate information from a variety of bioelectric signals; without the need for batteries or wires.

1.4 Thesis Organization and Contributions

1.4.1 Thesis Organization

Chapter 2 of this dissertation delves into background information on relevant material like biosignal sensing, data transmission and RFID technology. Chapter 3 describes a novel RFID based approach for biosignal data transmission and presents some simulations to verify the viability of the proposed method. Chapter 4 illustrates the steps involved in designing a hardware prototype for the RFID based heart rate monitoring along with tests conducted to characterize the system. An algorithm to improve heart beat detection accuracy in noisy environments is presented in Chapter 5. Chapter 6 discusses further system characterization and applications. Chapter 7 concludes this thesis and provides an insight into possible future work.

1.4.2 Thesis Contributions

The main contributions of this dissertation are summarized in Fig. 1.3. This section provides an overview of these contributions.

1.4.2.1 Data Transmission Method

The main innovative contribution of the thesis is a method for transmitting biosignal data by simply turning RFID tags on and off. The proposed method employs a variation of On-Off Keying (OOK) modulation to RFID tags by interrupting RFID data transmission based on the biosignal being monitored.

1.4.3 Hardware Design and Integration

Another contribution of this dissertation is a low power hardware realization of an RFID based battery free and wireless heart rate monitor. The hardware design involved circuits for biosignal amplification, wireless power harvesting and biosignal

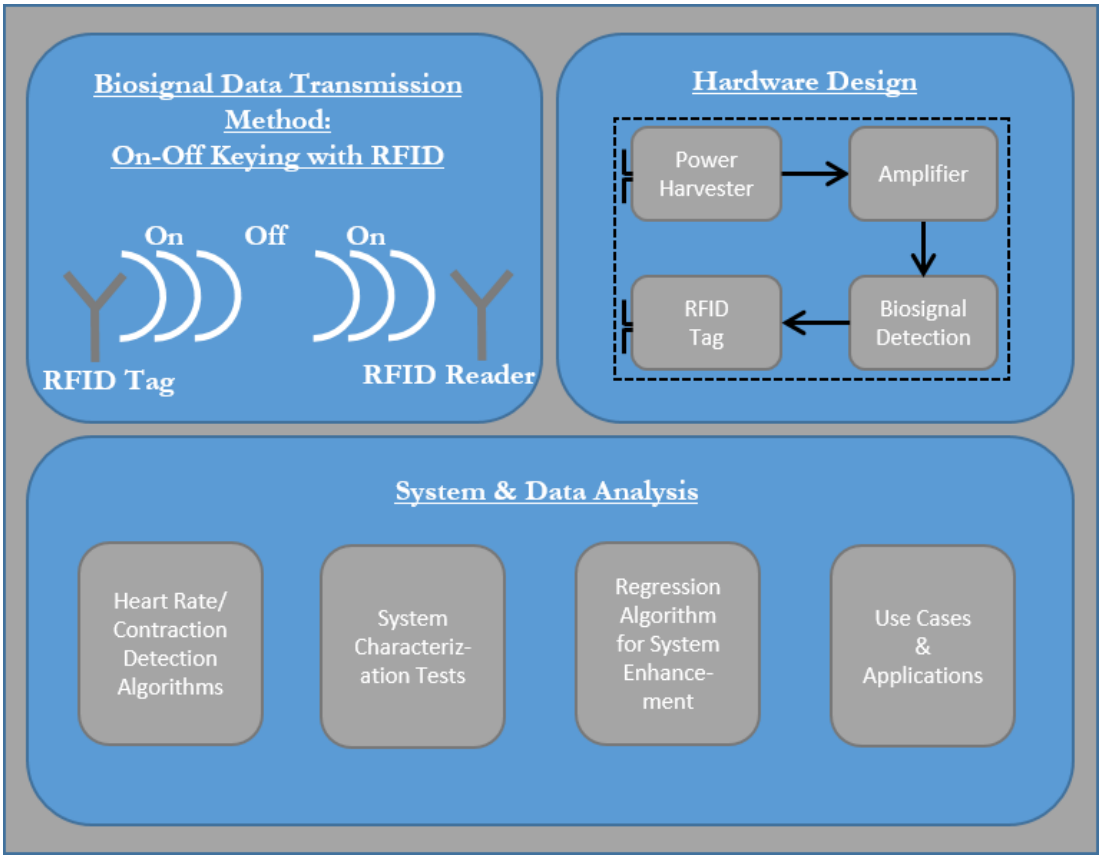

Figure 1.3: Thesis Contributions

detection in addition to overall system integration. Commercially available components like RFID tags and timer integrated circuits were creatively re-purposed for implementing the system. Additionally, fundamental research was also conducted for integrating a power harvesting antenna with the heart rate monitor.

1.4.4 System and Data Analysis

The dissertation contains extensive analysis to verify and validate the proposed method for biosignal analysis. Algorithms for monitoring heart rate and uterine contraction employing the RFID on/off method are evaluated with simulations. The heart rate monitor hardware is characterized using multiple tests that include validation with human data. A regression algorithm to improve heart rate detection data in noisy environments is demonstrated. A detailed study on a specific use case of a baby monitor is also presented.

1.4.5 Publications

The following articles have been published in relation to the work described in this thesis.

- S. Vora, O. Montgomery and T. Kurzweg, "Enabling Uterine Contraction Monitoring with Passive RFID Tags", *2017 IEEE-EMBS International Conference on Biomedical and Health Informatics (BHI)*, Orlando, FL, 2017, pp. 213-216

- S. Vora and T. Kurzweg, "Unconventional Biosignal Sensing with Passive RFID Tags ", *IEEE HKN The Bridge*, vol. 112, no. 3, pp. 25-29, Oct. 2016.

- S. Agezo, Y. Zhang, Z. Ye, S. Chopra, S. Vora and T. Kurzweg, "Battery-Free RFID Heart Rate Monitoring System", *Proceedings of IEEE NIH Wireless*

Health 2016, Bethesda, MD, Oct. 2016, pp. 136-142. (Best Paper and Presentation Awardee)

- W. Mongan, E. Anday, G. Dion, A. Fontecchio, K. Joyce, T. Kurzweg, Y. Liu, O. Montgomery, I. Rasheed, C. Sahin, S. Vora and K. Dandekar, "A Multi-Disciplinary Framework for Continuous Biomedical Monitoring Using Low-Power Passive RFID-Based Wireless Wearable Sensors," *2016 IEEE International Conference on Smart Computing (SMARTCOMP)*, St. Louis, MO, 2016, pp. 1-6.

- S. Vora and T. Kurzweg, "Modified logistic regression algorithm for accurate determination of heart beats from noisy passive RFID tag data," *2016 IEEE-EMBS International Conference on Biomedical and Health Informatics (BHI)*, Las Vegas, NV, 2016, pp. 29-32.

- S. Vora, W. Mongan, K. Dandekar, A. Fontecchio and T. Kurzweg, "Wireless heart and respiration monitoring for infants using passive RFID tags," *2016 IEEE-EMBS International Conference on Biomedical and Health Informatics (BHI)*, Las Vegas, NV, 2016.

- S. Vora, K. Dandekar and T. Kurzweg, "Passive RFID tag based heart rate monitoring from an ECG signal," *2015 37th Annual Int. Conference of the IEEE Eng. in Medicine and Biology Soc.*, pp. 4403-4406, 25-29 Aug. 2015.

The following articles are yet to be published.

- S. Vora, W. Mongan, K. Dandekar, G. Dion, A. Fontecchio and T. Kurzweg, "On Implmenting an Unconventional Wireless Infant Health Monitor with Passive RFID Tags", *11th Annual IEEE International Conference on RFID (RFID Live)*, Phoenix, AZ. (accepted).

- S. Vora and T. Kurzweg, "Passive RFID Heart Rate Monitor for Wearable Platforms", *IEEE Journal of Translational Engineering in Health and Medicine.* (in preparation)

2. Background

Extensive research is ongoing to make wearable devices smaller, lighter and efficient [94]. As was shown in Fig. 1.1, sensing, amplifying, digitizing and transmitting are the four primary steps involved in biosignal monitoring. In this chapter, methods and state of the art for biosignal sensing and data transmission are discussed with a focus on wearable technology applications. Additionally, as this work focuses on an RFID based solution, a discussion on passive RFID technology is also included to provide a foundation for later chapters.

2.1 Sensing and Amplification

The human body produces multiple signals that can be monitored to ascertain the health and function of body parts. These signals can be mechanical or electrical in nature. The focus of this work is on electrical biosignals; collectively called bioelectric signals.

2.1.1 Types of Bioelectric Signals

Bioelectric signals measured to monitor different organs have been given specific names; electrocardiograms (ECG) are measured for heart, electroencephalograms (EEG) are measured for brain, electromyograms (EMG) are measured for muscle activity and electrooculograms (EOG) are measured for eye activity. Typical examples of graphical representations of these bioelectric signals are shown in Fig. 2.1.

The hardware and apparatus used for measuring these biosignals are similar. For each of these measurements, conductive electrodes are placed on the surface of the skin close to the organ being monitored. The electrodes detect a mixture of biosignals

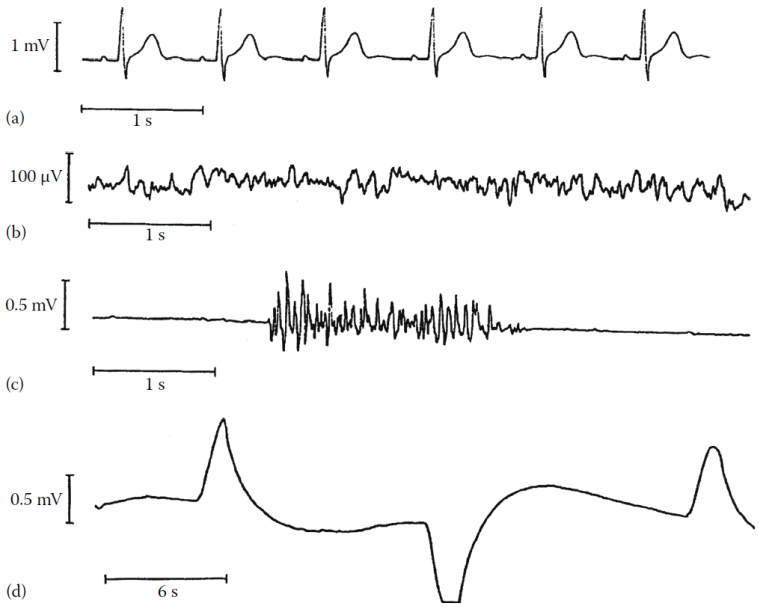

Figure 2.1: Examples of different bioelectric signals: a) ECG, normal sinus rhythm; b) EEG, normal patient with open eyes; c)EMG, flexion of bisceps; d) EOG, movement of eyes from left to right [130]

due to various organs. However, as can be seen from Fig. 2.1 and summarized in Table 2.1, biopotentials due to different organs vary in their amplitude,shape and frequency. To obtain the biosignal of interest, the sensed electric potential (biopotential) is first amplified with an appropriate voltage gain. The amplified signal is then passed through an appropriate filter for the desired biosignal. This filtered signal is then digitized using analog to digital converters.

The focus of this work is on parameter extraction from two special types of bioelectric signals (electrocardiograms (Section 2.1.2.1) and electrohysterographs(Section 2.1.3.1)). However, the approach and techniques discussed here can potentially be adapted for other bioelectric signals as well.

Table 2.1: Comparison of Bioelectric Signal Parameters [130]

Bioelectric Signal	Amplitude (mV)	Bandwidth (Hz)
ECG	1-5	0.5-100
EEG	0.001-0.001	0.5-40
EMG	1-10	20-2000
EOG	0.01-0.1	dc-10

2.1.2 Cardiac Monitoring

Globally, cardiovascular diseases continue to remain the leading cause of death; killing more people than any other disease [8]. This alone makes a strong case for development of convenient continuous cardiac monitors. Heart rate, which specifies the interval between heart beats, is the most important and commonly monitored cardiac feature. Nowadays, heart rate monitors have started finding applications in diverse areas from optimizing athletic performance [2] to monitoring health for those employed in risky professions like firefighters [47]. Several technologies, new and old, are used for heart rate monitoring. These include, but are not limited to, ballistocardiography [5, 39], pulse oximetry [108], phonocardiogram [33] and electrocardiogram [74, 128]. Of these, the electrocardiogram (ECG), is a primary monitoring technique. An ECG has several features that can provide significant insight into a patient's cardiac health [137], as discussed in the next section. Hence, heart rate monitors and ECG devices have received wide attention from researchers in academia and industry.

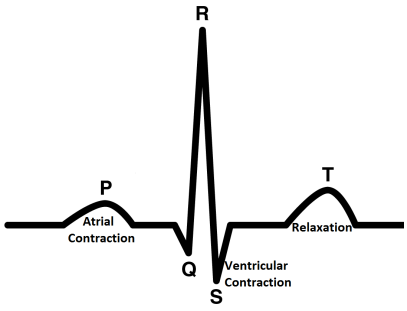

Figure 2.2: PQRST complex in an ECG Signal

2.1.2.1 Electrocardiogram

The way an ECG device works is that it detects and amplifies the tiny electrical charges on the skin that are generated when the heart depolarizes during each heartbeat cycle. A typical ECG signal is shown in Fig. 2.2 and it has several sub-waves which indicate the steps in the cardiac rhythm [24]. The heart cycle is initiated by the cells in the tissue called the sinoatrial (SA) node. The SA node can be referred to as the 'pacemaker' of the heart. This node sends an impulse to the cells in the atria which causes atrial contraction. This is represented by the 'P' wave in Fig. 2.2. Once the atria depolarize, the cells in the atrioventricular (AV) node cause the ventricles to depolarize. The ventrical contraction is represented by the 'QRS complex'. The 'T' wave represents the relaxation of the ventricles.

The most common cardiac parameter extracted from the ECG signal is the heart rate which conveys the frequency of the cardiac cycle. As the 'R' wave is the most prominent of these waves, the heart rate can be directly measured by calculating the time between successive 'R' waves [24].

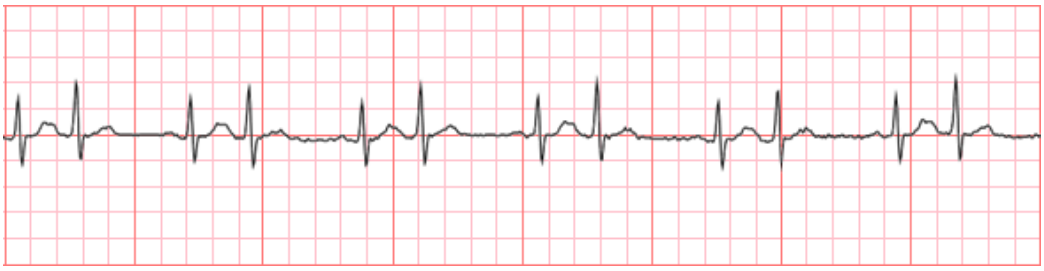

Figure 2.3: ECG of bigeminy condition [132]

2.1.2.2 Arrythmias

Deviations from the regular sequence of events in the generation of 'PQRST' waves may indicate critical cardiac events. Such changes from the normal cardiac rhythm are collectively called 'arrythmias'. A primer on different types of arrythmias along with cardiac conditions that they indicate can be found in [70] and methods of computationally simulating such arrythmias can be found in [13].

Some arrythmias affect the position of the 'R' wave and thus directly impact the 'R-R' intervals. Such arrythmias are called 'rate arrythmias'. For example, a condition called 'bigeminy' where there is an occurrence of alternating long and short 'R-R' intervals, is shown in Fig. 2.3. Many of the arrythmias manifest as a change in shape of the normal ECG waveform. For example, Fig. 2.4 shows atrial fibrillation, a type of shape arrythmia where the atria cannot effectively transfer blood to the ventricles due to abnormal electrical triggering. The 'P' waves represent atrial contraction and the 'P' wave is noticeably absent in the top plot of Fig. 2.4 thereby changing the shape of the ECG wave. Such arrythmias are called 'shape arrythmias'.

2.1.3 Uterine Contraction Monitoring

Another set of biosignals to be considered in this dissertation are uterine contractions. Timely detection of labor onset is critical in ensuring a safe delivery for

Figure 2.4: ECG of atrial fibrillation (top) and normal sinus rhythm (bottom) [131]

pregnant mothers and their new-borns. The onset of labor is typically indicated by frequent and regular contractions of the uterine muscles. Hence, uterine contraction monitoring becomes increasingly important towards the end of pregnancy. Any indication of a preterm delivery can help reduce risk to the fetus [65]. Though it cannot definitively predict preterm delivery, premature increased frequency of uterine contractions is a strong indicator of preterm delivery[53].

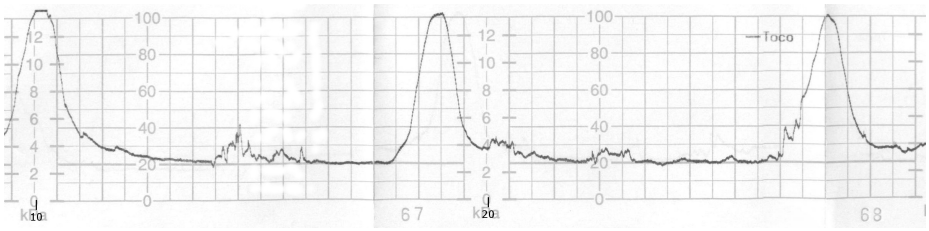

Figure 2.5: Tocodynamometer strip with contractions [7]

Intra-uterine pressure catheters (IUPC) are the gold standard in uterine contraction monitoring and can produce very reliable uterine contraction signals that

provide accurate contraction strength and frequency information [42]. However, the procedure to place these catheters is highly invasive and it is only performed when absolutely necessary; for accurate oxytocin regulation or if non-invasive monitoring is not possible due to maternal obesity [50]. On the other hand, tocodynamometry is the most common technique for measuring uterine contractions as it only involves strapping a sensor to the mother's belly [25]. A typical tocodynamometer strip is shown in Fig. 2.5 with uterine contractions clearly visible as humps over the baseline. However, the equipment used is bulky, requires expecting mothers to be tethered to a monitor and it only measures relative strength of contractions. Uterine EMGs or electrohysterograms (EHG) are non invasive and nearly as relaiable as IUPC [49]. Hence, there is a lot of interest in utilizing EHGs for uterine contraction monitoring.

2.1.3.1 Electrohysterograms

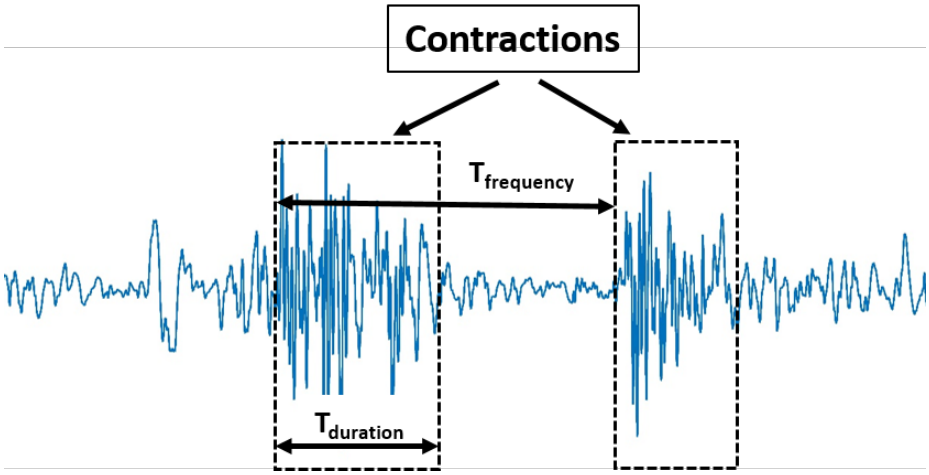

Figure 2.6: Contractions in an EHG Signal

A typical EHG signal for a pregnant woman in labor is shown in Fig. 2.6. Con-

tractions are marked by a rapid increase in frequency and amplitude of the signals and can be easily distinguished from the non-contraction state for parameter extraction. The primary parameters of importance for contraction monitoring are the duration and frequency of contractions. The EHG signal mainly differs from other bioelectric signals in terms of frequency. The bandwidth of these signals is in the range of DC to $3Hz$ [77], making it is possible to distinguish EHG signals from other bioelectric signals.

2.1.4 Biosignal Electrodes

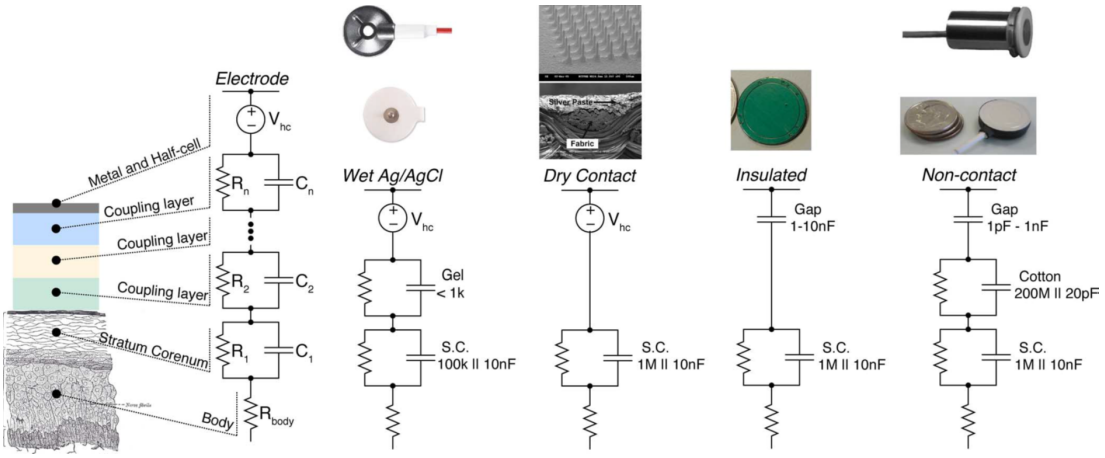

Figure 2.7: Electrodes for sensing bioelectric signals [32]

Electrodes are used to sense bioelectric signals like ECG and EHG from the surface of the skin. Several types of biosignal electrodes are shown in Fig. 2.7 alongwith their equivalent circuit diagrams [32]. Conventionally bioelectric signals have been sensed using flexible conductive electrodes with a silver chloride gel layer between the skin and the electrode. This gel layer, which may be wet or semi-dry, serves to

reduce the skin-electrode impedance and improves signal quality. Such silver chloride electrodes have several problems; they need to be replaced regularly as the effect of the gel wears off, they are not reusable and the adhesive-gel combination makes the electrodes unpleasant to wear. Thus, researchers have been trying to design electrodes that are comfortable and can be used for prolonged monitoring.

Textile electrodes are an attractive alternative to conventional electrodes as they can be integrated as a part of the garment a user already wears. However, the true potential of textile electrodes can only be realized by doing away with the need for conductive gels and adhesives for contact. To overcome these challenges, significant research has been done in characterizing conductive fabrics and yarns for textile electrodes [11, 17, 99, 103], comparing textile electrode types [32, 48, 78] and studying the interface between the skin and textile electrodes[118]. Materials like polymers [12, 72] and manufacturing techniques like screen printing [103] have been employed to create novel wearable electrodes.

Fabric electrodes are yet to receive widespread acceptance primarily because of the poor signal quality caused by inadequate contact between the electrode and the skin. Researchers have tried to solve this problem by exploring several techniques like introducing micro-barbs in the electrode [135] and improving the signal quality by making active electrodes that include low noise pre-amplifiers packaged with conductive surfaces [84]. Furthermore, research has also been done on creating contactless electrodes that are capacitively coupled to the skin for biosignal sensing [73, 117].

It should be noted that further research on electrodes is not conducted in this thesis and standard gel electrodes are used for human data collection described in Chapter 5.

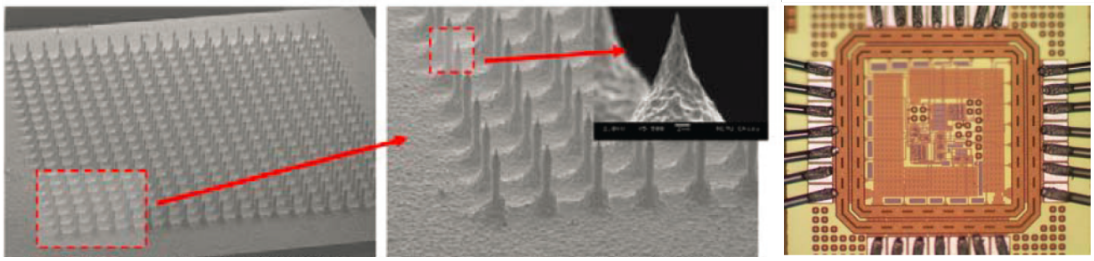

Figure 2.8: Integrated system with electrodes (left) and amplifier (right) on a single chip [29]

2.1.5 Low Power Biosignal Sensors

Another step in making wearable monitoring devices more practical is to reduce the power required for amplifying the sensed signal and packaging the circuits into compact integrated chips. There are several biosignal sensing systems-on-chip (SoC) in literature that are novel and utilize very little power [64, 105, 121]. An attempt has also been made to combine an eletrode and an amplifier into a single integrated circuit device [29]. This system is shown in Fig. 2.8 with a magnified image of electrodes on the left and an integrated chip with amplifiers on the right. With the advent of subthreshold conduction circuits, the power required to amplify bioelectric signals can be drastically reduced and [62] describes an ECG amplifier circuit that only consumes 2.6μW of power. Such low powered operation can make battery free signal sensing and amplification easier to achieve.

In conclusion, major strides have been made in sensing and amplifying biosignals. The power required for sensing and amplification has been significantly reduced. However, challenges still exist for a practical and comfortable alternative to gel electrodes.

2.2 Wireless Data Transmission

Wireless transmission of the acquired biosignal is essential to prolonged monitoring as it allows a person to be mobile. To wirelessly transmit biosignal data researchers mainly use established methods like bluetooth [31, 74] and cellular technologies[128] or develop their own prototype RF transmitters [80]. These transmission systems consume power for relaying the biosignal data. In fact, the most power hungry aspects of wearable monitors are not the sensors but the data storage and transmission parts [110]. Hence, optimizing the power required for data transmission is critical for prolonged wearable health monitoring.

2.2.1 Types of Wireless Data Transmision Methods for Wearable Monitoring

Table 2.2 compares the range and typical packet power consumption for commonly used wireless data transmission methods. As can be seen, different technologies are suited for operations at varying distances.

Table 2.2: Range and power requirements of commonly used data transmission methods [111, 114]

Wireless Technology	Range (m)	Frequency (GHz)	Power (μW)
ZigBee	10-100	0.868,0.915,2.4-2.5	3500
Bluetooth Low Energy	1-10	2.4-2.5	147
ANT/ANT+	10-30	2.4-2.5	183
WLAN	35-125	2.4,5.8	210
UHF RFID	0-10	0.86-0.96	NA

2.2.1.1 Medium to Long Range Data Transmission

The category of transmission methods discussed here are suitable for collecting data from a large number of devices and transmitting over large distances which can range over 100 m. ZigBee[136] is a popular wireless communication standard that is used for low-cost, low-speed and medium range data transfer [114]. ZigBee has been proposed as a wireless platform for several health monitoring devices [34, 63, 129]. It is easy to implement and provides a medium for communication between different devices. However, as can be seen from Table 2.2, the power required to transmit a single data packet is very high, making ZigBee difficult to use for wearable devices.

WLAN or cellular technologies are more suitable for transmitting sensor data over long ranges [114]. They are capable of compacting data more densely in each packet but components and power required for these communications make them prohibitive for continuous transmission from a biosignal sensor. Even so, researchers have looked into the possibility of direct data transmission from the sensor using cellular technologies [10].

2.2.1.2 Sensor to Hub: Short Range Data Transmission

The transmission methods discussed in this section are used for short range communication within a room or a small building between a sensor and a data collection hub like a cell phone. Bluetooth and specially bluetooth low energy (BLE) are widely used for data transmission from biosignal sensors. These technologies are very attractive for personalized wearable monitoring due to the pervasiveness of bluetooth compatible smart devices like phones and tablets. Hence, a bluetooth enabled sensor can easily transmit data to a host of already existing devices. BLE has additional features suitable for wearable devices like ultra low power idle modes and easy device discovery functions [114]. Thus, there is an abundance of health monitors in literature

that employ bluetooth to transfer data [19, 20, 61, 68]. It should be noted that power saving measures like alternating between data transmission and idle modes are often applied which introduce an inherent latency in the system and prevent continuous monitoring.

ANT/ANT+ is a proprietary technology that is designed to meet the needs of wearable sensor networks. It has features that allow for optimization between data latency and power consumption [114]. Researchers have thus looked at this technology extensively for use in wearable monitors [83, 123, 138].

Even though BLE and ANT are low power transmission technologies, the requirement for local power means that sensors need to have batteries. Wearable systems benefit from being low-power as this prolongs usage and reduces the system down time for recharging or battery replacement. Since data transmission is the main power consumer in wearable monitors, any success in reducing the power consumed for this step helps in prolonging the use cycle of the wearable device.

Passive RFID (Radio Frequency Identification) is a communication method that does not rely on any local power source. Passive RFID tags work on power wirelessly harvested off an RFID reader, rather than make use of any local battery systems. Using passive RFID virtually eliminates the local battery's data transmission burden and can even enable the development of battery free monitors. Hence, the study of RFID tags for biosignal monitoring applications is particularly interesting.

2.2.2 Unconventional Biosignal Sensing

Recently, a couple of biosignal sensing approaches have been published that do not require any sensor to be placed on a person for monitoring due to the data transmission method used. For example, [3] exploits the effect of mechanical vibrations caused due to beating of the heart and respiration cycle on wireless RF signals to

determine heart and respiration rate. Another work [75], proposes a method that uses perturbations in ambient WiFi signals to measure a person's heart and respiration rate. These methods, however, are very sensitive to practical conditions that involve moving objects in the environment and require the monitored person to stay relatively still. Also, in an environment with multiple people or even with animals it is difficult to designate the monitored vital signs to a specific person.

2.3 RFID Technology

Table 2.3: Comparison of RFID Technologies [43]

Type	Frequency (MHz)	Range (m)	Primary Application
Low Frequency	0.135	<1cm	Access control
High Frequency	13.56	<1m	Smart cards
Ultra High Frequency	868, 915, 2500, 5800	>3m	Inventory management

In contrast with the transmission methods presented in the previous section, RFID systems can be passive, reliable and allow for unique identification of all subjects being monitored. RFID systems are categorized by frequencies into three broad categories: Low Frequency (135kHz), High Frequency (13.56MHz) and Ultra High Frequency (868/915 MHz/2.5GHz/5.8GHz). Of these, the UHF tags have the highest range which is of the order of tens of feet. UHF tags can thus allow a user to move around while being monitored. UHF RFID tags can either be active or passive; wherein the later are a category of tags that do not need any local batteries for operation.

A typical passive UHF RFID system is shown in Fig. 2.9. The picture depicts

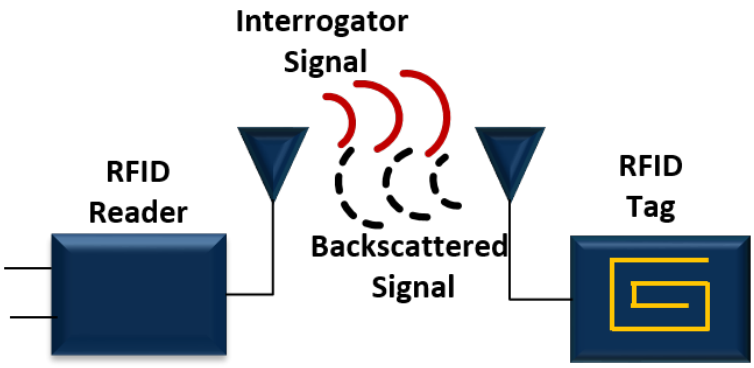

Figure 2.9: Passive Ultra High Frequency (UHF) RFID System

an RFID reader and a passive tag. The RFID reader sends a radio frequency (RF) interrogation signal which is received by the tag. The tag is powered wirelessly by this interrogating RF signal and it uses this energy to backscatter its unique tag ID. Backscatter communication is conducted by varying the load seen by the tag antenna with the data to be transmitted. The tag achieves this by changing its impedance between a high and a low impedance state wherein each state corresponds to a 0 or a 1. Thus, no battery is required on the tag to perform communication. With passive RFID, biosignal data can potentially be transmitted without using any sensor battery power thereby allowing significant reduction in power and size for a wearable monitor.

2.3.1 Data Transmission with RFID

Today, a large number of products are identified, cataloged and monitored using a unique RFID tag placed on them. Typically the only purpose served by these tags is to identify the object that they are attached to in a manner that is very similar to barcodes. Passive RFID tags have also started having increased visibility for inventory management and patient tracking in hospitals [120].

For RFID tags to be used in sensor networks, they have to be capable of trans-

mitting sensor data alongwith the tag ID. In its simplest form, the RFID tag can be considered to be a one bit transmission device. The status of this bit is dependent on the state of the tag; '0' while the tag transmits and '1' while it doesn't or vice versa. RFID tags, thus, can be connected to sensors and used to relay the signals detected by them. There are several devices that use RFID tags in this fashion, these include the initial version of the WISP platform [98] and a four bit transmission system for generic sensor data[28].

2.3.1.1 Contemporary Biosignal Sensing with RFID

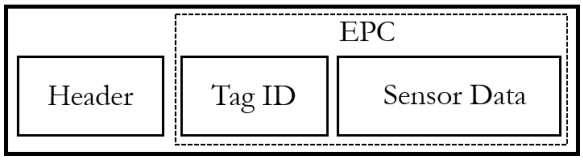

Figure 2.10: Contents of an RFID data packet

Contemporary RFID tags are capable of transmitting multiple bits of optional sensor data along with the tag ID. The contents of a typical RFID sensor data packet are shown in Fig. 2.10 which include a header for establishing a link with the RFID reader, a unique identifier (tag ID) and sensor data. Hence, RFID tags can transmit user defined data akin to other communication platforms. However, additional circuitry like analog to digital converters (ADCs) and microcontrollers are required to digitize and embed the sensor data with the tag ID. Such battery free RFID based ECG and EEG monitors have been suggested by [18, 37]. The additional components required not only increase the size of the system but also add to its power requirements. Another drawback of such systems is the requirement of significant

transmitted data redundancy to achieve an acceptable degree of reliability. For example, the electroencephalogram (EEG) system proposed in [37] (shown in Fig. 2.11) requires 92% data overhead and has a range of only 0.8m. The requirement for data overhead adds to the system power consumption. If this power is harvested wirelessly, higher power demand significantly degrades the system's range. Additionally, the system alternates between sleep/awake cycles to conserve power and eliminate the interference due to the continuous wave RFID reader signal on the processing circuit. Hence an alternative approach to biosignal data transmission with RFID tags that does not have these limitations is warranted.

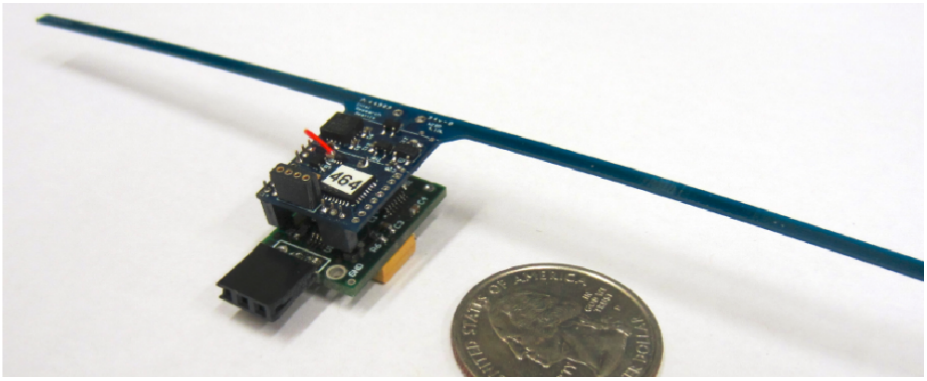

Figure 2.11: Passive RFID based EEG Monitoring System [37]

2.3.1.2 Unconventional Biosignal Sensing with RFID

One such RFID based sensor that does not follow the conventional process of biosignal sensing is presented in [97]. The operating principle of this RFID stretch sensor device is shown in Fig. 2.12. Here, an RFID tag is populated on a stretchable fabric antenna and integrated into a wearable band. This band can be placed around

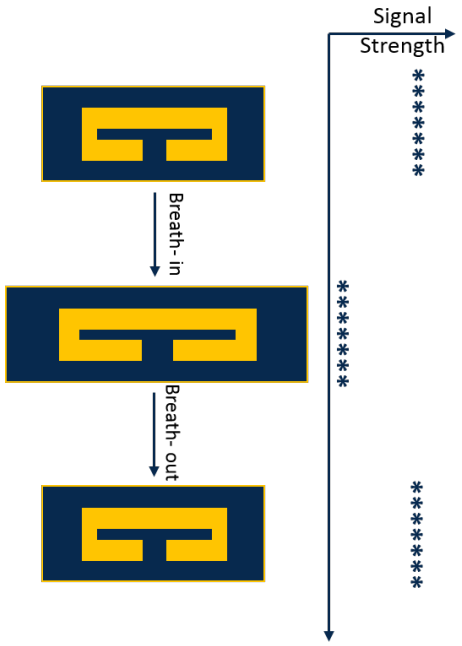

Figure 2.12: Operating principle of RFID respiration monitor

a subject's torso for respiration monitoring. The fabric antenna then stretches and relaxes as the subject's chest expands and contracts with each breathing cycle. The antenna geometry changes with the breathing cycle which causes variations in the signal strength backscattered by the tag as the subject breathes. These variations in received signal strength can be correlated to the respiration rate. Such a stretch sensor has no need for local data storage as the sensing and transmission steps are combined. An unconventional sensor for bioelectric signals, however, is still needed.

2.4 Conclusions

In this chapter, a variety of bioelectric signals produced by the human body were described and it was shown that they can be separated on the basis of their bandwidths and amplitudes. Extensive ongoing research for low power detection and

transmission of these bioelectric signals was also discussed. Passive RFID technology shows great promise for wireless and battery-free biosignal monitoring and several contemporary RFID biosensors from literature were described in this chapter. However, an altogether different approach is necessary for monitoring bioelectric signals without batteries. The following chapters describe a novel RFID based approach for sensing critical features of bioelectric signals.

3. Biosignal Monitoring with Passive UHF RFID Technology

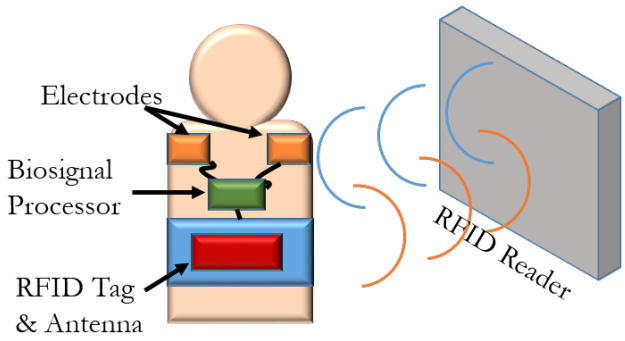

Figure 3.1: RFID Based Bioelectric Signal Monitoring

Biosignal monitoring with passive UHF RFID tags can be achieved wirelessly and without any batteries. As shown in Fig. 3.1, the integrated RFID sensor that includes electrodes, processing circuits and the RFID tag, can be worn by a person while the required biosignal is being monitored remotely using an RFID reader. Of all the different RFID technologies, UHF RFID is the most suited for biosignal sensing as it has enough range to monitor a mobile person indoors (up to 10 m). UHF RFIDs can cover a number a number of different frequency ranges between 860 MHz and 5.8 GHz. However, the lower end of this spectrum has received widespread acceptance across several industries due to the existence of a well-established and flexible standard. The standard that governs RFID tags in these lower frequency ranges is called EPC Class 1 Genration 2 (C1G2) UHF RFID protocol [58].

This chapter begins with a description of the C1G2 protocol. A novel method for biosignal monitoring using passive RFID tags is then introduced. The chapter

also includes an experimental analysis of a continuous RFID datastream. Finally, simulations are presented to discuss continuous heart rate and uterine contraction monitoring using the proposed novel method.

3.1 EPC Class 1 Gen. 2 UHF RFID Protocol

The EPC Class 1 Genreation 2 UHF RFID protocol [58] specifies the requirements of passive backscatter RFID systems that operate in the 860 MHz to 960 MHz range. This protocol is used for inventory and supply-chain management in retail, healthcare and manufacturing among other industries. Due to its large scale application, it is easy to obtain inexpensive commercial implementations for this RFID standard. However, a discussion of this protocol is warranted before studying biosignal monitoring using the C1G2 RFID standard.

3.1.1 Generalized Reader-Tag Communication

For systems compliant with the EPC C1G2 protocol, the reader always initiates communication with the tag. The tag can be either passive or active (battery powered to enhance range). In both cases, the tag communicates with the reader by modulating the signal backscattered from the reader's continuous wave signal. It should be noted that even in active tags, the reader-tag communication is always passive, the added battery is only used to power circuitry on the tag and not to enhance the strength of the backscattered signal [43]. The communication between the tag and the reader is in half-duplex mode which means that only one can transmit at a given time. An example of this communication between a reader and a tag is shown in Fig. 3.2 [110]. In this figure, note that the interrogation signal from the RFID reader initiates communication and the tag then backscatters a response. Not shown in the figure, is the fact that the reader continues transmitting an unmodulated continuous

wave signal while the tag backscatters its response. Thus, the tag's backscattered response has an offset as it is a combination of the tag's backscattered signal and the readers continuous signal.

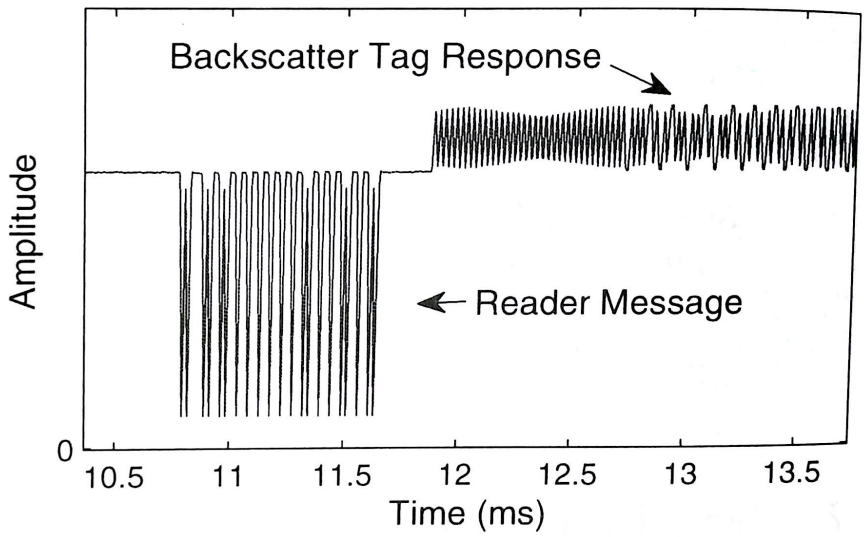

Figure 3.2: Half-duplex communication between an RFID reader and a tag [110]

The primary modulation scheme used for data transmission is Amplitude Shift Keying (ASK) [109]; though several forms of this modulation scheme like double sideband, single sideband or phase reversal ASK are allowed as per the protocol. The protocol allows a wide bandwidth of operation between 860 MHz and 960 MHz to allow for flexibility in usage across allocated spectrums in different geographical regions. For example, the allotted spectrum for UHF RFID in North America is 902 MHz to 928 MHz [43]. In order to minimize interference and free up spectrum for other devices, FCC specifies that UHF RFID systems hop frequencies in 500 kHz bands with not more than 400 ms per channel [110]. The protocol is compliant with

this frequency hopping requirement. Additionally, the protocol allows for reading multiple tags. The protocol does not specify a standard method for reading all tags but provides primitive commands that can be combined as per the user's choice to optimize for speed, efficiency, power and other factors. Hence, the C1G2 protocol offers a great deal of flexibility in UHF RFID system design.

3.1.2 Tag Read Process

The C1G2 protocol specifies a set of steps to identify and read individual tag reads. These steps ensure that tags are read efficiently and reliably. A study of these steps is essential to understand the effect of C1G2 protocol on biosignal monitoring with UHF RFID.

3.1.2.1 Single Tag Read

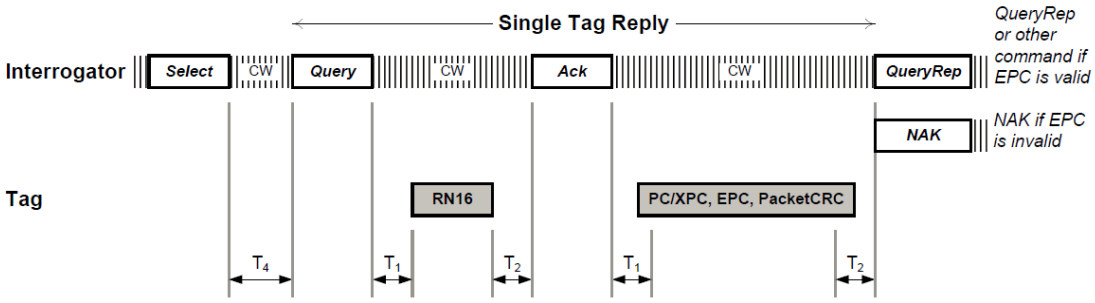

Figure 3.3: Single Tag Response [58]

Fig. 3.3 shows the typical process of reading a single RFID tag. The process starts with the RFID reader powering up and transmitting a continuous wave (CW) signal for a predetermined time. This CW signal is used to wirelessly power up the

tag; no query is sent by the reader for a fixed initial time to allow the tag to power on. Thereafter, a query is sent by the reader which indicates a 'Q' parameter among other protocol related details. The 'Q' parameter allocates the necessary number of slots for a tag to respond and its value is between 0 and 15. Once a tag receives a query, it generates a 16-bit pseudo-random number (RN16) between 0 and 2^Q-1. The generation of this RN16 number is an anti-collision measure and its function will be discussed in the next section. The tag then transmits the generated RN16 number to the reader. After receiving the RN16, the reader sends an acknowledgement (ACK) back to the tag. On receiving the 'ACK', the tag transmits its EPC code which is its unique ID back to the reader. The symbols 'T_x', are tolerance values assigned to allow for variations in communication times due to environmental reasons that will be discussed in Section 3.1.3. If the reader receives an invalid EPC, it sends a 'NAK' command for the tag to repeat the EPC code.

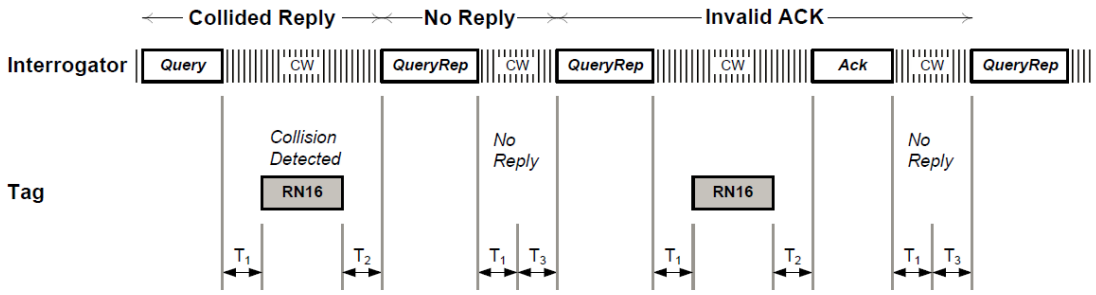

Figure 3.4: Query Repeat Cases [58]

The reader typically operates in an environment where there are more than one compatible tags. As the communication method is half-duplex, only the reader or the tag can be transmitting data at a given time. Thus, it is possible that more than one

tags might respond to the reader at the same time. The reader simply repeats the query if a collision is detected, or if no response is received from tags after waiting for a stipulated time as shown in Fig. 3.4. The reader initiates a new query after failing to receive the EPC three times. The protocol also has anti-collision features which will be discussed in the next section.

3.1.2.2 Collision Mitigation and Multiple Tag Read

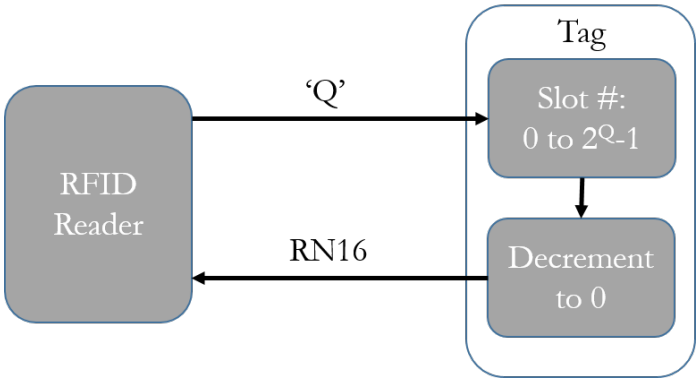

Figure 3.5: Procedure for tag response to RFID reader

The 'Q' parameter and the generation of the RN16 number together constitute the main anti-collision features of the C1G2 protocol. The procedure followed for initial handshaking between a single tag and the reader is shown in Fig. 3.5. The 'Q' parameter decides the number of available slots for the tags to respond. A higher 'Q' number is used for denser tag environments enabling a greater number of available slots for tags. Once the tags receive the 'Q' parameter from the reader, they generate the aforementioned random RN16 number. The higher 'Q' parameter, the lesser the likelihood of two tags generating the same random number. Each tag then starts

counting down from its generated random number. Once a tag reaches '0', it transmits its RN16 number to the reader and then completes the data transmission sequence described in the previous section. In this way collision between tags is avoided.

If a tag has been successfully read, it should be left out of the inventory process till all other tags in the environment are also read. Such exclusion ensures that the overall inventory cycle is not delayed by the same tag being read over and over again. The protocol uses flags to resolve this multiple read issue. At the start of an inventory cycle (when the reader powers up), all tags are set to a flag 'A'. Once a tag has been successfully read its flag is set to 'B' and it does not participate in the inventory process. Once all the tags in the environment have been read, the reader powers down momentarily causing all the tags to be reset to 'A'. All tags are then available in the next inventory round for a new read cycle.

3.1.3 Variations in Inter-Cycle Tag Read Time

Inter-cycle tag read time is the time taken by the reader to read the same tag again after completing an inventory cycle as described in the previous section. As will become evident in the following sections, this inter-cycle tag read time is critical for this work's biosignal sensing method. The EPC C1G2 protocol only provides a wide framework for UHF RFID systems to operate in, however, the flexibility offered by this protocol means that the time between same tag reads may vary significantly. The variation in tag read times can be due to several factors which are broadly divided into three categories; protocol related variations, tag related variations and channel dependent variations. These sources of variation are enumerated in Fig. 3.6.

Protocol related variations can be due to several adjustable parameters in the EPC C1G2 standard. Firstly, the 'Q' parameter that decides the allowable time slots for tags to respond can vary. Higher the 'Q' parameter, longer the allowable time for

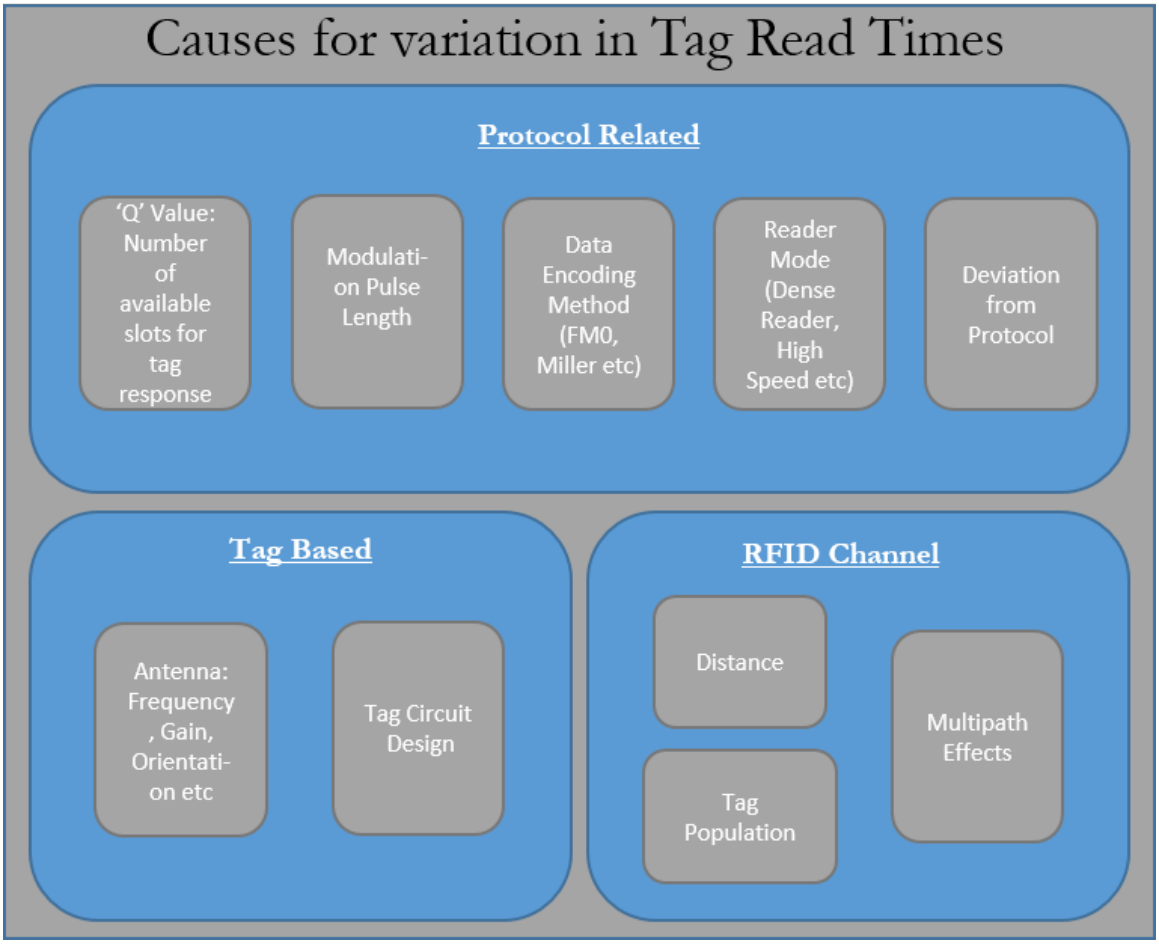

Figure 3.6: Causes of Variation in Tag Read Cycles

tags to respond. The protocol also allows for variation in modulation pulse length. Modulation pulse length is the duration of every bit of data. Longer pulse lengths are used to mitigate errors in noisy or low signal level environments, however, this causes an increase in tag read time as well. Several data encoding methods like FM0, Miller-2, Miller-4 etc are allowed by the protocol [58]. The choice of data encoding method influences the tag read time. Commercial RFID readers come programmed with several reader modes like 'High Speed Mode', 'Dense Reader Mode', 'Standard Mode' etc. These modes allow for predetermined selections of protocol parameters

suitable for different environments. Thus, time for tag reads also depend on the reader mode selected. Finally, some readers may also deviate from the protocol [27] while maintaining functionality with tags that follow the protocol, these deviations may also cause changes in tag read times.

Time between tag reads may also vary with individual tags. Some of the variation is introduced due to the tag antenna. As mentioned in Section 3.1.1, the reader is required to hop across several frequencies. The response of each tag at different frequencies might be different due to manufacturing tolerances. Thus tag read times may vary dependent on the frequency at which a particular tag is interrogated. The tag read times may also vary based on power and timing requirements of the circuit design for a given variety of tags. Tag read times may change because of the changes in the RFID channel due to environmental reasons as well. Misses in tag reads can be caused due to increasing distance and multipath effects. A higher tag population increases inter-cycle tag read time and may also cause repeated reader queries due to collisions. Fig. 3.7 shows the reduction in number of tags read per second with increasing distance for different reader modes [27]. It should be noted that a reader setting that yields high tag read rates at lower distances (HS1 and HS2) can be outperformed by other settings at higher distances.

From the above discussion it can be concluded that tag read times depend on a large number of factors. Accurately estimating tag read times for RFID systems thus, is non-trivial.

3.2 Biosignal Data Detection by Turning RFID Tags On and Off

As discussed in Section 2.3.1.1, passive RFID tags have already started finding applications in bioelectric signal sensing. However, so far, the RFID technology has merely replaced conventional data transmission methods like bluetooth. The sensed

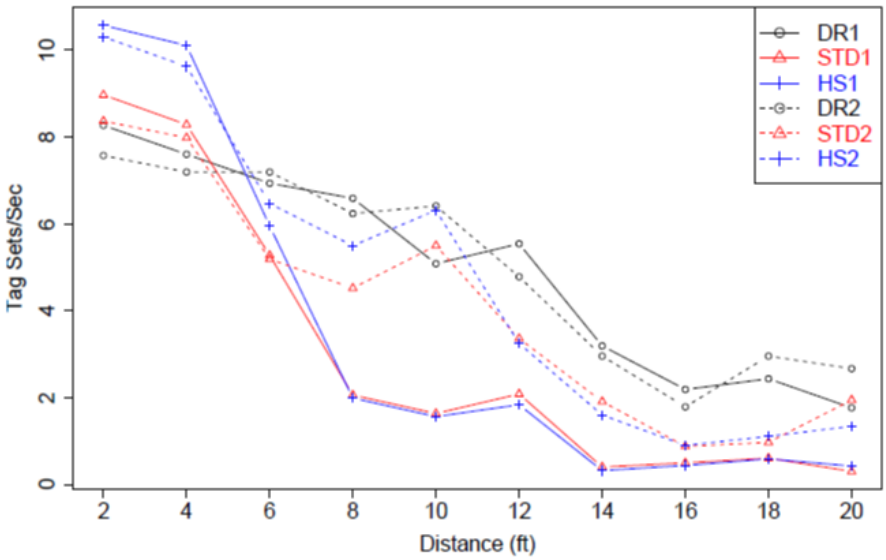

Figure 3.7: Variation in tag read times with increasing distance from the reader for different reader modes [27]

data is still digitized using analog-to-digital converters and stored on flash memories before transmission. In this section, a novel way to transmit biosignal data by simply turning RFID tags on and off is proposed.

3.2.1 Principle of operation

On-off keying (OOK) [81] can be considered to be the simplest form of amplitude shift keying modulation. Here, the presence or absence of a carrier wave represents a bit of data. An example of OOK modulation scheme is presented in Fig. 3.8 [69]. In the figure, the bit '1' is represented by the presence of the carrier RF wave while '0' is represented by the absence of any RF signal. The duration of each bit is fixed so as to resolve the occurrence of repeated 1's and 0's.

Now, the same concept of OOK can also be applied to an RFID datastream. The RFID tag can be turned on and off to transmit binary data. In doing so, one can

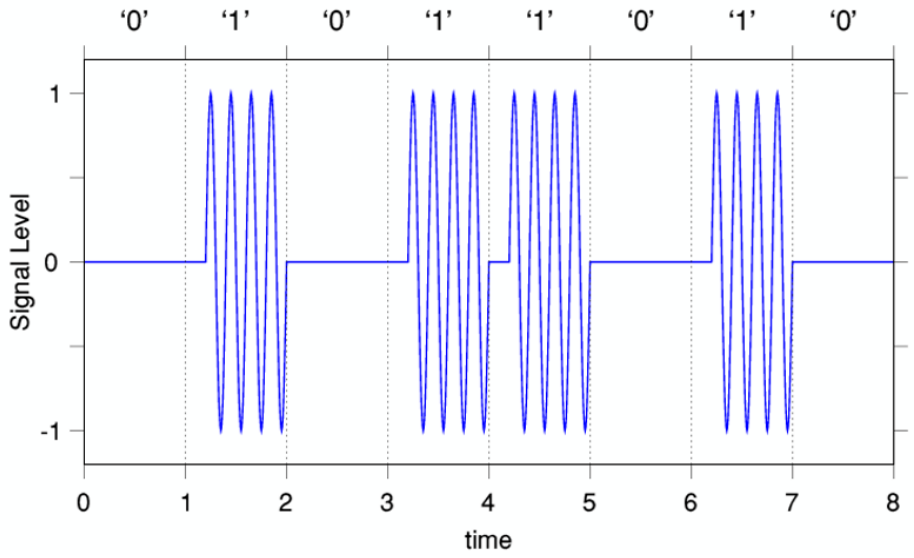

Figure 3.8: On-Off Keying Modulation [69]

turn the RFID tag off for a fixed duration every time a biosignal feature is detected, thereby creating an RFID tag data outage at the reader. Hence, the presence or absence of a biosignal feature is transmitted simply by monitoring an outage at the RFID reader.

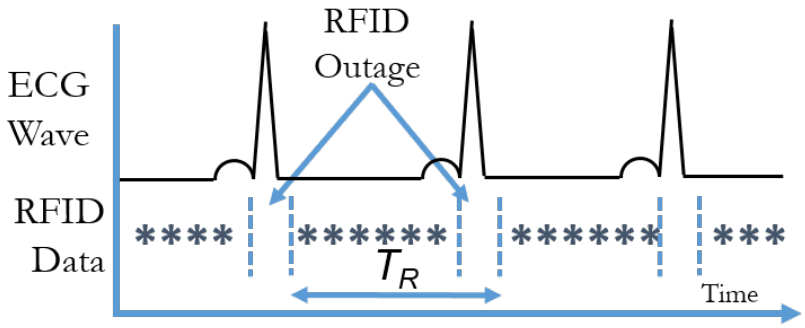

Figure 3.9: Biosignal monitoring by turning an RFID tag on and off

Fig. 3.9, explains the above concept using an ECG signal as an example. The biosignal feature of interest in this case is an ECG 'R' wave. The top part of the figure shows an ECG wave with 'R' waves clearly visible as the dominant spikes. The receipt of an RFID tag ID is denoted by a blue asterisks in the bottom part of the figure. Here, a single RFID tag is turned off for a brief period every time an ECG 'R' wave is detected. These outages can be easily detected at the RFID reader. In this way, biosignal information can be transmitted without the need to store any data locally and all analysis can be done at the reader. Such a method can significantly reduce the power requirements and circuitry on the local sensor.

It should be noted that 'OOK' in a strict sense is not used for data transmission in the discussion above. In fact, one might argue that the above method of monitoring has parallels to pulse width modulation [16] as the time between outages corresponds to a heart rate. The comparison to OOK is simply provided to provide a conceptual basis for transmitting data by turning an RFID tag on and off.

3.2.2 Benefits and Limitations of the RFID On-Off Method

There are several advantages to transmitting biosignal data by turning an RFID tag on and off. Firstly, it doesn't require any local data digitization or storage which not only eliminates the power required to perform digitization but also minimizes the cost and circuitry associated with that function. As no data is stored locally, biosignal monitoring is real-time. Additionally, data transmission is carried out passively using the power harvested off the reader. The savings in power thus achieved, can greatly enhance the range of RFID based biosignal monitors when compared to the systems described in Section 2.3.1.1 without using batteries. The reduction in system complexity can allow for sensor development with minimal circuitry which can be easily and better integrated with wearable platforms. As each monitored person can

be recognized based on the RFID tag placed on them, this system has the capability to monitor several people at the same time using a single RFID reader. In general, this technology has the potential to enable prolonged, comfortable, battery-free and wireless monitoring.

The proposed method, however, does have some limitations. The system can only operate in the presence of an RFID reader which may constitute an initial capital investment in large facilities. Additionally, the method only provides a way to transmit specific biosignal features and not the entire biosignal. However, transmitting features alone could be enough for many monitoring applications like heart rate, respiration rate, muscle response etc. Detecting these features with simple low power electronic circuits may also be a considerable challenge. Because the system relies on time between RFID outages, the variation in tag read times as discussed in Section 3.1.3 introduces a systemic source or error in the system.

The following sections and chapters discuss the steps that can be taken to mitigate the limitations and challenges of the proposed method so as to realize the full potential of its benefits.

3.3 RFID Datastream

In typical RFID applications which consist of inventory control and item identification, a tag is read only once. Biosensing applications, on the other hand, demand continuous reading of the same tag over and over again. However, extensive data for multiple reads of the same tag over hundreds of cycles is not available. In this section, data for time between RFID tag reads is empirically studied to understand the practicality of the RFID on/off method for biosignal monitoring and gain some intuition in determining RFID outage durations.

3.3.1 Tag Read and Tag Outage Durations

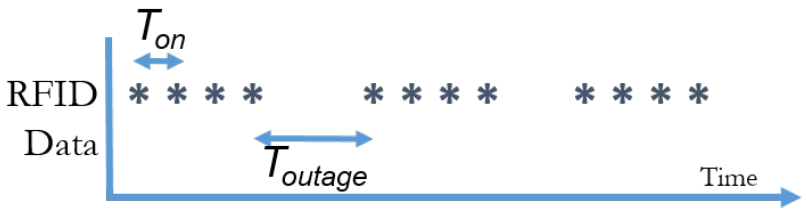

Figure 3.10: RFID time between tag reads: Continuous response and outage response durations

When biosignal monitoring is done by turning an RFID tag on and off, the resolution of the measurement is entirely dependent on the time between tag reads. Fig. 3.10 shows two important parameters, 'T_{on}' or the time between tag reads and 'T_{outage}' or the duration of an RFID outage that indicates the detection of a biosignal feature. Let us first talk about the outage time. The outage duration should be much smaller than the time between biosignal features or else the feature might be missed entirely. The lower limit on the outage duration, however, is imposed by the time between tag reads. The outage duration needs to be larger than the typical time between tag reads other wise it would be impossible to distinguish an outage in the regular RFID datastream. Hence, the duration between tag reads and the variation in them need to be small so that smaller outage durations are possible.

Section 3.1.3 discussed the causes of variations in tag read times. A detailed study of variation in tag read time is presented in [27] where the impact of various factors like protocol settings, varying tag populations, distance, environment etc. are elaborated. It should be noted that varying time between tag reads would cause for the biosignal data to be transmitted at irregular intervals which could cause information to be

delayed or even missed. An understanding of the time between tag reads and its distribution is important to implement a biosignal monitor that employs the RFID on/off method. Hence, an empirical study of distribution of time between tag reads is conducted.

3.3.2 Experimental Setup

The experimental setup for collecting tag read time data is shown in Fig. 3.11. This data collection was conducted in an office furnished with standard items like computers, desks, chairs etc. An RFID reader and an RFID tag were placed at varying distances from each other between 1 and 3 meters. To simulate the effect of additional tags in the environment, two more tags were added, one after the other, at the same aforementioned distances from the reader antenna. In the presence of additional tags, time between tag read data was calculated for the same tag and not for the additional ones. Data was collected at each setting for a period of three minutes. The timestamp for each tag read was recorded and the difference between successive timestamps was calculated to determine the time between tag reads.

The devices and equipment needed for this data collection were RFID tags, an RFID reader, an RFID antenna and a personal computer for data logging. All the above readings were collected using Impinj Monza X Dura tags [55]. A Monza X-2k evaluation kit (shown in Fig. 3.11c as the larger black rigid PCB) was used for data collection. The dummy tag consisted of additional Monza tags on flexible substrates (also shown in Fig. 3.11c). The RFID reader used was an Impinj R420 Speedway Reader [56]. The antenna used was an RFMAX S9028PCLJ [104]. The code for controlling the RFID reader was obtained from [87]. The reader setting was 'MaxMiller'[54] mode with 'M4' encoding.

A faster read setup was also tested using only the flexible Monza tag at 1 meter

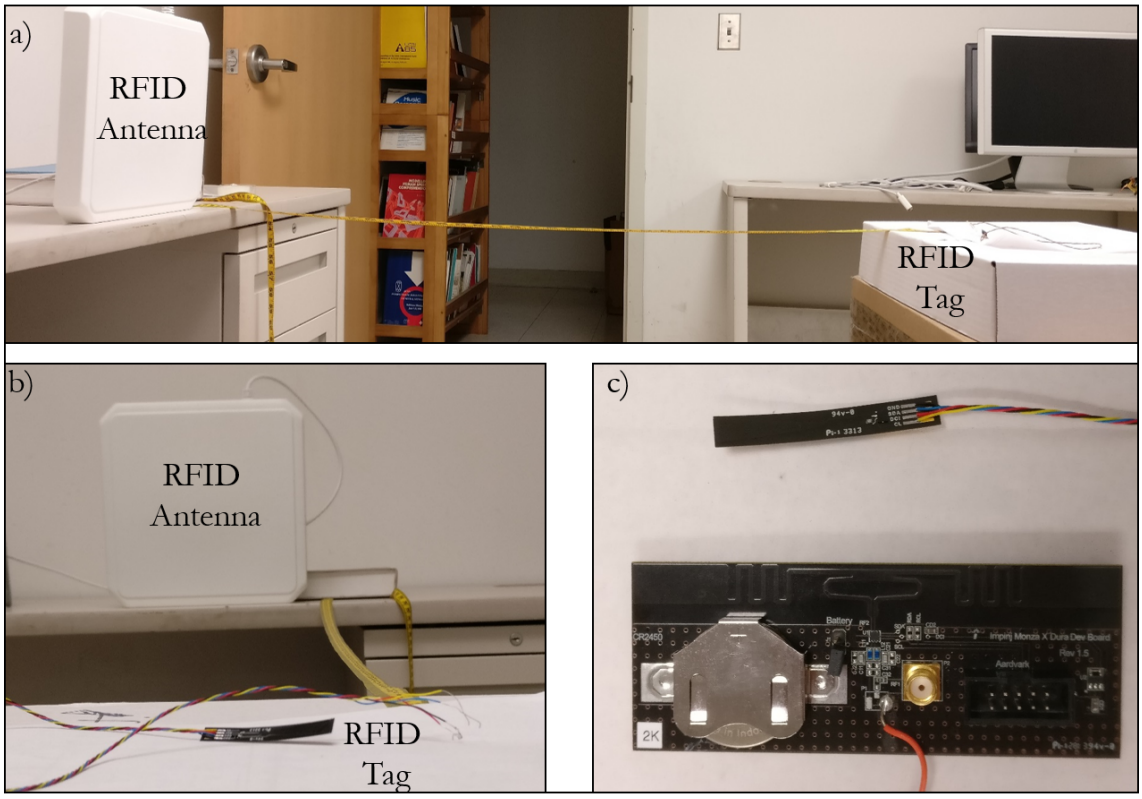

Figure 3.11: Setup for acquiring RFID time between reads data: a) RFID reader antenna with RFID tag (lateral view), b) RFID reader antenna with RFID tag (tag in foreground), c) RFID tags used

distance from the antenna. The reader setting in this case was 'Dense Reader Dual Target' [54].

3.3.3 Continuous RFID Datastream

Fig. 3.12 shows the distribution of time between tag reads when a single tag was placed at a distance of 1 m from the RFID antenna for a period of about three minutes. The time between tag reads is very regular and for the most part, tag reads happen in between 27 and 30 ms. The variation is expected due to the factors discussed in Section 3.1.3. There is an additional group of tag read times around 34 ms and this

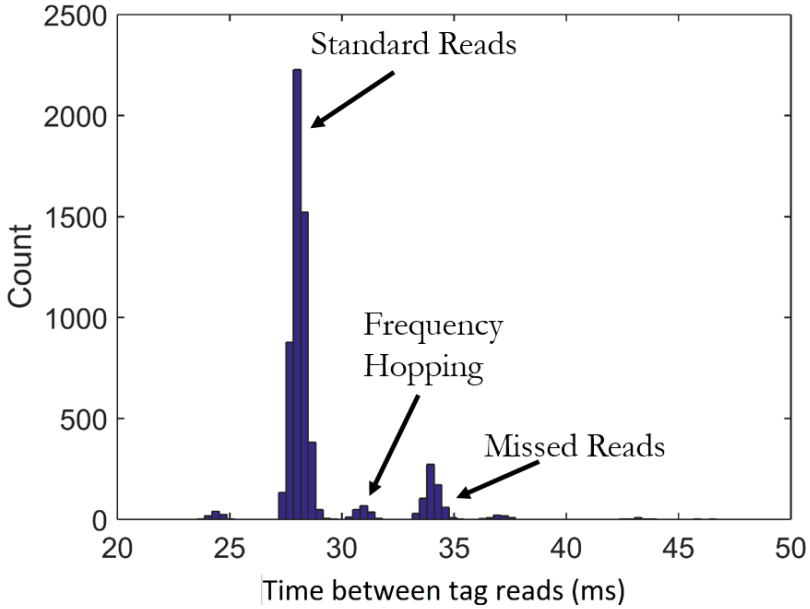

Figure 3.12: Distribution of time between tag reads (MaxMiller Mode) with one tag at $1m$ from the antenna

delay can be attributed to tags that were missed on the first attempt. The smaller groups following these two relatively larger groups of tag read times happen mostly due to the delay caused by periodic frequency hopping. Almost all tag reads happen in under 40 ms. Fig. 3.13 shows the composite distribution of tag read times from all setups mentioned in the previous section. It can be observed that the distribution looks very similar to the one plotted for the single tag at 1 m case. This result shows that the time between tag reads can be expected to be consistent for the distances tested and in the presence of multiple tags.

It should be noted that there were some tag read times over 50 ms in Fig. 3.13 which are not shown in the graph. Their count was very small in relation to the ones in between 20 and 50 ms and were not visible on the linear scale plotted here. Hence, the same data was plotted using a log scale and is shown in Fig. 3.14. In a data set of over 60,000 tag reads, fewer than 100 tag reads took between 50 and 90 ms

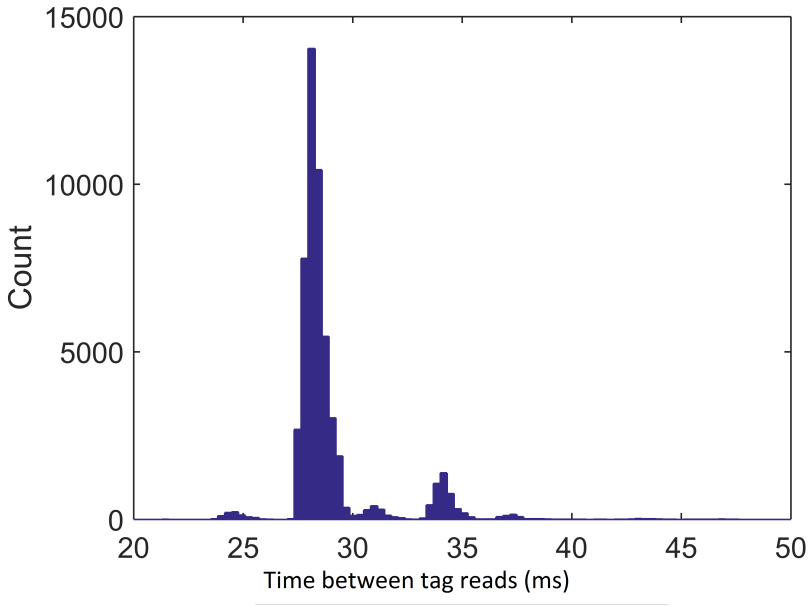

Figure 3.13: Distribution of time between tag reads (MaxMiller Mode):Combined data for all combinations of tag placements

(approximately 0.17%). These delayed reads mainly happened at greater distances from the reader and in the presence of multiple tags; both factors can cause missed tag reads. Even though the delayed reads are few in number, there could be situations where the delays are increased. Hence, the choice of an outage duration should take into account these delayed reads.

Fig. 3.15 shows the read time distribution for a single tag at 1 m distance from the antenna with the reader in the 'Dense Reader' mode. The change in the protocol setting has changed the distribution as well. The time between tag reads is nearly three times lesser than the previous setting chosen or about 10 ± 4 ms. Hence, this setting can be used when faster biosignal measurements with greater resolution are desired.

It can be summarized from the plots that we have seen so far that time between tag reads can be in the vicinity of 6 ms to about 40 ms depending on the RFID

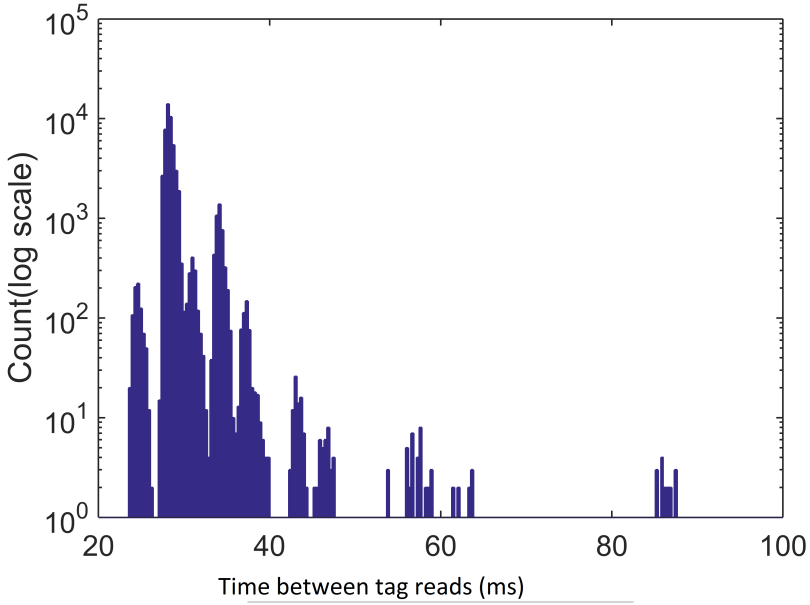

Figure 3.14: Distribution of time between tag reads (MaxMiller Mode):Combined data for all combinations of tag placements (log scale)

reader setting. The tag read time can increase due to various issues that cause tag read misses but the aforementioned numbers are typical. The RFID outage duration should be significantly greater than the typical tag read time. An outage duration of about 100 ms thus might be sufficient.

The data collected above can be used to gain an understanding of the viability of the RFID on/off method for biosignal monitoring. However, the time between tag reads can vary due to many factors that include the reader mode and simulating the effects of all these factors is beyond the scope of this dissertation. The dense reader mode supports a very high tag read rate and is designed to operate in a multiple tag environments. Hence, this reader mode is suited for biosensing applications where a tag needs to be read continuously. The data collected using this mode is thus used in the simulations conducted in the next section.

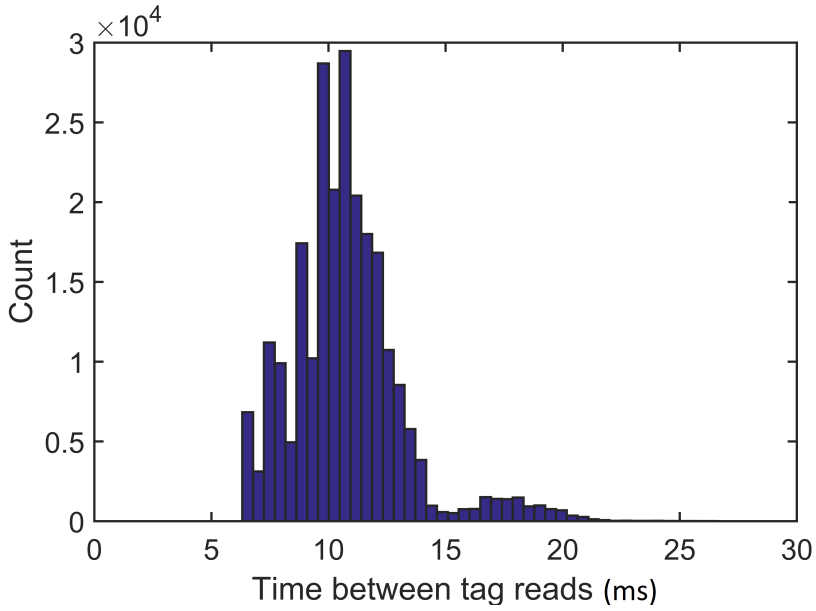

Figure 3.15: Distribution of time between tag reads (Dense Reader Mode) for a single tag at 1 m

3.4 Biosignal Detection with UHF RFID

The previous section showed that the typical time between RFID tag reads is of the order of tens of milliseconds which is much smaller than the time between biosignal features like heart beats which start at several hundreds of milliseconds. Hence, the time between tag reads is sufficiently small for monitoring typical low frequency biosignal features. However, the success of the RFID on/off method depends on translating the electrical biosignal into a reliable RFID datastream. Hence the system requires integration of multiple steps which include biosignal detection and RFID outage generation on the sensor side and outage detection and processing for biosignal feature extraction on the reader side. In this section, simulations are conducted to gain insights into practically integrating these steps for detecting heart beats and uterine contractions. The simulations are based on empirical datasets and are meant

to motivate hardware design and data processing for monitoring heart rate and uterine contractions. For the purposes of this exercise, empirical ECG and EHG data was obtained from publicly available databases on PhysioNet [45].

3.4.1 Heart Beat Detection

A brief example of heart beat detection with the RFID on/off system was presented in Section 3.2. In this section, two empirical datasets were used to simulate an RFID datastream complete with outages corresponding to heart beats from ECG data.

The first dataset was the RFID time between tag read data that was empirically collected as described in Section 3.3. The dataset used here was the one collected with Dense Reader mode and the set included nearly 250,000 individual tag read times. The second set was a publicly available ECG database [76] which contained 310 individual ECG records. The sampling rate at which the ECG data was collected was 2 ms per sample which is much faster than the typical time between RFID tag reads. The first ten records from the ECG dataset were used in this simulation.

3.4.1.1 Simulation Algorithm

The Fig. 3.16 describes the algorithm used to complete the simulation. The ECG dataset contains regularly spaced timestamps as per the sampling rate of the ADC used and the associated value of the ECG signal at that time. The simulation converts this regularly time spaced ECG signal to a varying time RFID stream that has an outage every time a heart beat is detected. The output of the simulation is a series of timestamps that indicate the time of successive tag reads. To achieve this result, the variable that stores the RFID timestamp is first initialized to zero and then the first timestamp from the ECG dataset is compared to it. The timestamp from the ECG dataset would naturally be greater than zero and the simulation progresses to the

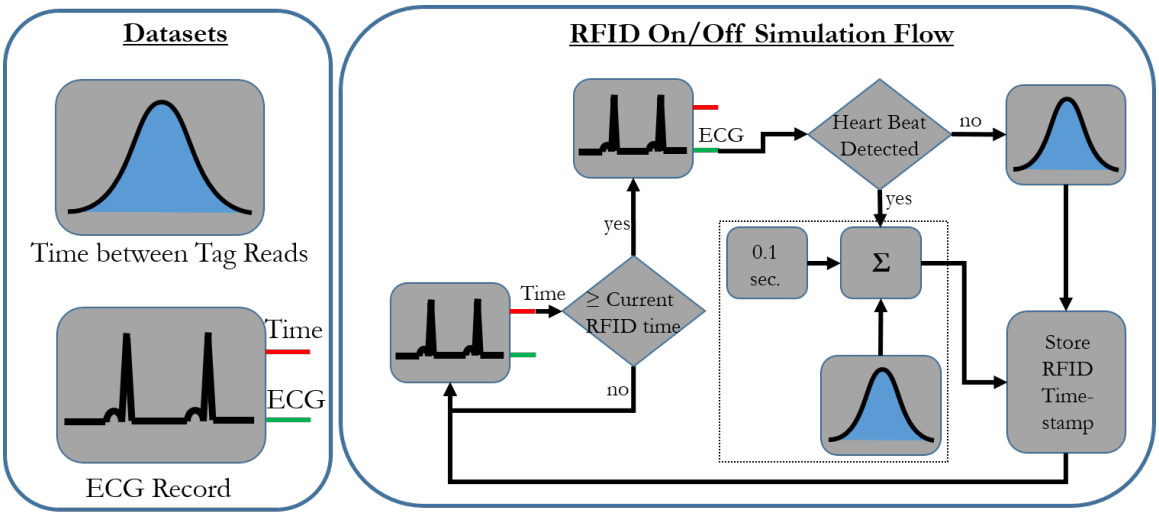

Figure 3.16: Flowchart of simulation to generate an RFID datastream with outages for heart beats

next stage where the associated ECG value for the given time is found and checked to see if that value corresponds to a heart beat. Heart beats are detected by simply setting a threshold such that a detection happens only when an 'R' wave appears in the ECG signal. If there is no 'R' wave detected, the algorithm simply picks a random tag read time from the RFID dataset and increments the RFID timestamp variable by that duration. The ECG timestamp is then incremented till it is greater than or equal to the stored value of the RFID timestamp. Again, an associated ECG value is picked and the presence of a heart beat is checked. If a heart beat is detected, then a random tag read time is picked from the RFID dataset and it is incremented by the tag outage duration. The outage duration for this simulation was chosen as 0.1 seconds. This choice of the outage duration was made based on Fig. 3.14 where all tag read times were less than 0.1 seconds. Hence, it is possible to easily distinguish an outage from a regular tag read. Additionally, the time between heart beats is expected to be over 0.3 seconds so there is no risk of a 0.1 second outage covering

more than one heart beat. After recording the RFID timestamp after the outage, the process is continued through to the end of each ECG record and repeated for ten records.

The MATLAB code for the simulations can be found in Appendix A.

3.4.1.2 Simulation Results

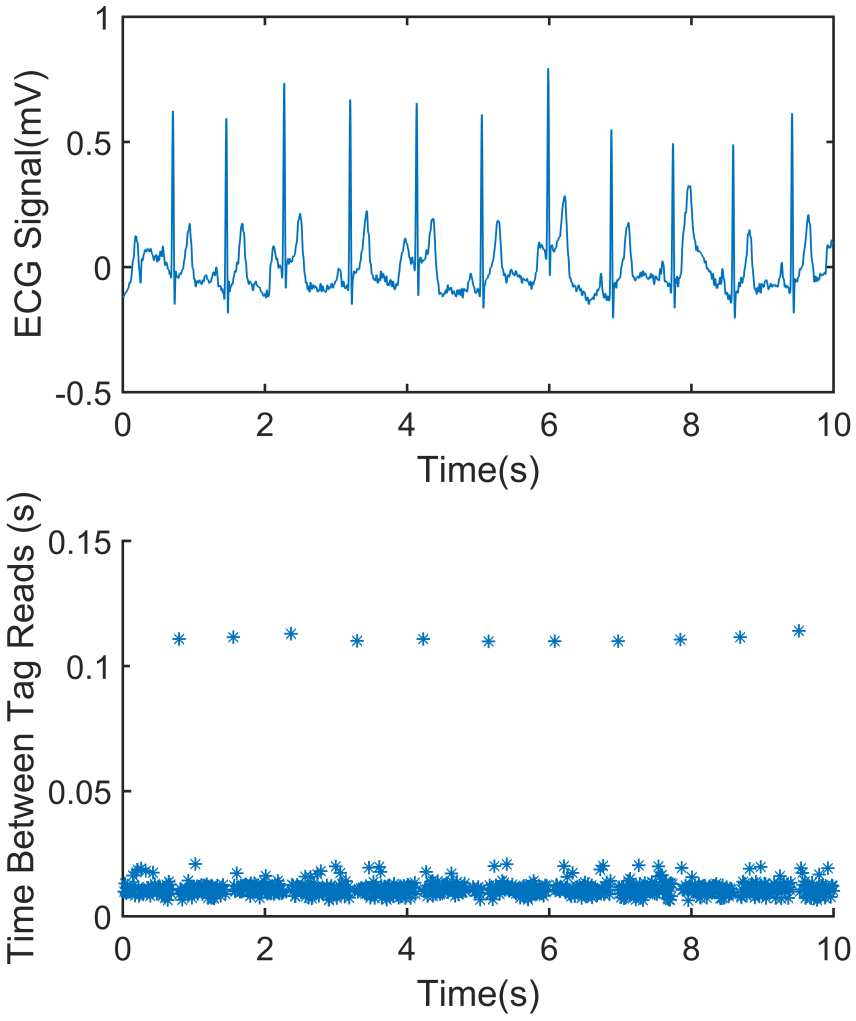

Figure 3.17: Comparison of RFID data outages with ECG data

Fig. 3.17 shows the first ten seconds of one of the ECG records on the top. The bottom plot shows the RFID data as obtained from the simulation algorithm discussed above. The y-axis in that plot represents the time between each successive RFID tag read received by the reader. This time is very small as long as an outage is not created due to the detection of a heart beat. However, jumps in the time between tag reads are clearly visible and these jumps indicate RFID outages. As expected, one can observe that there is an outage associated with every 'R' wave in the original ECG record. Hence, an RFID outage at the reader can be said to correspond to the detection of a heart beat.

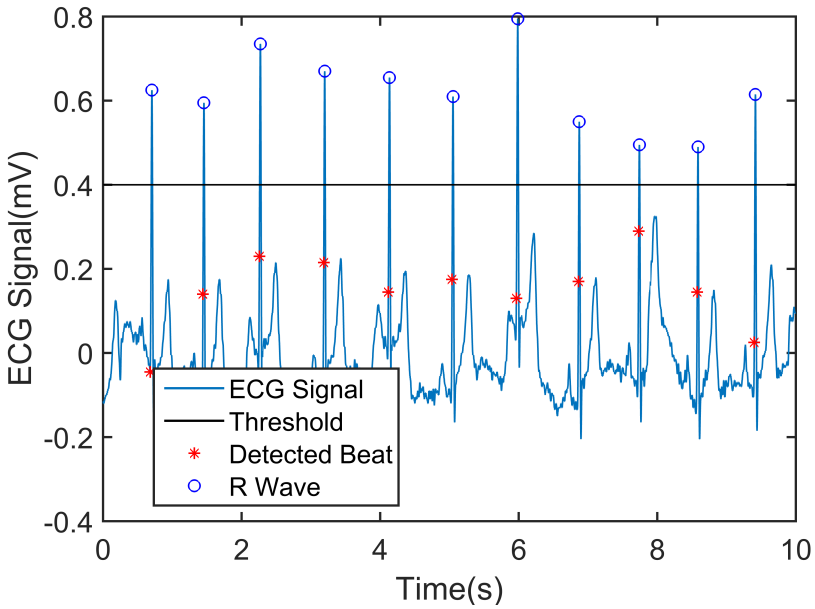

Figure 3.18: Heart Beats as detected by RFID

Fig. 3.18 compares the heart beats as detected from the RFID data (red stars) with the actual positions of 'R' waves (blue circles). The threshold selected to detect 'R' waves is also shown on the graph. It can be seen that the detected beats do not

coincide exactly with the threshold position. The tag is turned off for 0.1 s as soon as the threshold is reached. However, for the detection algorithm, the outage starts at a point where a tag was last read successfully before being turned off. Thus, a slight variation is introduced in the detected time between beats. This variation is entirely dependent on the time between tag reads and therefore smaller tag read times are desirable. However, the effect of this variation on heart rate calculations should be understood.

$$HeartRate = \frac{60}{T_{R-R}} \tag{3.1}$$

Heart rate is calculated by finding the time between successive 'R' waves. For the RFID datastream, a heart rate calculation thus depends on the time between successive outages. Equation 3.1 gives the heart rate in beats per minute (BPM) where '$T_{R\text{-}R}$' is the time between successive RFID outages in seconds.

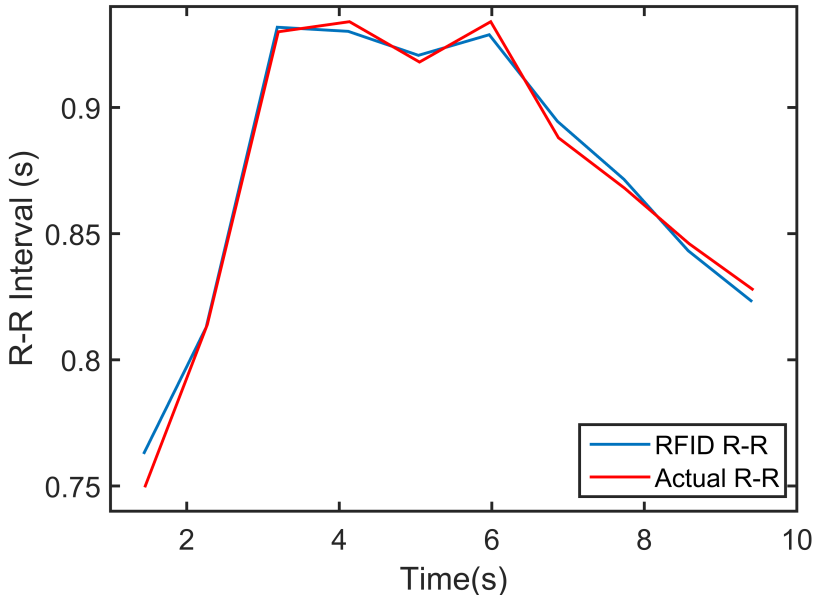

Figure 3.19: Error in detection of R-R intervals due to RFID

The RFID detected beat-to-beat interval (also called 'R-R' interval) is compared to the actual interval in Fig. 3.19. It can be seen that the RFID determined beat interval is very close to the actual one. The reason for the small difference can be understood by looking at Fig. 3.20 where the distribution of error in beat intervals from all simulated ECG records is shown. The error in RFID beat interval is less than 10 ms for most data. This error is considerably smaller than typical beat intervals which run into several hundreds of milliseconds. Thus, the error produced by the RFID tag read time can be considered negligible for the selected setting. However, if the time between tag reads were to increase, the error could also increase marginally.

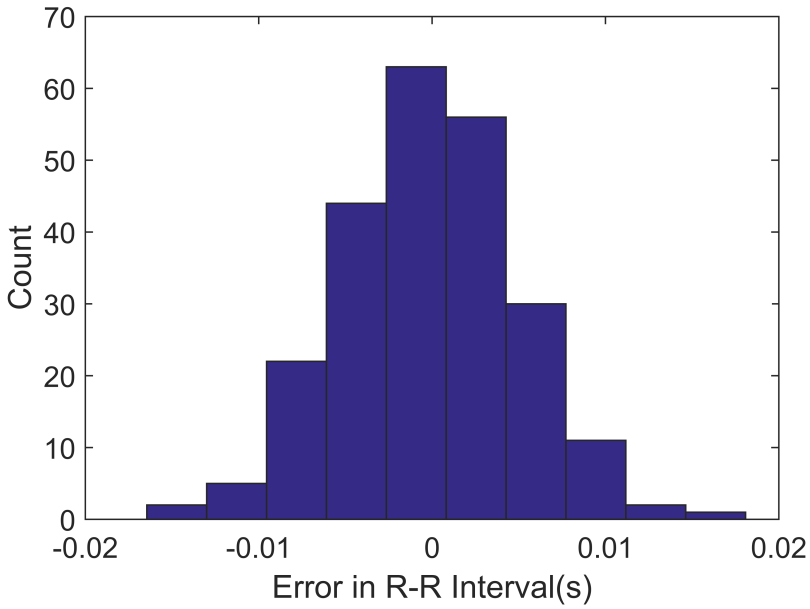

Figure 3.20: Distribution of error in R-R interval determination due to RFID

It can be concluded that the RFID on/off method is viable for continuous heart rate monitoring. The outage duration of 100 ms is easily discernible from regular tag reads. In addition, the typical variation in tag read times does not create a significant

error in the calculated heart rate.

3.4.2 Uterine Contractions

Another example of signals that can potentially be monitored with the RFID on/off system are uterine contractions for pregnant women. For simulating an RFID datastream with uterine contractions, the source biosignal database used was an online EHG database [7]. This database contains 122 EHG records obtained from women at various stages of pregnancy. Each record is about sixty minutes in duration. Not all records had contractions, so five records that had multiple observable contractions were used for this simulation.

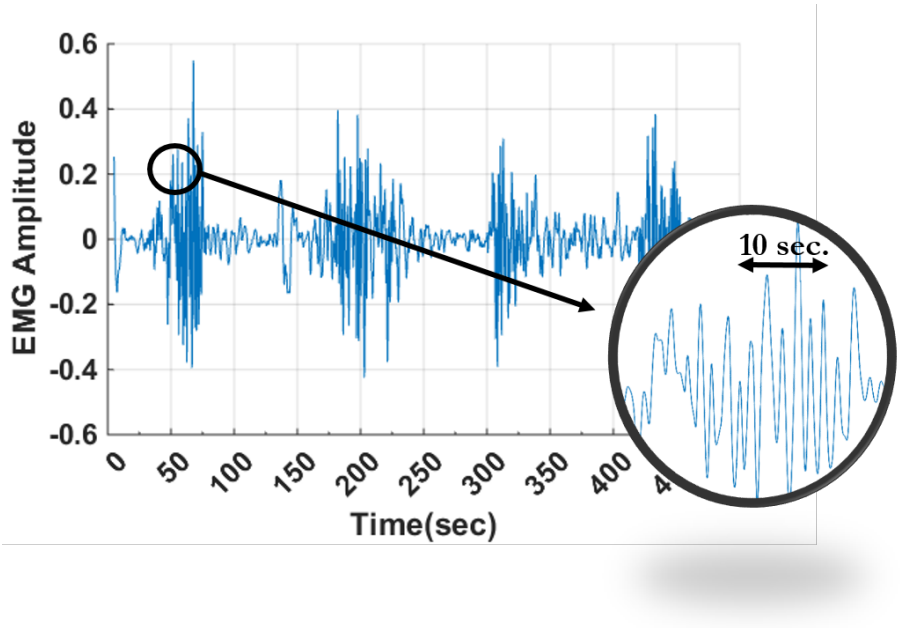

Figure 3.21: Uterine EMG during labor with contractions highlighted in the inset

Fig. 3.21 shows the EHG signal for a woman in labor. Contractions are clearly

visible as groups of spikes. It should be noted that an EHG signal is a very low frequency signal and each individual spike can stretch several seconds. Thus, a threshold based approach of creating outages might trigger multiple outages that are several seconds long. Long outages may be undesirable as they could be indistinguishable from tag reads due to poor signal quality. Thus, outages in this case are triggered by detecting a rising edge which ensures a single outage per contraction spike. The EHG signal is not flat in the absence of contractions and hence, false detection of non-contraction rising edges needs to be prevented. It can be seen that the signal amplitude is relatively low between contractions. The problem of false triggering can thus be avoided by adding hysteresis around the baseline which establishes a non-zero threshold for detection of rising edges. Thus, RFID outages are only created for the large amplitude contraction edges.

3.4.2.1 Simulation Algorithm

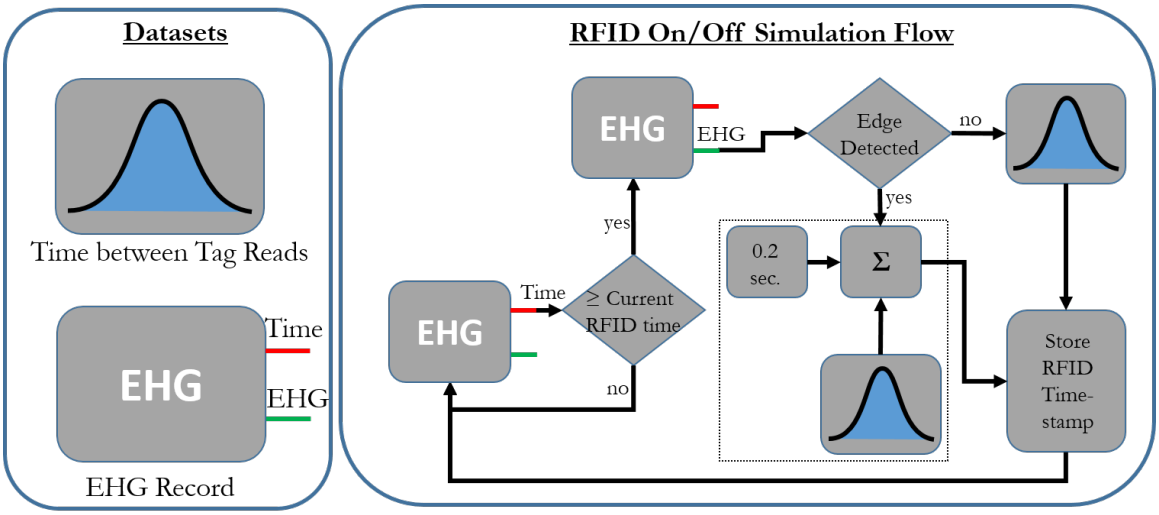

Figure 3.22: Flowchart of simulation to detect uterine contractions by turning an RFID tag on/off

The simulation steps for uterine contraction are shown in Fig. 3.22. The steps are very similar to the ECG simulation except for the change in database and detection mechanism (edge instead of threshold). Additionally, hysteresis has been added so that there is some buffer around zero-crossing points to avoid outage triggering from smaller non-contraction signals. The outage duration is also increased to provide an additional buffer for slower tag read times. This increase is possible because of the low frequency of the EHG signal.

MATLAB code for the simulations can be found in Appendix A.

3.4.2.2 Simulation Results

An EHG signal with several contractions can be seen in Fig. 3.23. The detected contraction spikes are shown in red stars. The locations of uterine contractions can be easily recognized from the outages in the RFID data stream in the bottom graph. The uterine EMG signal has a lot of activity during contractions which cause multiple outages. There are relatively few outages in the absence of contractions. The outages can be grouped to calculate the duration and frequency of contractions.

Further analysis of EHG signals will be briefly discussed in Chapter 5. The rest of this work will focus on heart rate monitoring from ECG signals.

3.5 Conclusions

The details of the C1G2 protocol in relation to varying time between RFID tag reads were discussed. A novel method for biosignal monitoring by turning an RFID tag on/off was introduced. The time distribution of an RFID datastream was empirically studied for use in simulations to ascertain the method viability. Simulations for heart beat and uterine contraction detection using the RFID on/off method were also completed which proved the possibility of using this method for biosignal monitoring.

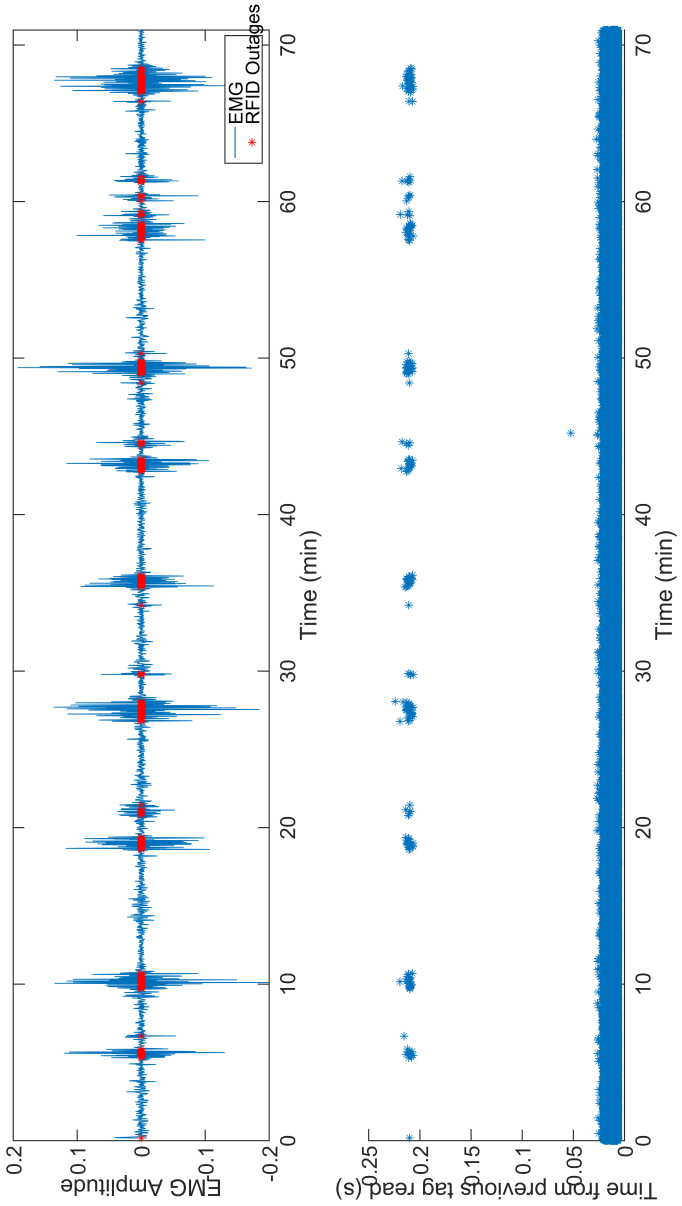

Figure 3.23: Comparison of RFID data outages with EHG data

4. Hardware Implementation for RFID based Heart Rate Monitoring System

Through simulations, Chapter 3 proved that RFID tags can be used to transmit intervals between heart beats by turning the RFID tag on and off. In this chapter, a hardware implementation of this RFID technology is discussed to achieve heart rate monitoring. The broad focus of this chapter is on low power circuit implementations with minimal foot print, component selection and system integration.

4.1 System Design Considerations

The main requirements of the heart rate monitoring system are that it be wireless and battery-free. The use of RFID technology eliminates the power required for data transmission but power is still needed for signal sensing and amplification. For the proposed RFID heart rate monitor to be battery-free, the system would have to rely on harvested power for operation. Thus, the system needs to have very low power consumption. The range of the system is dependent on the RFID tags used and the wireless power required to operate the sensing circuitry. Hence, the power required by the additional circuitry should be roughly the same magnitude as that consumed by the RFID tags so as to not limit the system range. The power requirement of the system can be minimized by choosing optimal circuit topologies and low power components. Efforts should also be made to reduce the footprint of the overall design to ensure easy integration with wearable platforms. Additionally, the circuit should provide continuous operation with minimal latency to provide real-time monitoring.

Low power operation and small footprint, therefore, will be the prime motivating metrics for a successful design.

4.2 System Block Diagram

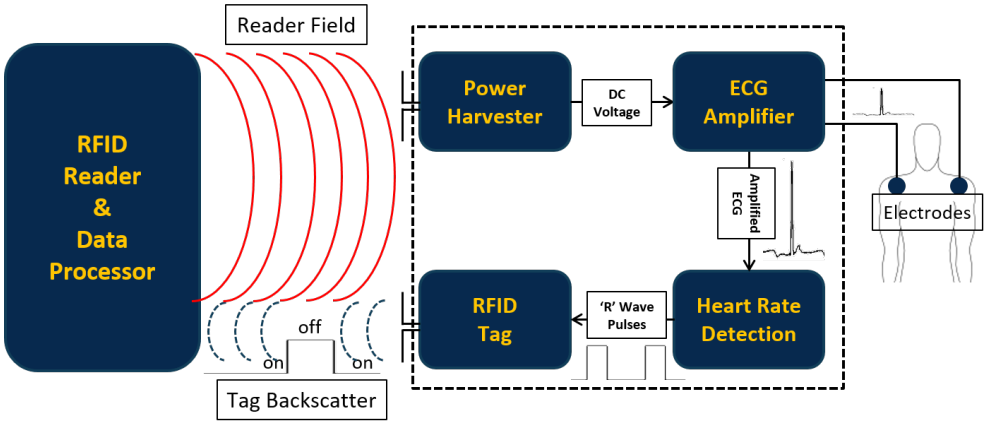

Figure 4.1: Block diagram of passive RFID based heart rate monitor

A detailed block diagram of our RFID based heart rate monitoring system taking into account the wireless and battery-free requirements discussed in Section 4.1 is shown in Fig. 4.1. The main components of the system are the RFID reader, ECG amplifier, power harvester, heart rate detection circuit and the RFID tag. All components, except the RFID reader, are to be placed on the person being monitored and these components are shown in the dotted block in Fig. 4.1. The RFID reader and data processor are remote or off the body. The complete process is described below.

4.2.1 RFID Reader and Data Processing

The RFID reader and the data processing unit constitute the first and the last part of the RFID based heart rate monitoring system. The RFID reader emits continuous RF signals in order to continuously interrogate the RFID tag for heart rate data. These RF signals also serve an additional use of providing power for ECG amplifi-

cation and heart rate detection, as discussed in the next section. Hence, the reader serves the dual purpose of acquiring heart rate data and also powering the sensing circuit. The RFID reader is connected to a processor that calculates the heart rate based on the data received from the reader.

4.2.2 Power Harvesting

A constant DC voltage is required to operate the ECG amplifier and the heart rate detector circuit. A wireless power harvester is used to provide this DC signal. The power harvester circuit uses its antenna to capture the continuous waves emitted from the RFID reader. These RF waves are rectified and regulated to create a constant voltage source for other circuitry.

4.2.3 ECG Amplification

The ECG signal can be acquired by placing a pair of electrodes across the cardiac axis on the human body. The amplitude of this ECG signal, however, is very small (about 1mV). Hence, an amplifier is needed to magnify the small ECG signal to a level that can be detected by the heart beat detection circuitry. Additionally, due to the presence of other bioelectric signals (Section 2.1.1) and noise, the ECG amplifier also needs a bandpass filter. The filtered and amplified ECG signal is fed to the heart beat detection circuit.

4.2.4 Heart Beat Detection

The role of the heart beat detection circuit is to identify the ECG 'R' waves and then generate a pulse of a specified duration to turn the RFID tag 'off' momentarily. In other words, this circuit creates a series of square pulses that are used to turn the RFID tag on and off in accordance with the source ECG signal. This detection

hardware is critical to the work described in this thesis.

4.2.5 RFID Tag

The RFID tag uses its antenna to continuously backscatter its unique EPC code to the reader. The tag is powered directly by the reader and does not require any energy from the wireless power harvester. The continuous transmission between the tag and the reader is interrupted when the heart rate detection circuit transmits a signal to turn the tag off causing the tag to go silent for a short period. These period of silences are seen as outages at the RFID reader and can be correlated to the detection of 'R' waves. The heart rate can be determined by calculating the time between these outages.

The above setup enumerates the minimal constituent blocks required to implement the RFID based heart rate monitor. There is no provision to store data locally and the data is continuously transmitted. All the processing and analysis is done at the RFID reader in real-time. The following section describes the hardware implementation of the blocks described in Fig. 4.1.

4.3 Circuit Design and Component Selection

While integration with a wearable platform is not discussed in detail in this work, the system design takes into account this integration as the eventual goal. Hence, the key to a successful design for this work are minimal power, fewest components and smallest footprint for the system monitor to be placed on the body. The overall design is a mix of choosing optimum commercial components, innovative solutions and repurposing existing technology for novel uses. This section describes the hardware design for proof-of-concept tests on the proposed RFID based heart rate monitor.

4.3.1 ECG Amplifier

Setups for ECG sensing have been investigated since William Einthoven proposed the first clinical arrangement at the turn of the twentieth century [113]. Hence, the circuits for ECG amplification have reached a point where dedicated integrated chips are available for the sole purpose of amplifying and digitizing ECG signals [9]. However, standard ECG circuits may not be ideal for the low power design required for this work. An analysis of the main amplifier requirements is thus required before choosing components and a circuit topology.

4.3.1.1 Design Requirements

Table 4.1: ECG Amplifier Requirements

Parameter	Target
Electrodes	2
Bandwidth	0.5-100 Hz
Gain	1000-2000
Power	< 500 μW
Dynamic Range	0-3 V

The main requirements for the ECG amplifier are listed in Table 4.1. For this work, only the ECG 'R' waves are of interest and a single pair of electrodes will suffice for this measurement. The bandwidth of the ECG signal is between 0.5 Hz and 100 Hz, therefore, the ECG amplifier must be able to provide linear gain in this

region. ECG signals are of the order of a few millivolts, an amplifier gain of between 1000-2000 is required to bring the signal amplitude to a few Volts so that it can be processed by the heart beat detection circuit. The power consumption of this circuit is targeted to be less than 500 μW as this current is comparable to the power required for biosignal amplification and data processing by other RFID based sensor systems [37, 110].

In addition to the above requirements, the designed ECG amplifier should have high input impedance so that most of the input signal is available to the amplifier. As the required gain is very high and the noise appearing at the input of the amplifiers is also amplified, the chosen amplifier should have very low noise. It should also have high common mode rejection ratio (CMRR) to eliminate noise that is common to the electrode pair.

4.3.1.2 Circuit Design

Instrumentation amplifiers are commonly used for amplifying biosignals and are able to achieve many of the requirements stated in Table 4.1[35]. These amplifiers have input buffers which provide very high input impedance in addition to low noise and high CMRR. However, it is important that the instrumentation amplifier have very low power dissipation. The Texas Instrument's (TI) INA321 [60] is a micropower instrumentation amplifier with a quiescent current dissipation of less than 40 μA. Fig. 4.2 shows our ECG amplifier circuit implementation based on the INA321 chip.

The ECG signals are delivered to the amplifier through inputs IN1 and IN2. These input signals are pulled to the mid-rail common mode voltage using resistors R7 and R8. IC2 is the INA321 instrumentation amplifier which provides a gain of about five. Additional gain is thus needed and is provided by an amplifier stage which also doubles as a low pass filter. Another opamp, indicated by IC1B, provides feedback and acts

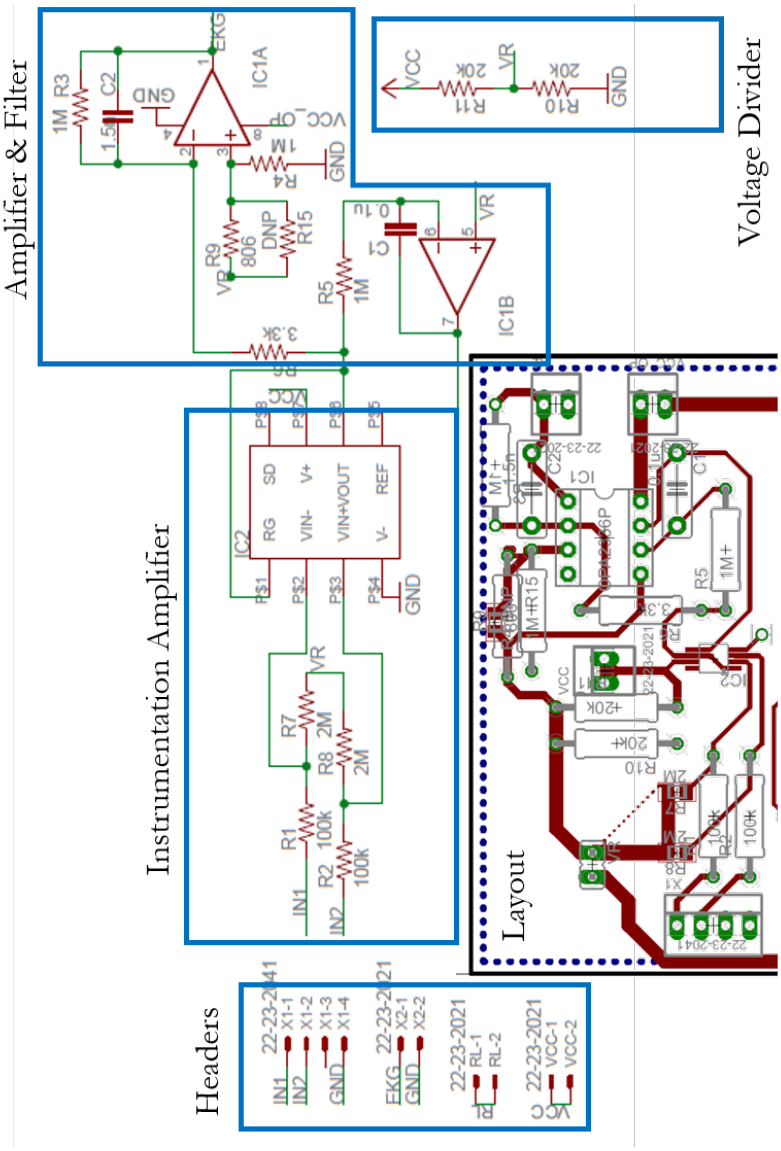

Figure 4.2: ECG Amplifier Schematic with Layout

as a high pass filter to set the lower cut-off frequency of the amplifier. The values for the filter components were chosen after simulating this circuit using a SPICE tool. The frequency response of the simulated circuit is shown in Fig. 4.3. The opamps used were TI's OPA336 [119].The voltage divider formed by resistors R10 and R11 provides mid-rail (half of supply) DC voltage for biasing the instrumentation amplifier

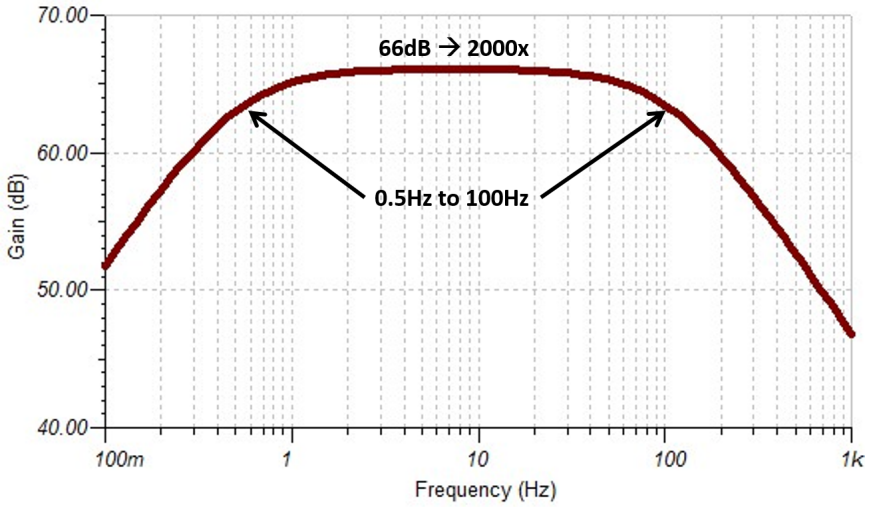

Figure 4.3: ECG Amplifier Frequency Response (simulated)

inputs. The layout of this circuit is also shown in Fig. 4.2.

4.3.1.3 Functional Verification of the ECG Amplifier Circuit

The primary function of the ECG amplifier circuit is to provide a clean and amplified ECG signal from which an 'R wave' can be easily discerned. To verify that the ECG amplifier circuit is operating satisfactorily, the circuit was connected to an ECG wave simulator [51]. The features (amplitude, shape, frequency etc.) of the simulator output are identical to actual ECG signals obtained from humans. Since the amplitude of the ECG signals is very small, the simulator also has an inbuilt amplifier for comparison with the ECG amplifier being tested. The outputs of the designed ECG amplifier and that of the simulator pre-amplifier are compared in Fig. 4.4. The figure shows that the ECG amplifier faithfully reproduces the input ECG signal. The signal shape and 'R' wave peaks of the amplified ECG wave line up very well with the simulator output.

Figure 4.4: Comparison of the ECG Amplifier output with the ECG simulator preamplified output

4.3.2 Heart Beat Detection

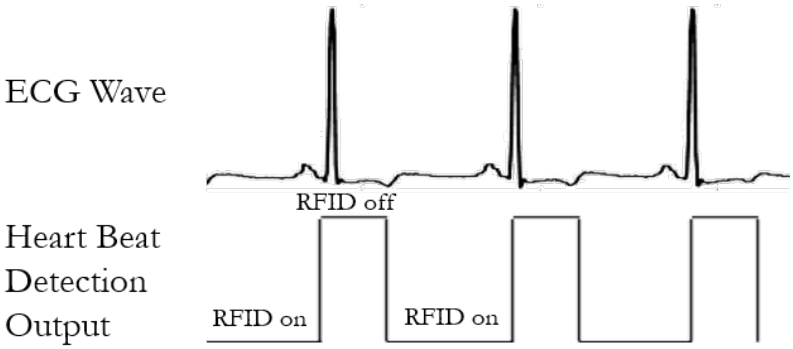

Figure 4.5: Heart beat detection circuit output

The ECG 'R' wave has a very short duration of only a few milliseconds which

may not be enough to produce a recognizable RFID outage or even turn the RFID tag off. Thus a heart beat detection circuit is required to detect ECG 'R' waves and convert this signal to a well defined square wave pulse to turn the RFID tag on and off reliably. The function performed by the heart rate detection circuit is shown in Fig. 4.5. A common way to design an 'R' wave detection circuit is to use a programmable microcontroller, however, this approach has several limitations and a more efficient approach is employed in this work. Both are described below.

4.3.2.1 Microcontroller Based Approach

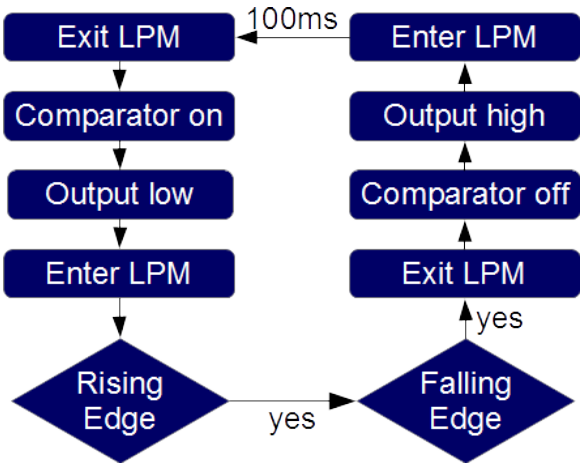

Figure 4.6: Microcontroller based heart rate detection algorithm

A low power microcontroller like TI's MSP430 [59] series of microcontrollers can be used for heart beat detection. The microcontroller has inbuilt comparators, ADCs, clocks, flash storage and consumes less than 1 μA of current while in sleep mode. An algorithm that can be followed to detect 'R' waves is shown in Fig. 4.6. When the system is initialized, the designated output pin on the microcontroller is set to

low, the inbuilt comparator is turned on and the microcontroller enters a low power mode to conserve power. The comparator is set to look for a rising edge that exceeds an appropriate threshold. The microcontroller then looks for an immediate falling edge to confirm the detection of an 'R' wave. Once the 'R' wave is detected, the microcontroller momentarily exits its low power mode, turns the comparator off and sets the output to high for 100ms. This outage duration was chosen based on the discussion in Section 3.4.1. After the outage is complete, the microcontroller again enters a low power mode and the comparator starts looking for a rising edge. The entire process can be completed by using less than 100 μA of current.

The above procedure provides a robust method to detect 'R' waves and reliably produce square pulses to turn RFID tags on and off. However, the use of a microcontroller is not only expensive but also requires a larger circuit footprint. More importantly, the power consumption is still very high (approximately 300 μW) and lower power solution is desirable.

4.3.2.2 IC 555 Timer Based Approach

An innovative approach to obtain 'R' wave correlated RFID outage pulses is to use an IC555 timer. When used as a monostable multivibrator [46], IC555 produces a single square wave pulse of a desired duration every time it is triggered with a narrow negative going edge. The process of using a monostable multivibrator to obtain an outcome similar to the one shown in Fig. 4.5 is described below.

4.3.2.3 Circuit Design and Functional Test

A very low power IC555 chip, CSS555[36], which has a current consumption of less than 5 μA, is used for this work. The circuit diagram for the monostable operation is shown in Fig. 4.7. The main design components of the circuit are the resistors R_A and

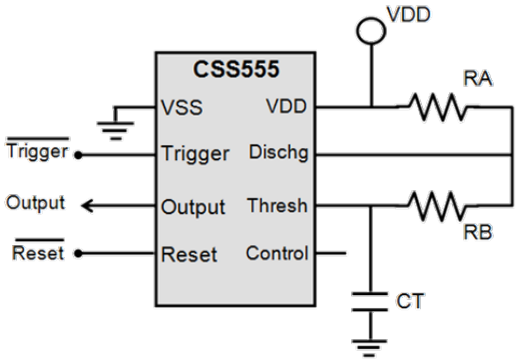

Component	Value
V_{DD}	1.8-3V
RA	9MΩ
RB	10kΩ
CT	10nF

Figure 4.7: Circuit for using IC555 as a monostable multivibrator with component values for heart beat detection

R_B, and the capacitor C_T. R_A and R_B are in the charge path of the capacitor C_T. Due to the internal configuration of the IC, only resistor R_B is in the discharge path of the capacitor. In the absence of a negative edge trigger below 2/3 V_{DD} (supply voltage), the output of the circuit is low. In this state, the capacitor constantly discharges through R_B as the discharge pin is internally connected to ground. However, when a trigger is applied to the circuit, the discharge pin is disconnected from ground, the capacitor starts charging and the output of the circuit is turned high. The capacitor charging continues till the voltage across it reaches an internally set threshold after which the output of the circuit is low again. Thus, the charging cycle through R_A, R_B and C_T decide the duration for which the output of the circuit is held high. The component values were chosen based on the Eq. 4.1 [36]. The recovery time of the circuit depends on how soon the capacitor discharges and thus the resistor R_B needs to be small. It should also be noted that there is a direct path from source to ground via the resistor R_A while the discharge pin is internally grounded. Thus, this resistor needs to be very high to reduce current consumption. The component values shown in Fig. 4.7 were chosen with these considerations in mind. The system was designed for an outage duration of about 100 ms and a recovery time of less than 50 μs. It

should be noted that the circuit needs a negative edge trigger for operation. The negative trigger is achieved by simply reverting the polarity of the ECG signal.

$$OutageDuration(s) = 1.1 \times (R_A + R_B) \times C_T \tag{4.1}$$

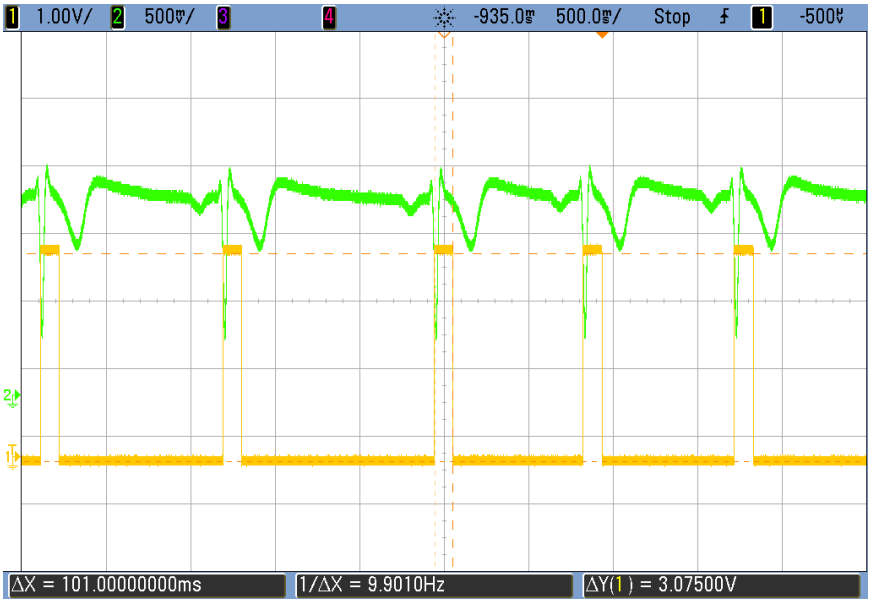

Figure 4.8: Heart beat detection circuit output

Fig. 4.8 shows an oscilloscope capture of the output of the multivibrator circuit when it is triggered using an amplified ECG signal. The ECG signal is inverted as the detection circuit is triggered with negative edges. As can be seen in the capture, the circuit creates square wave pulse for every ECG 'R' wave and the outage duration is approximately 101 ms.

4.3.3 Power Harvester

The ECG amplifier and the heart rate detection circuit both require power for operation. This power is provided using a wireless power harvester.

4.3.3.1 Power Harvester Requirements

Several methods exist for energy harvesting from vibrational and electromagnetic sources [102] for biosignal monitoring. For this work, however, a more stable and constant source of wireless energy is required to implement a reliable battery free solution. As per the method described in Section 3.2, a reader constantly interrogates an RFID tag for biosignal monitoring. Thus, the reader continuously emits RF waves which can be harvested for powering the additional circuitry besides the passive RFID tag. However, there are specific challenges with using the RFID reader as the power source.

The wireless power harvester needs to operate in the same frequency band as the UHF RFID system. Same band operation can be achieved by appropriate antenna design of the power harvester. The bigger challenge, however, is the fact that RF power degrades quickly with distance. The power received by a wireless power harvester can be roughly estimated using the Friis transmission equation which is shown in Eq. 4.2 [14]. Here, the variables P, G, R and λ stand for power, antenna gain, distance and wavelength, respectively while the subscripts 'r' and 't' stand for receiver and transmitter, respectively. In this case, the RFID reader is the transmitter and the power harvester is the receiver. It can be seen that the power received increases with wavelength, however, since the system operates in the UHF band, the wavelengths are very small. Additionally, the received power decreases by a factor of distance squared. Hence, the power received by the harvester reduces very quickly with small increases in distance. The received power can be increased by increasing the trans-

mitter and receiver antenna gain, but there are limitations on this increase also [14]. Hence, the power harvester needs to be very sensitive so that it can operate at very low power levels while being efficient enough to ensure that most of the harvested power is transferred onto the sensor circuits.

$$P_r = P_t G_t G_r (\frac{\lambda}{4\pi R})^2 \tag{4.2}$$

4.3.3.2 Powercast

Commercial chipsets are available for wireless power transfer but many of them are for other frequencies or cannot drive enough power at the RFID UHF frequency of interest [41, 106, 115]. The Powercast P2110B [100] is a wireless power harvester receiver that integrates all the necessary components of a wireless power harvesting in a single daughter PCB board. It operates in the UHF RFID frequency band of 902 MHz to 928 MHz. The minimum power at which the chipset operates is -12 dBm which is equivalent to about 63 μW. The efficiency of the device depends on the reeceived power and the efficiency is above 50% as long as the received power is above -9.5 dBm. The constant DC output voltage is adjustable between 1.8 V to 5.25 V. The P2110B harvester does require some external components which include an antenna and a storage capacitor. The antenna can be designed to optimize for size, directivity and antenna gain while the capacitor can be optimized for start-up time and continuous operation in face of intermittent input power loss. The Powercast evaluation module is shown in Fig. 4.9. Optimization of external components will be discussed in Section 4.5.

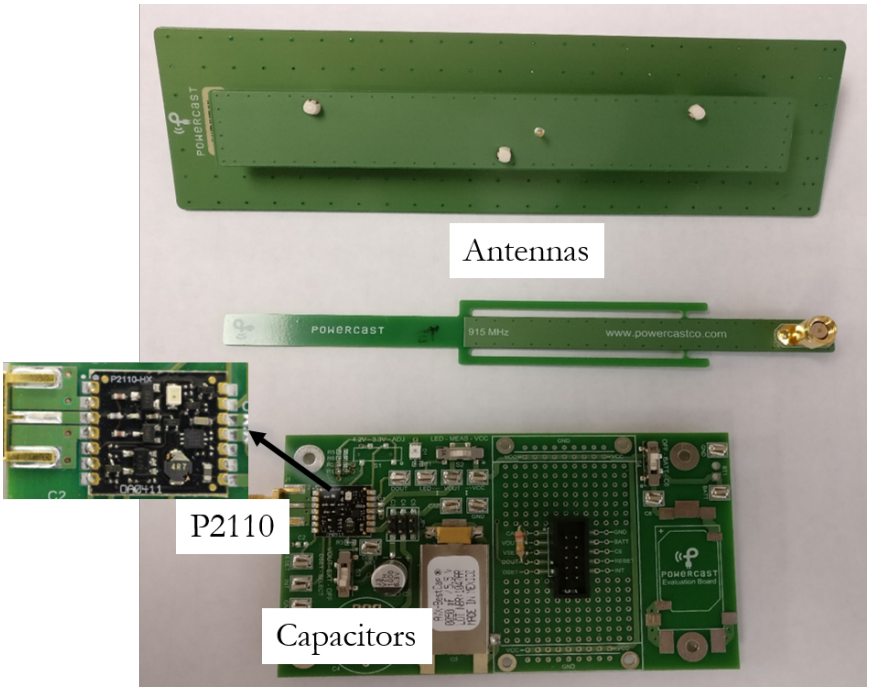

Figure 4.9: Powercast P2110 evaluation kit

4.3.4 RFID Tag

This work employs RFID tags in an unconventional application. RFID tags are not meant to be turned on and off multiple times in a duration of seconds. Hence, it is difficult to find commercial RFID tags that can be turned off with a local analog or digital voltage signal. This section describes how the objective of turning an RFID tag on/off for biosignal monitoring can be achieved by repurposing existing commercial tags.

4.3.4.1 Turning RFID Tag On/Off

An RFID tag consists of an RFID chip which does all the data processing and a tag antenna which captures and transmits RF signals. If the connection between the RFID chip and its antenna are broken, the tag is unable to communicate and can be

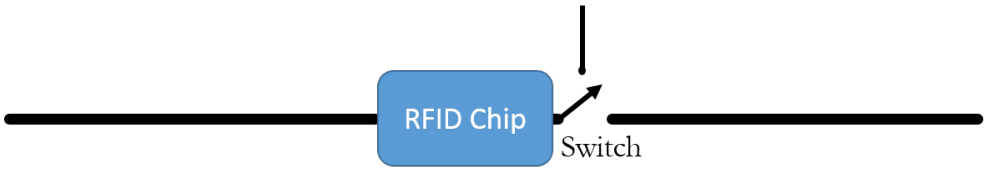

Figure 4.10: Turning an RFID tag on and off with a switch

considered to be turned off. Hence, an RFID on/off mechanism can be implemented by connecting a switch in between the RFID chip and the antenna as illustrated in Fig. 4.10. However, introducing such a switch also introduces losses which directly effect the range of the RFID tag. Additionally, power is required to change the state of the switch which is an additional burden on the power harvester circuit. Hence, an alternate approach that does not have these limitations is required. Ideally, an RFID chip that has features that allow it to be turned on and off with an external signal is desired. One such chip is discussed in the next section.

4.3.4.2 Impinj Monza X2K Dura

Figure 4.11: Impinj Monza X2k Dura pin configuration [55]

The pin configuration of Impinj Monza X2k Dura chipset is shown in Fig. 4.11. This RFID chip can be connected to two antennas to increase sensitivity, and it also has provisions for transmitting user defined data by using serial communication pins. Additionally, the chip has a DC input (DCI). A passive RFID tag does not need any DC input to operate, however, on this particular chip a DC voltage can be applied to enhance the tags sensitivity from -17 dBm to -24 dBm [55]. However, this approach can be reversed to suppress all communication from the tag and effectively turn the tag off. To achieve this on/off ability, an internal register [1] in the tag needs to be reset first. Once the register is set, the RFID tag is turned off every time a DC voltage between 1.8 V and 3 V is applied to the DCI pin. In this way, the RFID tag can be turned off without any additional lossy components or a substantial power draw.

The above method of turning RFID tags on and off was tested by supplying a square wave pulse of about 110 ms duration to the DCI pin of the Monza tag every second and recording the time between tag reads similar to the procedure described in Section 3.2. Fig. 4.12 shows the time between tag reads for the described test. The RFID outages are clearly visible in the plot. The variation in the RFID outage durations can be attributed to a combination of factors described in Section 3.1.2 and the total time taken to turn the Monza tag on, which could be anywhere between 2 ms and 20 ms. The current consumed for turning the RFID tag off was measured and it was found to be only 17.6 μA.

4.3.5 RFID Reader and Data Processing

The primary requirement of the RFID reader is to provide adequate range for reading tags. Additionally, it needs to provide wireless power for auxiliary circuits. The reader is remote and thus has no limitations on size and can be energized using

[1] `DCI_RF _EN` register

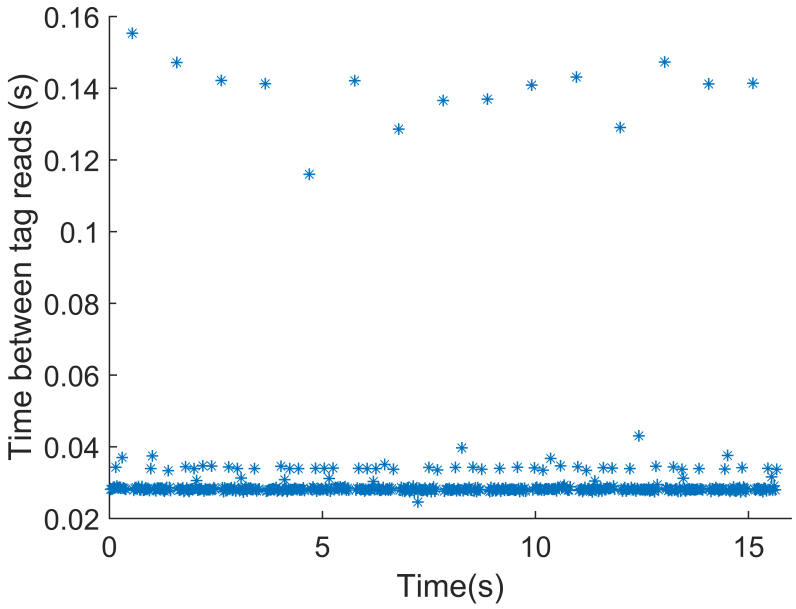

Figure 4.12: Time between tag reads when an RFID tag is turned on and off

plugged-in power. Hence, the requirements of the RFID reader, in many ways, are relaxed compared to those of the other components. The RFID reader needs to transmit maximum allowable power to maximize RFID range. The RFID reader also needs to have the flexibility to allow for different EPC protocol configurations as described in Section 3.1. The focus of this dissertation work is on the components of the sensor circuits described above and the RFID reader is mainly used as a means to collect data. While many other RFID readers could have satisfied these requirements, the readers used for this work were the Impinj Speedway R1000 and R420 [56] as these were readily available. The RFID reader also needs a transmission antenna and the antenna chosen was RFMax S9028PCLJ [104]. All the RFID data was stored and processed on a personal computer connected to the RFID reader.

Individual components and circuits have been identified to complete the system blocks shown in Fig. 4.1. The next step is to integrate them to create a prototype RFID heart rate monitor.

4.4 System Integration and Functional Tests

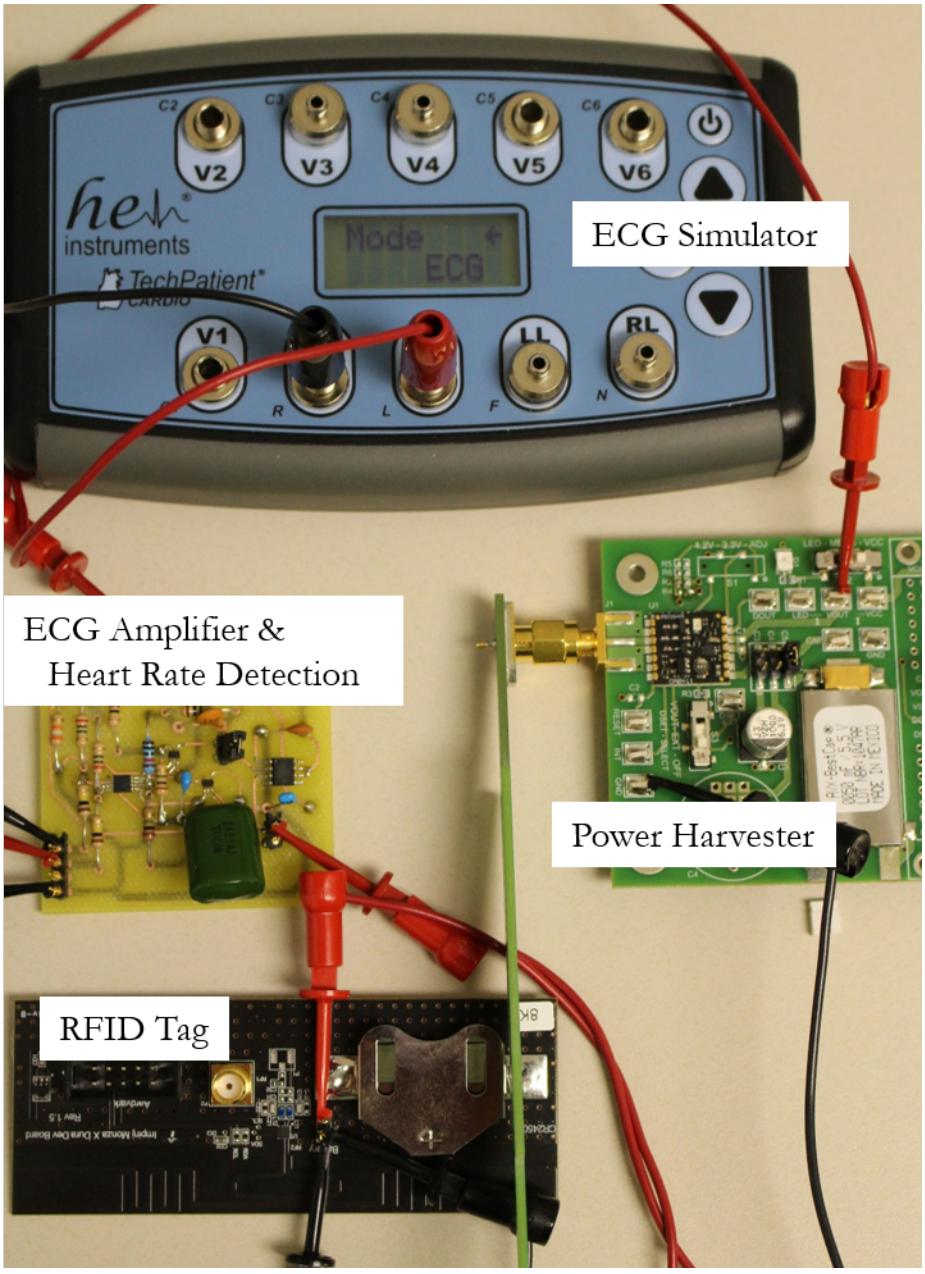

Figure 4.13: Hardware components for testing RFID based heart rate monitor

Fig. 4.13 shows the hardware components described in Section 4.3 and integrated as illustrated in Fig. 4.1. In this section, several functional tests are discussed to do a preliminary validation of the RFID heart rate monitoring hardware.

The ECG signal was generated using HE Instruments TechPatient Cardio ECG simulator [51]. This simulator is capable of generating ECG signals with heart rates from 30BPM through 300BPM and amplitudes between $0.5mV$ and $4mV$. The ECG simulator was used to generate five discrete heart rates between 30BPM and 300BPM. Each set of measurements was taken for a period of three minutes. The RFID reader and the system were kept approximately three feet away from each other. The reader was used to record the times at which a response from the tag was received. These time-stamped data points were then analyzed to determine the heart rate. The range of the system was analyzed by increasing the distance between the RFID reader and the rest of the assembly. For all these tests, the reader setting was 'MaxMiller'[54] mode with 'M4' encoding which was the slower read rate setting discussed in Section 3.3.

4.4.1 Overall Power Consumption

Table 4.2: List of system components with current consumption of each block

Block	Components	Peak Current
ECG Amplifier	INA321(TI), OPA336(TI)	145 μA
Beat Detection	IC 555(CSS)	3 μA
RFID Tag	Monza X-2k (Impinj)	18 μA
Total		166 μA

Table 4.2 lists the peak current consumed by each system block of the RFID heart rate monitoring system. These current levels are for a 2.7 V system. With these values, the peak power dissipation is 448 μW which is under the target of 500 μW. The main power consumption occurs in the ECG amplifier circuit and further power reduction in this system will improve system range. It should be noted that the RFID tag only consumes 20 μA of current for the 100 ms when the tag is turned off. The power can further be reduced by operating the system at a lower voltage, as the system can operate with a voltage as low as 1.8 V (30% reduction).

4.4.2 Heart Beat Detection

The amplified ECG signal for a 30 BPM wave is shown at the top of Fig. 4.14. For a 30BPM signal, the ECG pulse appears every two seconds. The amplified 'R' wave triggers the timer causing it to turn the output high for about 100 ms. These RFID control pulses can be seen in the middle plot of Fig. 4.14. To determine if the system described in Section 4.2 can be used to calculate the heart rate reliably, the time between successive tag reads is first calculated. It is expected to see a jump in time for every heart beat detected. The time between successive tag reads for the first five seconds is shown in the bottom of Fig. 4.14. Note that the 'y-axis' is time between tag reads and the 'x-axis' remains time. It can be clearly seen that there is a spike for every ECG pulse. Similar results were observed for other tested heart rates as well.

4.4.3 Detection of Varying Heart Rates

Tests were run at varying heart rates between 30 and 300 BPM. Data for these heart rates are summarized in Table 4.3. The second and the third columns in this table list the total time for each measurement and the number of heart beats detected

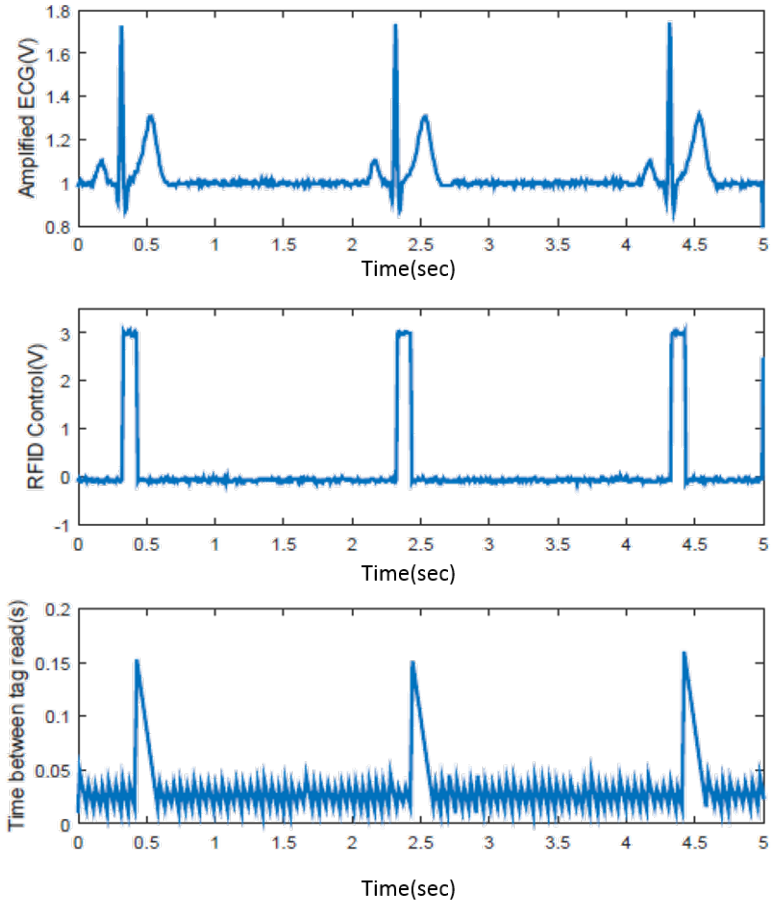

Figure 4.14: Heart beat detection for a 30BPM ECG signal: amplified ECG signal(top), microcontroller output to turn RFID on/off(middle), time between successive tag reads (bottom)

by the RFID system in that time, respectively. The third column, average heart rate, is populated by dividing the number of beats in the third column by time in the second column. The last column lists the standard deviation of beat-to-beat heart rate measurement. The beat-to-beat heart rate is determined by measuring the time between successive tag outages and using Eq. 3.1. The average heart rate calculated for all measurements are accurate when sampled over three minutes. Heart rates are always presented as an integer, but fractional values are included to compare accuracy.

Table 4.3: Analysis of tag read measurements at several heart rates

HR(BPM)	Time(min)	Beats	Average HR (BPM)	Beat-to-beat std dev (BPM)
30	2.99	90	30.00	0.20
60	3.00	180	59.95	0.82
120	3.00	360	119.99	3.67
180	2.99	540	180.04	6.90
240	2.99	720	240.02	15.86
300	2.99	899	299.92	25.65

For 30BPM and 60BPM, the standard deviation of the beat-to-beat measurement is less than 1, which means that for these heart rates one could simply measure the time difference between successive tag outages and expect to get a very accurate heart beat calculation. However, the standard deviation starts increasing steadily for faster heart rates and some kind of averaging may be required.

Fig. 4.15 shows the distribution of calculated 'R-R' intervals for three different heart rates. It is important to note that the accuracy of the tag timing measurements do not get worse with increasing heart rate. However, the same error in measurement has a larger significance for a higher heart rate. For example, a 50ms over-estimation in a 30BPM measurement will cause an error of 2.5% while a 50ms overestimation in a 300BPM measurement will cause the calculated heart rate to be lower by 20%. The system error remains the same regardless of heart rate. This notion is supported by the data in Table 4.3, where nearly 900 beats were detected in 3 minutes for the 300BPM signal even though the standard deviation was significant. The read error can be accounted for with read rates and the channel environment. As was

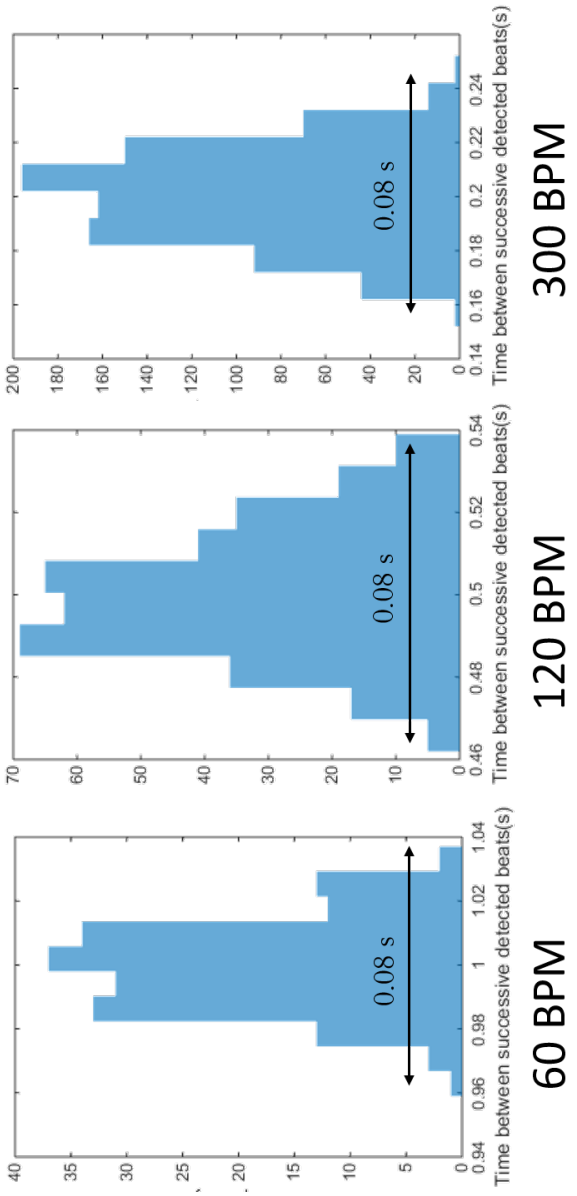

Figure 4.15: Distribution of 'R-R' intervals for three different heart beat sets

discussed in, Section 3.2, the distribution of tag read times is a function of reader settings. Hence, a faster read setting may be desirable for more accurate 'R-R' interval calculations. For slower reader settings, like the one chosen in this example, averaging might be necessary for faster heart rates. However, the three minute averaging window

used in Table 4.3 is both impractical and excessive. Hence, the next logical step is the determination of a minimum sampling time within which we can expect to get a fairly accurate heart rate calculation.

4.4.4 Averaging to Improve Heart Rate Calculation

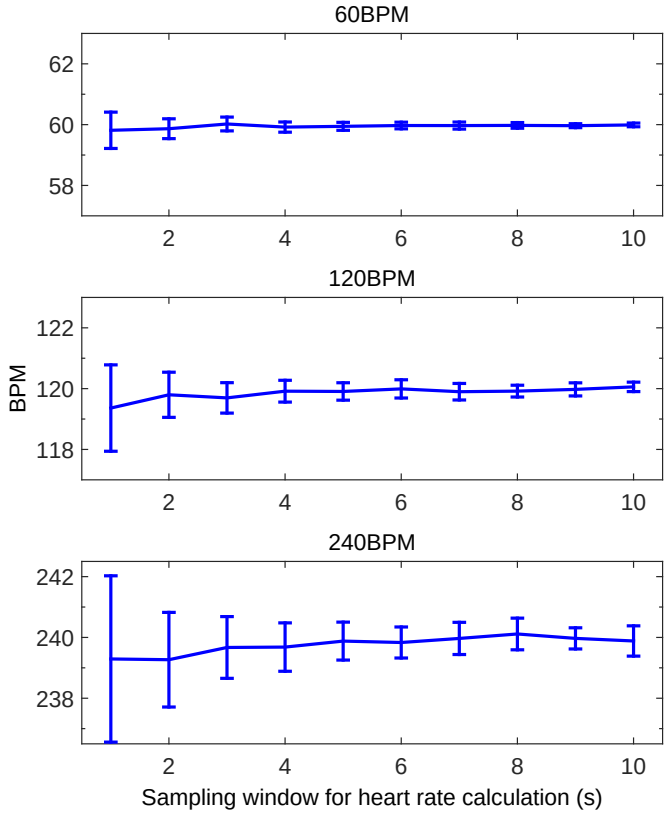

Figure 4.16: Standard deviation in heart rate calculations over different sampling windows

In Fig. 4.16, the mean and standard deviation of heart rate measurements over sampling windows between one and ten seconds for 60, 120 and 240 BPM signals are

plotted. Each window starts and ends with a detection of a beat. For the heart rate calculation, a modified version of Eq. 3.1 is used as shown in Eq. 4.3. Here, T_{sample} is the time of the window and 'Beats' represents the number of detected heart beats in the window.

$$HeartRate = \frac{60 \times Beats}{T_{sample}} \tag{4.3}$$

If a heart rate calculation accurate to within 1 BPM is required, a sampling window of one second is enough for the 60 BPM signal. However, to achieve the same accuracy for a 120 and 240 BPM signals, sampling times of 2 and 4 seconds respectively are needed. The higher standard deviation with increasing BPM can be attributed to the increasing significance of the same error margin as explained earlier. However, one should note that the standard deviation for 120 BPM and 240BPM is smaller than that observed in the beat-to-beat calculations shown in Table 4.3. This error reduction is because of averaging over a larger number of beats in the same time. For example, in a one second sample window, the 120BPM signal has two beats and the 240BPM has four beats. With a sampling window size of 4 seconds, all the measured samples are within 1 BPM of the actual heart rate. A window size of 4 seconds would thus be appropriate for the tested system setup.

4.4.5 Range Tests

The above measurements were taken with the reader approximately three feet away from the tag. Next, the performance of the system was evaluated as the tag was moved away from the reader. In Fig. 4.17, the standard deviation in heart rate measurement for 60 and 120 BPM signals is shown when the tag is four, nine and fourteen feet away from the reader. The amplifier and heart rate detection circuit was powered externally as the power harvesting circuit did not provide uninterrupted power beyond 6 feet. The sampling window for each measurement is set at four

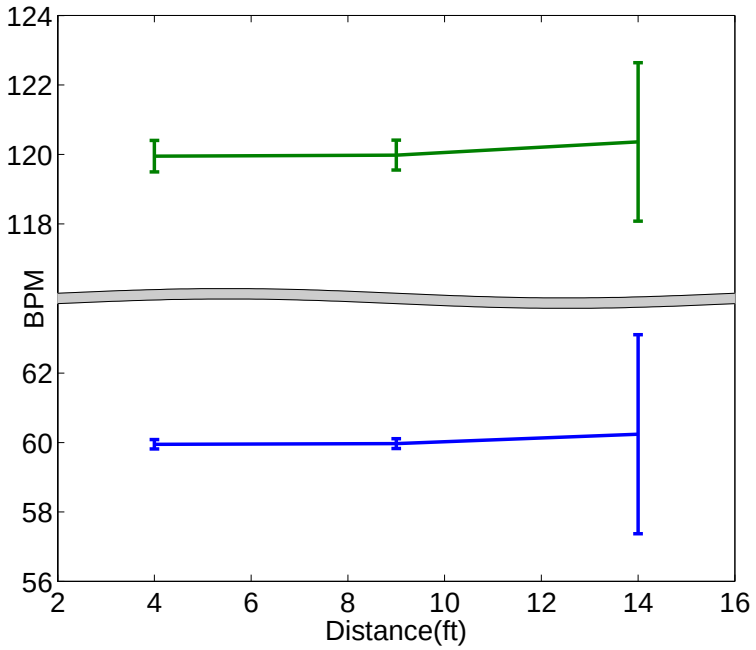

Figure 4.17: Standard deviation in measured heart rate with varying distance from the reader

seconds as described in the previous section. For both the heart rate signals, the standard deviation is very small for up to nine feet; though it is slightly higher for the 120BPM signal. At fourteen feet, the 60BPM and 120BPM signals have a standard deviation of 2.8 and 2.3, respectively. This is mainly due to the fact that a large number of tag reads are missed. The standard deviation for the 120 BPM setting is lower in this case compared to the 60 BPM signal; as its higher number of samples (twice as many) starts having a greater impact on the calculated average. In many cases, the error measured by the system may be acceptable but if greater accuracy is desired one can increase the sampling window size.

The assembled hardware showed that RFID tags can be turned off reliably for a wide range of heart rates. The outages thus created can be monitored at the RFID

reader to accurately calculate heart rate. However, averaging may be required in some cases to improve accuracy.

4.5 System Size Reduction and Optimization

Section 4.4 discussed preliminary tests on the feasibility of an RFID based heart rate monitoring system based on the method described in Section 4.3. The results show that it is indeed possible to transmit heart rate information by simply turning an RFID tag on and off. However, the system needs optimization on several fronts. The size of the system needs to be reduced for integration with wearable platforms. As shown in Fig. 4.18, the Powercast power harvester needs two external components; an antenna and a storage capacitor. These external components need to be optimized for size without significantly effecting performance. Besides the power harvester, integrating all system components on a single printed circuit board will also allow for further reduction in size. It was shown in Section 4.4.1 that ECG amplifier consumed more than 85% of the system's total power and thus, ways to optimize the amplifier should be explored. This section discusses these optimizations.

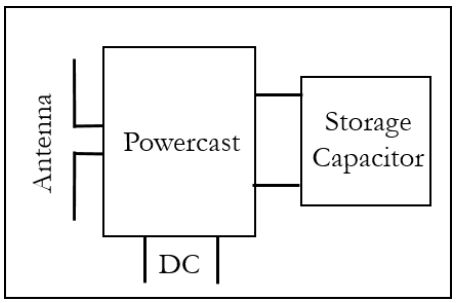

Figure 4.18: Components of the power harvester

4.5.1 Power Harvester Antenna

The size of the antenna is dependent on the wavelength of the transmitted or received RF waves [14]. Since the RFID system described in this work is designed to operate at 915 MHz, the wavelength is approximately 33 cm. The power harvester antennas shown in Fig. 4.9 are patch and dipole types and both are about 16 cm long. This length is about half of the wavelength and is a typical size for an antenna at 915 MHz. Reducing antenna size is possible but it comes at the cost of antenna gain and efficiency. Chip antennas are now available for portable wireless applications and they offer drastically reduced sizes with relatively limited loss of favorable antenna parameters [15]. A comparison between some of these chip antennas is offered in the next section.

4.5.1.1 Compact Chip Antennas

Table 4.4: Chip antenna comparison

Model	Make	BW(MHz)	Gain(dB)	Size(cm)
VJ5601M915MXBSR	Vishay	835-995	1.73	4×4
M6207010	Ethertronics	902-928	2.56	8×1.8
PC91.07.0100A.db	Taoglas	902-928	2.42	3.4×0.7
APAE915R2540ABDB1-T	Abracon	912-918	4.5	3.5×3.5

Table 4.4 compares several chip antennas for use with the powercast power harvester device. The antennas are compared based on their bandwidth, gain and size.

As per the EPC C1G2 protocol discussed in Section 3.1, the reader hops across frequencies from 902 MHz through 928 MHz in 500 kHz steps. Thus, the power harvester antenna has to satisfy this band. The antenna size listed here are approximate sizes that include the antenna chip and the necessary keepout area around the chip.

Gain of the antenna should be as high as possible to maximize the system range. An estimate of the desired antenna gain can be obtained from a modified form of the Friis transmission equation (Eq. 4.2). Eq. 4.4 describes the relevant formula to determine the receiver antenna gain where all variables are as described in Eq. 4.2. Assuming 1 W of transmit power which is the maximum allowed value, 250 μW of received power, 4 m of distance and 8.5 $dBiC$ gain for the transmit antenna (from [104]), the required receiver antenna gain is 2.13 dB.

$$G_r = (\frac{P_r}{P_t G_t}) \times (\frac{4\pi R}{\lambda})^2 \tag{4.4}$$

With gain being the main consideration, the Abracon antenna is the most optimal choice. It is smaller than all the considered antennas, except for the Taoglass antenna, yet provides nearly twice the gain as the other antennas. It should be noted that the bandwidth of the Abracon antenna does not span the entire range specified by the C1G2 protocol. However, the bandwidths shown in the table are -10 dB bandwidths which specify the range for which the antennas have a return loss of less than -10 dB. Thus, antennas do continue operating beyond the specified bandwidth but at a lower efficiency. Additionally, unlike the RFID system, the power harvester does not need to be fully operational in the entire range of the protocol frequency sweep. With sufficiently high gain, the power harvester can harvest enough power to last the entire duration of the sweep by operating in its fractional bandwidth. This harvested energy can be stored in the power harvester capacitor to last for an entire frequency sweep

cycle. Hence, the Abracon chip's limited bandwidth may not be a problem. However, due to the small bandwidth, correct tuning of the antenna is very important so that it operates close to the center of the RFID band. Tuning involves tweaking antenna geometry to achieve a desired antenna center frequency. The next two sections discuss the challenges and the procedure for tuning the antenna.

4.5.1.2 Antenna Tuning: Challenges

Figure 4.19: Abracon APAE915R2540ABDB1-T chip patch antenna [1]

The Abracon APAE915R2540ABDB1-T [1] is a miniaturized patch antenna shown in Fig. 4.19. The center frequency of such patch antennas can vary based on manufacturing variations, ground plane sizes, surrounding circuitry and a host of other factors. Hence, the antenna needs to be tuned for each system configuration to maximize gain and efficiency at the required frequency. The center frequency of patch antennas can be changed by introducing slits in the metal patch [21, 22, 71]. Change in center frequency based on the length of the slit in a patch antenna is shown in Fig. 4.20 [22]. It should be noted that there is no clear visible trend between slit length and antenna center frequency. This is because, the center frequency depends on a variety of parameters like substrate material properties, antenna geometry, position

of slit etc. A detailed analysis of tuning antennas utilizing slits is presented in [23]. An analytical procedure to determine the exact slit size and position to achieve a desired center frequency is complex. Hence, a simulation with a modeling software like Ansys HFSS is preferred to get an intuition about tuning these antennas. However, the material properties of the Abracon antenna are not known and they need to be figured out before simulating the effect of slits. The next section discusses the process of estimating material properties and studying the effect of slits on antenna center frequency. After learning through simulations, the antenna design will be verified using hardware.

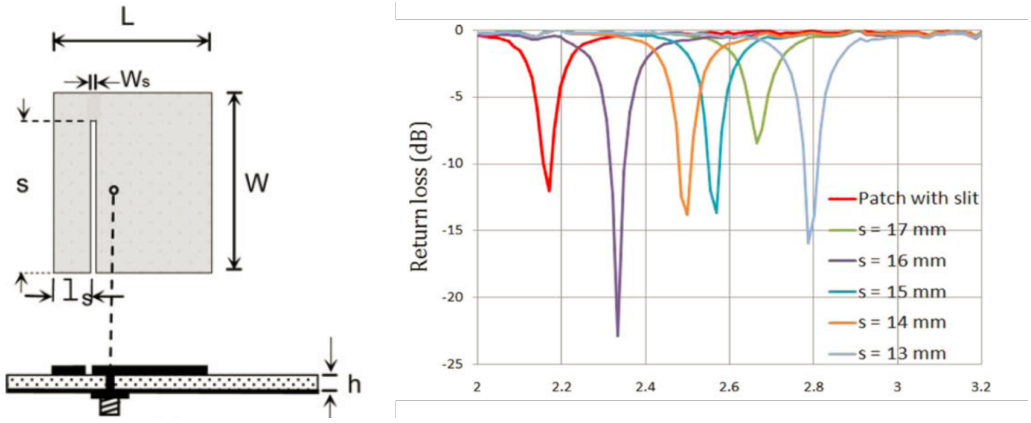

Figure 4.20: Effect of varying slit lengths on antenna center frequency [22]

4.5.1.3 Antenna Tuning Procedure: Simulations

Most geometrical dimensions of the Abracon patch antenna are available on the datasheet [1], while the rest can be measured directly from the antenna chip. Using these dimensions, a model of the patch antenna was created in the HFSS software as shown in Fig. 4.21. The metal patch and the ground plane were both assumed to be

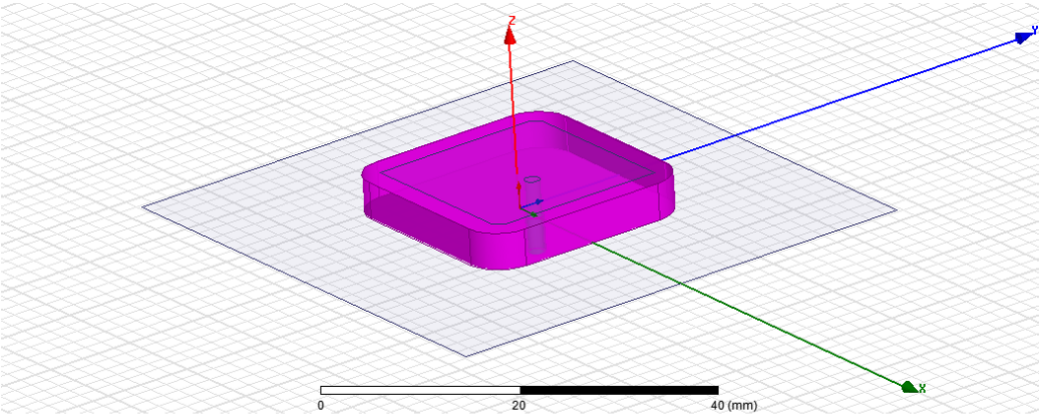

Figure 4.21: Patch antenna HFSS model

perfect electrical conductors. The substrate material property of relative permittivity is unknown. A rough estimate of the permittivity is used to obtain an understanding of slit effects on the center frequency of the Abracon patch antenna. To estimate permittivity, the patch antenna was populated on a PCB and its untuned return loss was measured using a network analyzer. The permittivity of the substrate in the simulation was then varied till the response looked similar to the actual measured return loss. The relative permittivity thus found was 55 F/m. Simulations are performed to tune the antenna by trying different slits on the patch antenna.

The goal of this exercise is to tune the antenna return loss peak close to 915 MHz, as this is the center frequency of the RFID band. Fig. 4.22 shows the steps involved in successfully tuning the simulated antenna. It should be noted that these steps were arrived at through trial and error after attempting a number of slit sizes and positions. The slit width used was 0.5 mm as that was the smallest available drill bit size to make slits experimentally. The change in center frequency as a 2 mm slit and then a 4 mm slit is cut are shown in Fig. 4.23. The antenna without any slits is centered outside the RFID band at about 938 MHz. As the slit is introduced and

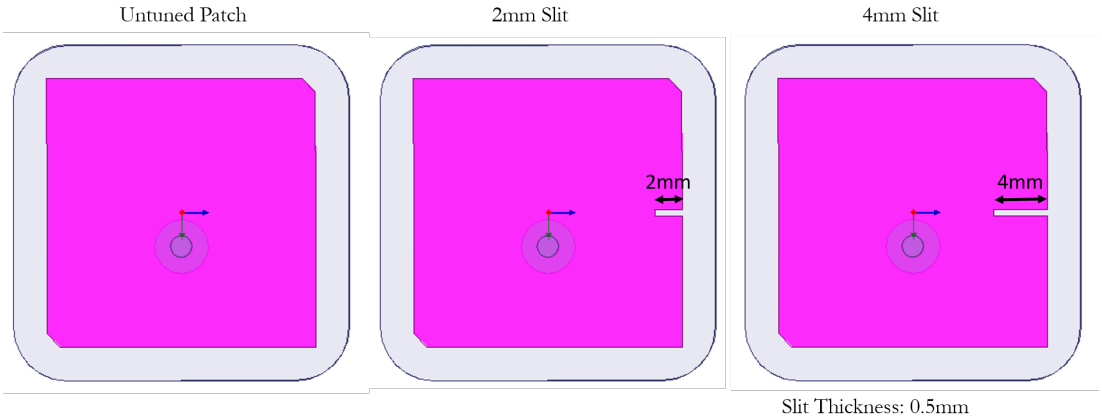

Figure 4.22: Patch antenna tuning steps

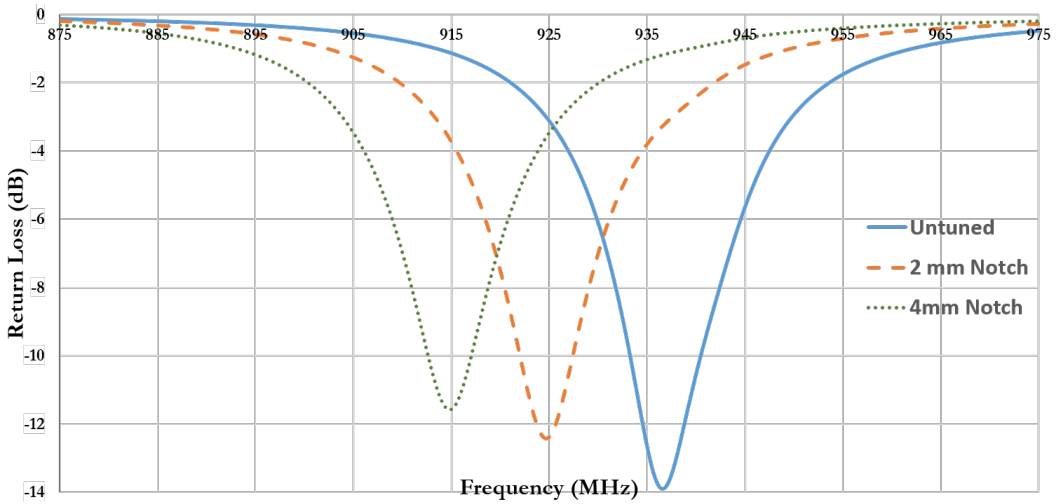

Figure 4.23: Center frequency change with slit length variation

then extended, the antenna is tuned closer to the desired frequency of 915 MHz. However, the return loss does increase marginally as the antenna is tuned.

As it was observed in Fig. 4.20, there is no linear relationship between slit length and frequency shift. Hence, when the slit length was increased from 2 mm to 3 mm

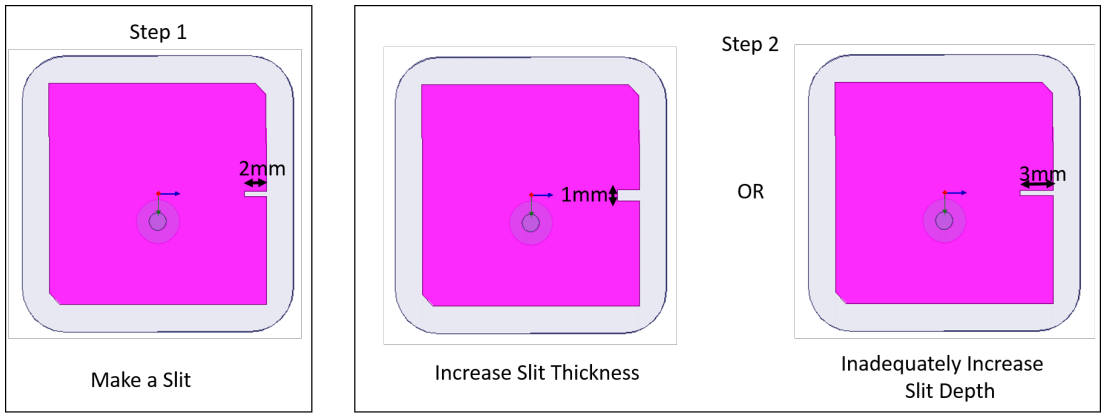

Figure 4.24: Incorrect tuning steps

as shown in Fig. 4.24, the center frequency, increased slightly instead of decreasing. Making the slit thicker also had the effect of increasing the center frequency. However, in general, it was observed that making small gradual increases in slit lengths tended to decrease center frequency while making wider slits increased the frequency. Finally, it should be noted that there is more than one way to tune the antenna to a desired frequency. For example, Fig. 4.26 shows another configuration where the antenna is tuned to 915 MHz with two slits and the corners chamfered to 1.6 mm instead of the original 1 mm. With these intuitions, practical hardware tuning of the patch antenna can be attempted.

4.5.1.4 Antenna Tuning Procedure: Hardware

The Abracon patch antenna was populated on a FR4 board of 45 $mm \times 45$ mm size. The center frequency of the antenna was determined using a network analyzer. A drill press with a 0.5 mm drill bit was used to create tuning slits in the antenna. Initially, the center frequency of the antenna was approximately 935 MHz. An iterative process of making slits in the antenna using the drill press and recording its center frequency was followed. The slit size was progressively increased till a center

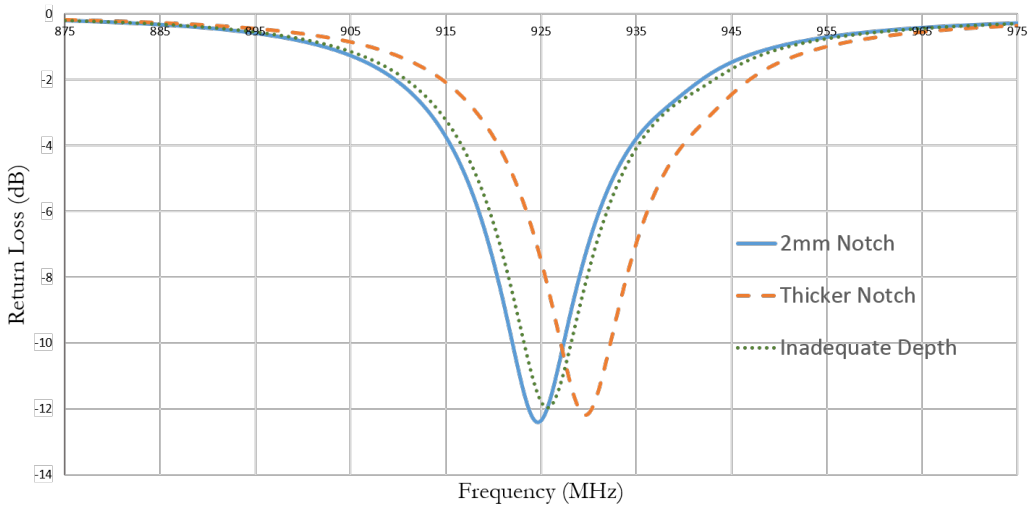

Figure 4.25: Center frequency change due to incorrect tuning steps

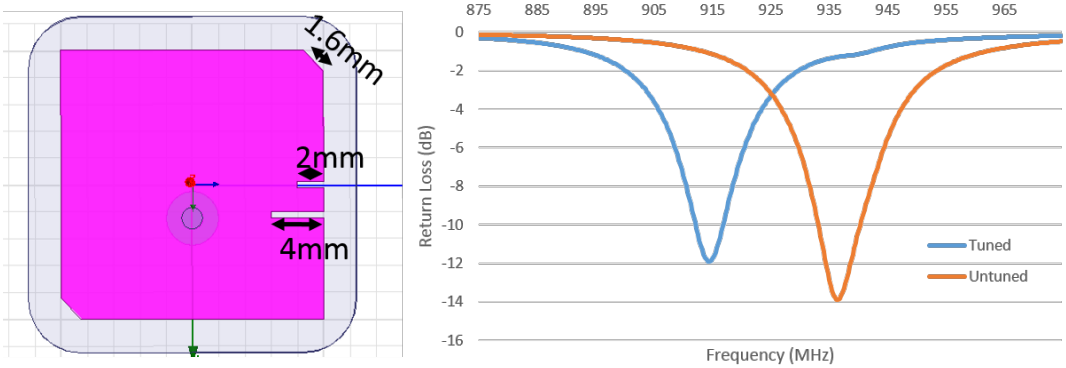

Figure 4.26: Alternate final tuning geometry

frequency of about 917 MHz was obtained at about 3 mm. The shift in center frequency with increasing slit size steps can be seen in Fig. 4.27. The tuned antenna is shown in Fig. 4.28 with the slit circled.

The performance of the tuned antenna was then compared to reference antennas from the Powercast evaluation kit [100]. The Powercast kit consists of a dipole an-

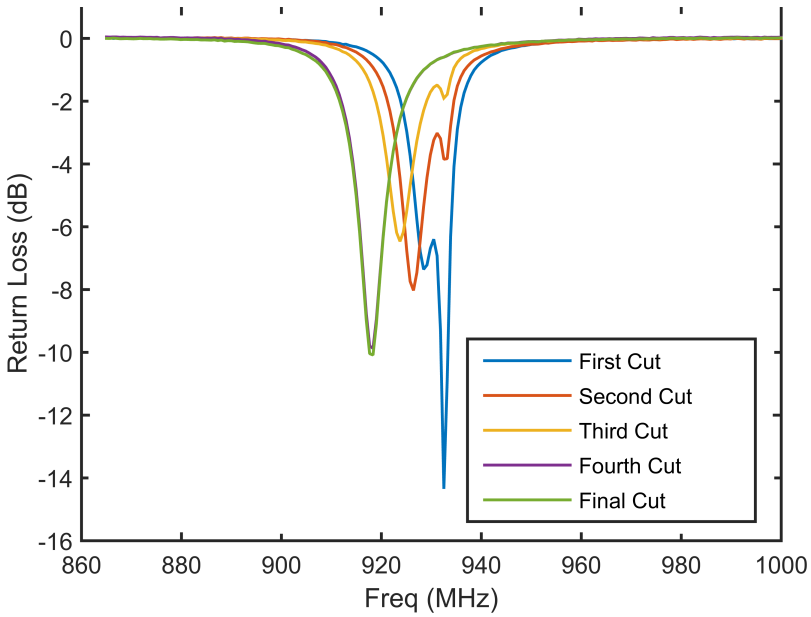

Figure 4.27: Center frequency change with antenna slit changes

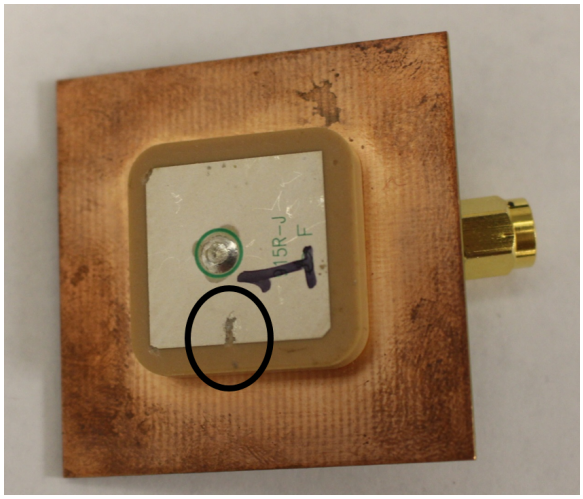

Figure 4.28: Tuned patch antenna

tenna and another patch antenna. The three antennas are shown in Fig. 4.29. The final Abracon patch antenna represents a significant size reduction. The reference

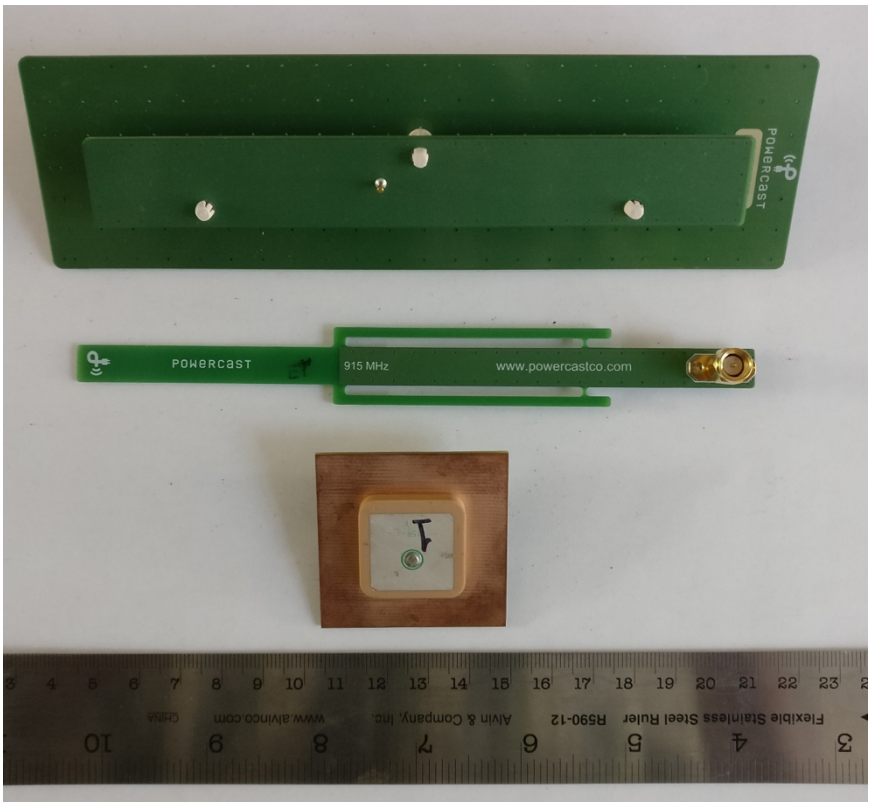

Figure 4.29: Size comparison of the tested antennas

antennas and the designed patch antenna were connected to the Powercast evaluation board which has an onboard LED to act as a load. The current passing through the LED is proportional to the power received from the antenna. Hence, this current was measured for each antenna while the setup (shown in Fig. 4.30) was placed at several distances from an RF transmitter. The results of this test are shown in Table 4.5. The reference patch antenna which has a gain of about 6 dB performs the best. However, the designed patch antenna is comparable to the reference dipole antenna, albeit with a considerably smaller size. The designed patch thus has a lower range when compared to the reference patch due to the significantly smaller aperture size but it can still be used to harvest power at reasonable distances from the RFID

reader.

Figure 4.30: Setup for comparison of designed patch antenna with reference powercast antennas

The power harvesting antenna is the largest component of the RFID heart rate monitoring system. The above exercise allows for size reduction with a small impact on performance. The reduction in antenna size as described above is a significant step in making the system wearable.

Table 4.5: Comparison of designed patch antenna with reference powercast antennas

	Powercast Patch	Powercast Dipole	Tuned Patch
	Dimensions (cms)		
	17.8 × 5	16.5 × 2	4.5 × 4.5
Distance (ft)	Current (μA)		
1	2490	1720	1550
2	1060	506	484
3	521	220	163

4.5.2 Power Harvester Capacitor

The power harvester capacitor serves the purpose of providing uninterrupted DC supply in the event of momentary changes in received RF power strength due to frequency hopping or other environmental reasons. The larger the capacitor value, the higher the charge stored to compensate for received power variations. However, larger capacitance values tend to be larger in size which opposes the design goal of reducing overall system footprint. The value of the capacitance can be determined using Eq. 4.5, where C is the capacitance value, V_{DC} is the desired rail voltage, I_{load} is the expected average load voltage and $t_{cut-off}$ is the desired time for which the capacitor should continue supplying power after the RF power source has been turned off [100]. As per this equation, for nominal values of 2.7 V, 75 μA and 5 s respectively, a capacitor size of roughly 15 mF is required. An additional consideration is the power loss in a capacitor due to its equivalent series resistance or ESR. To minimize these losses, capacitors with very low ESR are desired and Powercast recommends a series resistance of less than 200 $m\Omega$ [100]. In summary, the chosen capacitor needs to have a small footprint, low ESR and a capacitance value in the millifarad range.

$$C = 15 \times V_{DC} \times I_{load} \times t_{cut-off} \tag{4.5}$$

4.5.2.1 Capacitor selection and testing

Three super-capacitors that meet the above requirements were selected for testing. Two of the capacitors were sampled from Seiko (CPX- 3225A752 and 10080C104) while an additional capacitor was sampled from Kemet (T495D477M006ATE045).The sizes and capacitance of these components are summarized in Table 4.6. To compare these capacitors, a test board was designed and populated with the capacitors and the powercast power harvester. This board is shown in Fig. 4.31. The power harvester

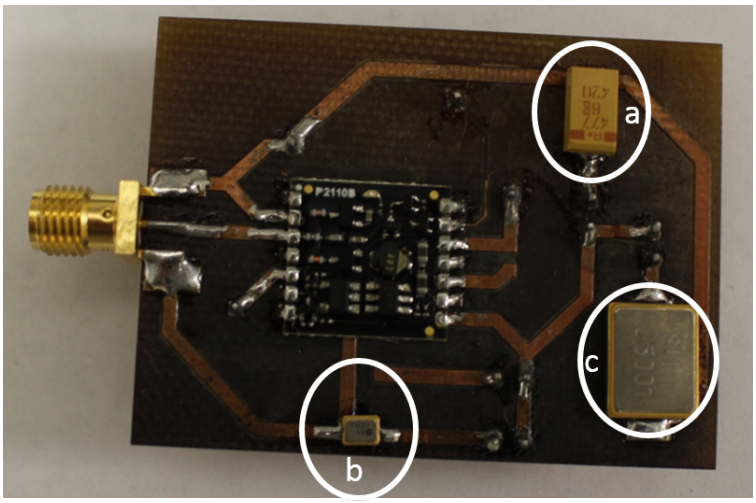

Figure 4.31: Board for testing compact supercapacitors (labels in Table 4.6

was set for an output voltage of 2.7 V and a load current of about 100 μA. Each capacitor was connected to the Powercast one at a time to gauge their performance. The start-up time was first measured by turning an external RF field on and measuring the time required for the set DC voltage to appear at the Powercast output. Next, the cutoff time was measured by turning the RF field off and measuring the time for which the Powercast continues to supply power to the load. The RF field was left on for 30 s every time before being turned off for measuring the cut-off time.

Table 4.6: Power harvester capacitor comparison

Model	Label	Capacitance (mF)	Size(mm)	Start time (s)	Cut-off time (s)
T495D477M006ATE045	a.	0.47	7.3 × 4.3	2.6	2.8
CPX3225A752D	b.	7.5	3.2 × 2.5	2.7	14.4
CPX10080C104F	c.	100	10 × 8	2.7	29.1

The results of the above test are shown in Table 4.6. The table also shows the capacitance value of each capacitor. The start-up time for all the capacitors is comparable which suggests that the overall system start-up time depends on the Powercast device itself and not so much on the capacitor for these capacitance values. The cut-off time however, differentiates these capacitors. As expected, higher capacitance values produce higher cut-off times. CPX10080C104F has the highest capacitance of 100 mF and also the highest cut-off time of 29 s. CPX3225A752D on the other hand has a capacitance of 7.5 mF but the cut-off time is only halved when compared to CPX10080C104F. Additionally, CPX3225A752D is also the smallest of all capacitors. Therefore, this capacitor was chosen for the system.

4.5.3 ECG Amplifier Optimization

As was discussed in Section 4.4.1, the ECG amplifier circuit consumes the highest amount of power in the system. Reducing the power consumption of this block could help in improving the system's overall range. Additionally, all system components need to be integrated on a single board to approach a more final design. Fig. 4.32 shows this optimized and integrated schematic. This schematic will be discussed in the next two sections.

4.5.3.1 ECG Amplifier Power Reduction

The first step towards power reduction was taken by increasing the resistor (R_{11} and R_{12}) values for the voltage divider to 500 $k\Omega$ each as compared to 20 $k\Omega$ earlier. This change, results in the current drawn by the divider to reduce by a factor of 25. However, such high resistor values could be loaded due to the input impedance of the circuits that are connected to the divider. Hence an opamp buffer is added to provide a stable voltage source.

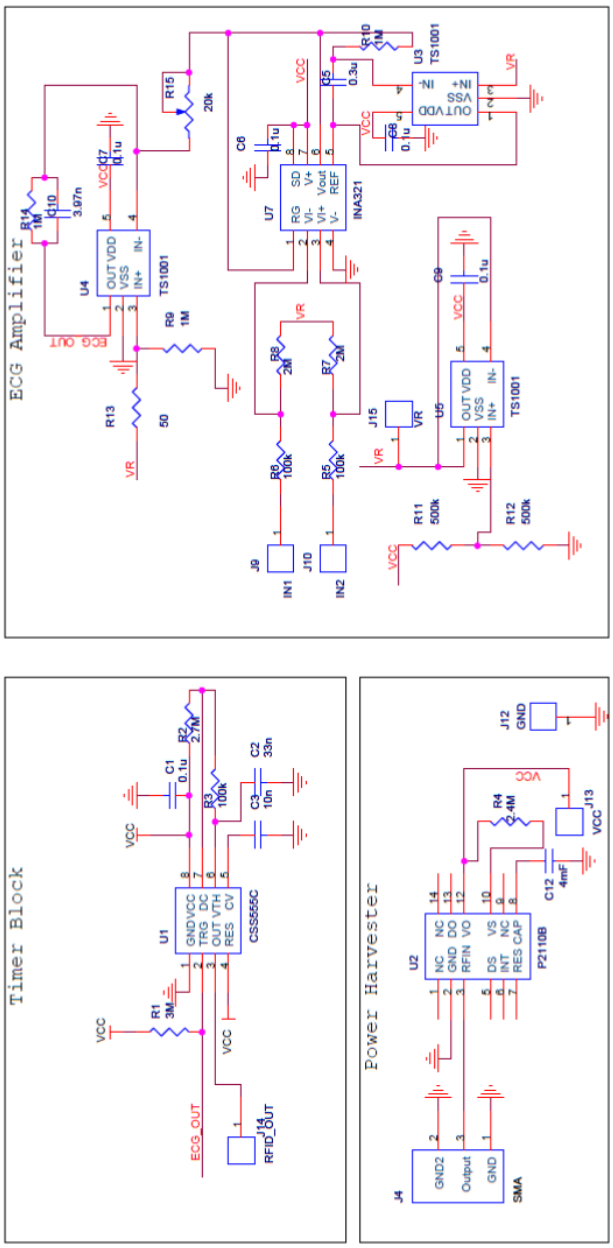

Figure 4.32: Integrated schematic optimized for power consumption

Another power saving change was to replace all OPA336 opamps with TS1001 opamps [107]. These opamps have a supply current of only 0.6 μA, compared to the 20 μA of the OPA336 opamps. This change almost eliminates the currents consumed

by the opamps. Hence, the main remaining power consuming source in the ECG amplifier circuit is now the INA321 instrumentation amplifier.

With these changes, the overall current consumption of the amplifier circuit is reduced from 145 μA to only 44.5 μA.

4.5.3.2 Integrated Heart Rate Monitor Board

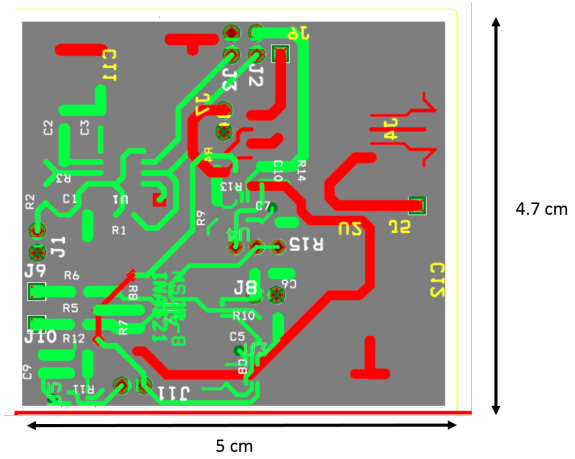

Figure 4.33: Layout for the circuit optimized for power consumption

The three system blocks; the power harvester, the ECG amplifier and the heart rate detection circuit have all been integrated into a single circuit board. This integrated schematic is shown in Fig. 4.32. Additional, minor changes were made to the original circuit as presented earlier. For example, the resistor R_{15} has been added as a potentiometer so as to provide variable gain for the ECG amplifier output. Resistor R_4 has been added to adjust the DC voltage output of the powercast system to 2.7 V. The layout for this schematic is shown in Fig. 4.33.

4.5.4 Final Circuit Design and Layout

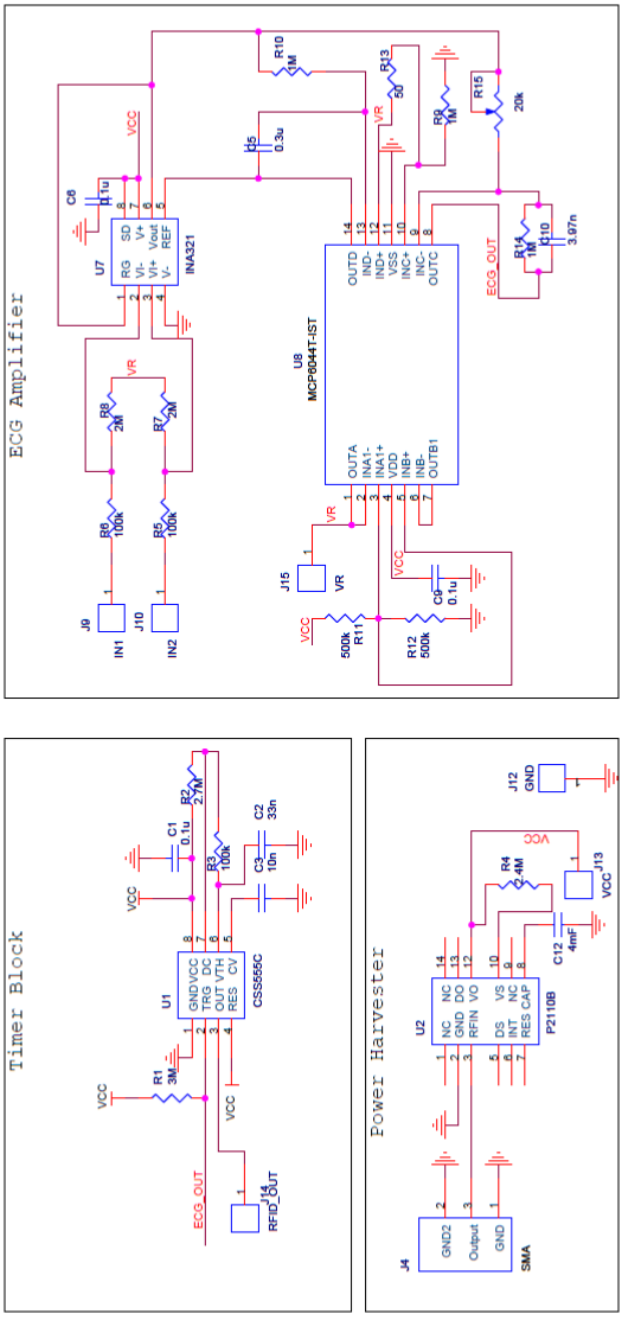

Figure 4.34: Final system schematic

Even though the circuit presented in the previous section is integrated and optimized for power, it is not optimized for size. Size optimization was left out so as to provide adequate testpoints and flexibility for making changes for the test board. A schematic which further reduces the footprint by integrating all three opamps into a single package (MCP6044 [85]) with a similar power consumption is shown in Fig. 4.34. The layout for the system is shown in Fig. 4.35 and the final system size is only 1" × 1". The layout for this circuit is included in Appendix D.

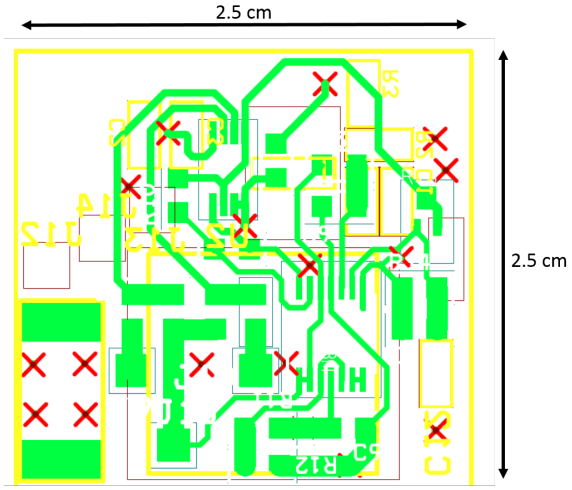

Figure 4.35: Final system layout

The integrated heart rate monitoring system (without the RFID tag) is shown in Fig. 4.36. The glowing green LED in the figure indicates that the system is drawing power wirelessly using the designed patch antenna.

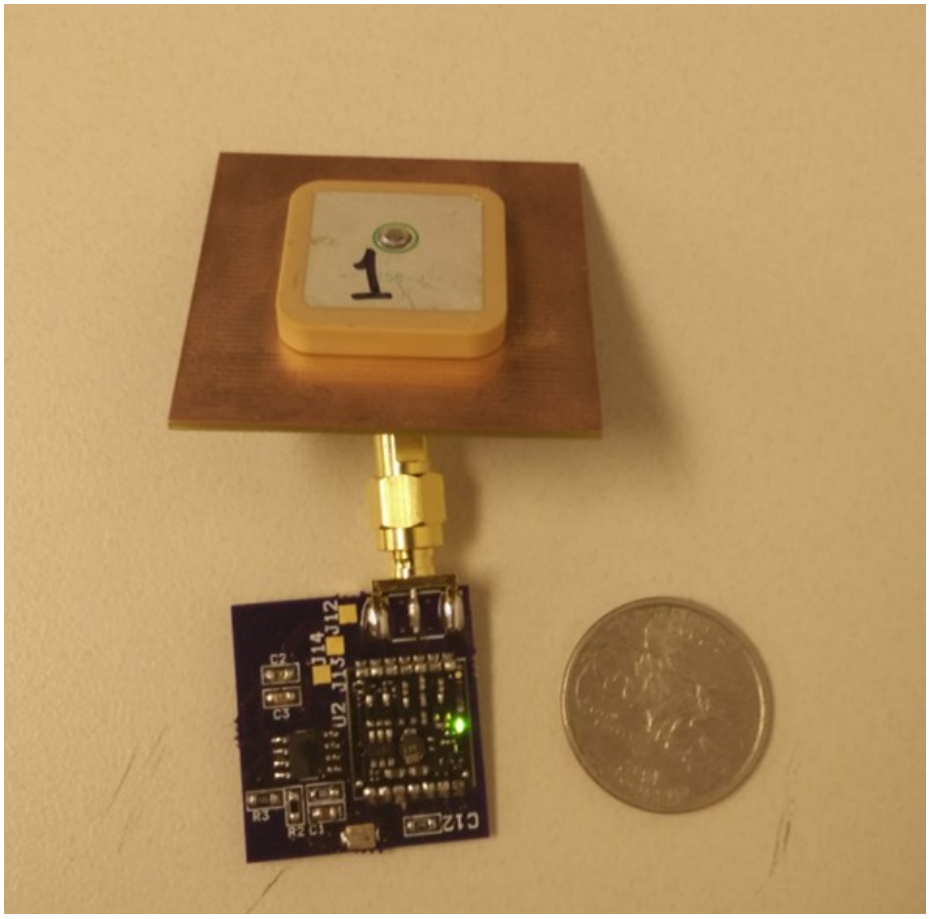

Figure 4.36: Final integrated RFID heart rate monitoring system

4.6 Conclusions

Table 4.7: System Specifications

Electrodes	2
Antennas	2
Heart Rate Monitor Size	2.54 $cm\times$ 2.54 cm
Monitor Power Consumption	127 μW
Power Harvester Antenna Size	4.5 $cm\times$ 4.5 cm
Power cut-off time	15 sec
RFID Tag	Monza X2k Dura
System Range	6 ft

The final system specifications are listed in Table 4.7. The total power consumption of 127 μW does not include about 50 μW of power that is consumed every time the RFID tag turns off. The focus of the design was the ECG amplifier and the heart rate detection circuit. The power harvesting antenna and the RFID tag are external and can be altered if desired.

In this chapter, a hardware realization of the RFID based heart rate monitoring system was presented. The discussion included design of a low power ECG amplifier with under 45 μA of current consumption. An innovative approach for heart beat detection was demonstrated using IC555. A commercial power harvester design was completed by selecting a low footprint power harvester and an antenna. A detailed

discussion on antenna tuning was also presented. A commercial RFID tag was re-purposed to transmit heart rate information by turning it on and off without any additional components. Finally, the entire system was integrated into a compact printed circuit board measuring a size of 1" $\times$ 1" in addition to an external antenna and an RFID tag.

5. Algorithm for Heart Beat Detection Improvement in Noisy Environments

The RFID heart rate monitoring system described so far can be expected to perform well in noise free environments, that is, without significant channel interference and at short distances from the RFID reader. However, for practical applications, the environment may not be not ideal. In this chapter, a logistic regression model is implemented to improve heart beat detection from RFID data for the RFID on/off system in noisy environments.

5.1 Effect of Additional Tags

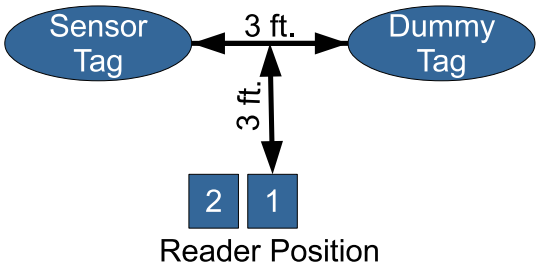

Figure 5.1: Reader and Tag positions for tests involving an additional dummy tag

It is possible that there might be more than one RFID tag in the environment and system behavior in the presence of an additional tag is of interest. To test performance in a situation like this, the sensor tag and a dummy tag were placed about one and a half feet from each other and the reader was kept at a distance of about 3 feet from them. In position 1, the reader is kept at the center of the two tags such that

about 53% of the reader measurements are from the sensor tag. For position 2, the reader is slightly closer to the sensor tag such that about 64% of the measurements are from the sensor tag. The reader setting was Maxmiller mode with 'M4' encoding [54]. It should be noted that the reader setting plays a critical role in the observed time between tag reads and thus on the effect played by the additional tag.

Table 5.1 shows 60BPM and 120BPM ECG signal measurements for the two mentioned positions. This table lists the average heart rate and standard deviation calculated over a four second sampling window, and also presents the percentage of false beats detected in the measurement. Three minutes of data was collected for each setting. It is evident that the performance suffers slightly due to the presence of an additional tag. As the reader spends time in reading the dummy tag, the time between measurements of the sensor tag increases thereby creating a larger variation in the time between successive beats detected. It is also possible that the reader may not read the sensor tag for a duration longer than 100ms in which case the system would assume it to be a detected heart beat. It is the detection of these false beats that cause the over estimation of the average calculated heart rate in Table 5.1. Even so, in spite of the presence of an additional tag, the system is able to calculate the heart rate relatively well for the tested setups.

Table 5.1: Heart rate measurements in the presence of two tags. Position 1: Reader placed in center of two tags. Position 2: Reader placed closer to the sensor tag

Position	60 BPM			120 BPM		
	HR(BPM)	Std Dev	False Beats	HR(BPM)	Std Dev	False Beats
1	61.66	4.43	3.33%	122.12	5.33	1.39%
2	60.37	0.92	0%	120.1	2.4	0.5%

5.2 Need for Beat Detection Improvement

As was seen in the above section, false outages may start appearing when additional tags are placed close to the sensor. Such outages can be created due to multipath effects, poor signal strength, and noise induced triggering of the heart rate detection circuit. Based on a given scenario, there could be a lot more false outages than observed in Section 5.1. It is difficult to distinguish between a real heart beat and a false outage as the tag data is similar in both cases. Conversely, the heart rate detection circuit may sometimes miss a heart beat due to spurious noise in the circuit. In the presence of false or missing outages, the calculated heart rate will be incorrect. Thus, an algorithm to correctly determine real and missed heart beats could help to make this RFID system more reliable in noisy environments.

Time-domain methods that essentially find average heart rates over several seconds can only help to overcome problems posed by poor data quality to a certain extent. Additionally, averaging removes beat-to-beat interval variation which may be critical for health monitoring (to be discussed in Section 6.1.1). Hence, a method to identify individual heart beats more accurately from RFID data is required. Machine learning algorithms have been successfully employed for improving accuracy of other heart rate monitoring systems [26, 93]. However, these algorithms relied on conventional ECG data and the challenges posed by heart rate data in our RFID on/off system are very different. Hence, an algorithm that is suited for the RFID on/off system needs to be developed.

5.3 Beat Detection Algorithm

The objective of the beat detection algorithm is to accurately determine heartbeats by identifying unintentional outages. A secondary objective is to eliminate the need for averaging so as to retain beat to beat variability information. A supervised

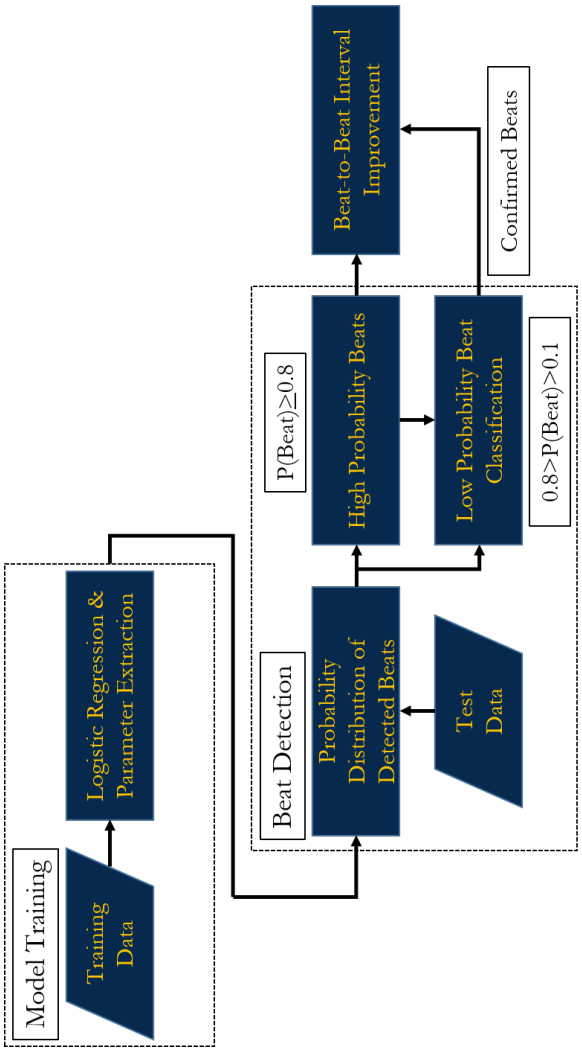

Figure 5.2: Algorithm for probabilistic heart beat classification from RFID data

learning algorithm based on logistic regression [52] is proposed to achieve these goals. The proposed algorithm utilizes the probabilities obtained from a logistic regression model to estimate the likelihood of an outage indicating a real heart beat. The entire process is summarized in Fig. 5.2 and will be explained in the remainder of this section. The process will include model training, beat detection and beat confirmation.

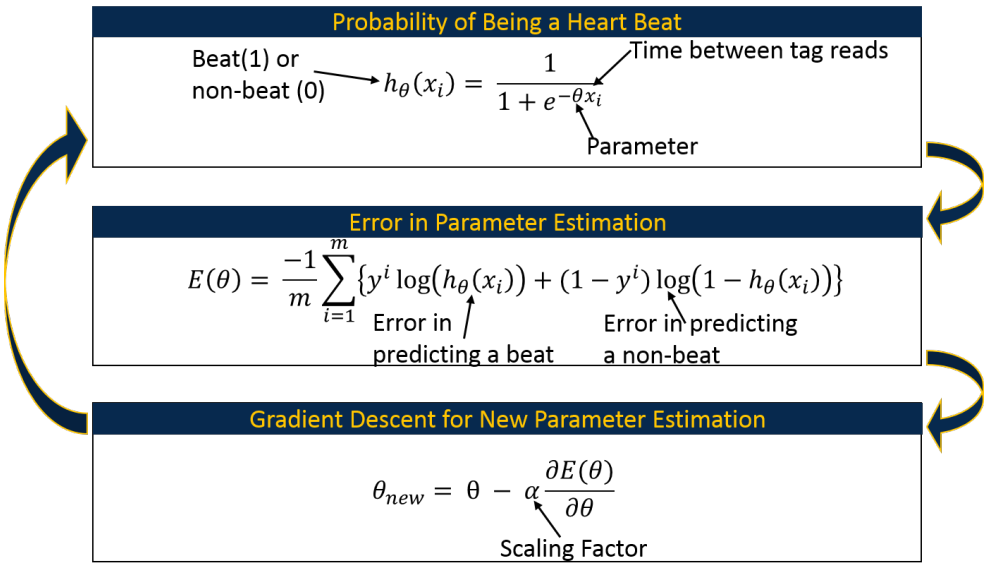

Figure 5.3: Iterative steps taken for logistic regression model training

5.3.1 Model Training

The goal for model training is to obtain parameters (θ) that fit RFID on/off data so that when unknown data is presented it can be accurately classified as a beat or a non-beat. The steps taken to obtain these parameters are illustrated in Fig. 5.3. The time between successive sensor RFID tag reads is the primary feature (input) used in the model. For data points that are not heart beats, this time is usually much lower than the predetermined duration of the RFID outage. However, the time between tag reads for false outages could be much higher or comparable to the predetermined RFID outage duration. Hence, a binary decision tree cannot be used to separate the real beats from non-beats and false outages. Therefore, polynomial features of time between tag reads are used as inputs to the model. Each feature data point has an associated state; all real beats are assigned as '1' and all non-beats (including false outages) are assigned '0'.

The probability of a given tag outage being an actual heart beat is given by

the logistic function in Eq. 5.1. Here '$h_\theta(x_i)$' is the probability that a data point represents a beat (1) or not a beat (0), 'x_i' represents the training data feature with index 'i' and 'θ' represents the parameters of the model.

$$h_\theta(x_i) = \frac{1}{1 + e^{-\theta x_i}} \tag{5.1}$$

Before training, the parameters 'θ' for the fit are unknown. To obtain these parameters, they are first assumed to be '0' and the error with this assumption is calculated using Eq. 5.2, where 'm' is the number of training samples with index 'i', and 'y' is the actual state of the output (1 for beats and 0 otherwise). The first term in this equation accounts for the error in determining beats and the second term represents the error in determining non-beats. Once the error due to the choice of θ is determined, a new assumption for the parameter is made using Eq. 5.3 where 'α' is a scaling factor that adjusts the step sizes for new values of θ. The process of finding the error and new parameters is continued until the value of θ converges and that value is chosen as the parameter for the model.

$$E(\theta) = \frac{-1}{m} \sum_{i=1}^{m} [y^i log(h_\theta(x_i)) + (i - y^i) log(1 - h_\theta(x_i)] \tag{5.2}$$

$$\theta_{new} = \theta - \alpha \frac{\partial E(\theta)}{\partial \theta} \tag{5.3}$$

The model training needs to be done before the algorithm can be applied to eliminate false outages. The training can be done on any annotated heart rate data set, regardless of the actual heart rate value. Training data length should be long enough to adequately represent the appearance of false outages for a given RFID channel. About 60 seconds of data is typically enough.

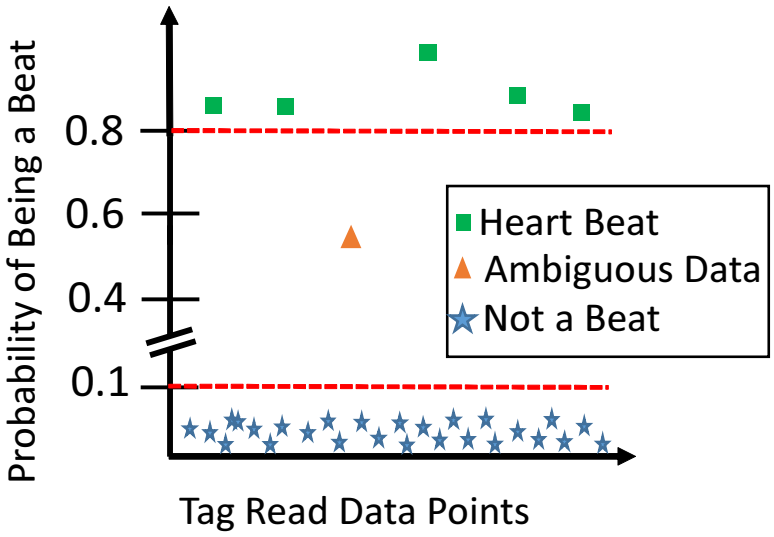

Figure 5.4: Classification of tag data points based on probability of being a heart beat

5.3.2 Beat Detection

The parameters obtained from model training are verified by inserting the test data features into Eq. 5.1. This operation yields the probability of each test data point being a heart beat. Fig. 5.4 shows how tag data are classified into three categories; heart beats, non-beats and ambiguous data, based on the probabilities obtained from the model. Tag data that have a probability of less than 0.1 of being an actual beat are classified as non-beats. Data points that have a greater than 0.8 probability of being a real beat are directly classified as beats. Very few tag data points have intermediate probabilities and they could represent real beats or false outages. To correctly classify these ambiguous beats, a linear regression analysis is done using the previous two accurately determined beats. If the ambiguous data point follows the linear trend with a margin of 20%, it is classified as a heart beat. This margin is sufficient to account for typical heart rate variability for humans [90].

Table 5.2: Time between successive detected beats: An example of a missed beat

T_{1-2}	T_{2-3}	T_{3-4}	T_{4-5}	T_{5-6}
0.99	1.02	0.98	**2.01**	0.99

5.3.3 Beat Interval Improvement

Heart beats can sometimes be missed due to a hardware glitch, noisy environment or incorrect classification from the above algorithm. One such example for a 60BPM heart rate signal is shown in Table 5.2 where the time between successive detected beats is shown in seconds. Here, the time between the fourth and fifth beat (T_{4-5}) is twice as long as the previous three samples, which most likely indicates a missed beat. When this case is identified, a beat is inserted using the arithmetic mean of the previous two beats. It should be noted that the beat insertion is only done when an approximately 50% jump is noticed in time between tag reads. This feature should be disabled if a person is being monitored for heart conditions where missed beats occur naturally.

5.4 Data Collection and Algorithm Testing

To verify the algorithm, data was collected using a commercial ECG simulator (HE Instruments' Tech-Patient Cardio ECG Simulator) as a source for the heart rate signal. The ECG simulator was used to generate three discrete heart rates; 45BPM, 60BPM and 120BPM with 0% variability. The simulated ECG signal was fed into the RFID heart rate monitoring system described in Chapter 4. The RFID outage duration for detected 'R' waves was set to be about 110 ms. RFID data was recorded by an RFID reader (Impinj Speedway Revolution R420 UHF Reader). The RFID reader and the tag with the heart rate detection system were placed six

feet away from each other. If an additional RFID tag is close to the heart rate tag, it could interfere with the heart rate tag's radiation, resulting in poor data quality. Thus, a noisy environment was simulated by placing an additional RFID tag five centimeters away from the sensor tag. However, poor data quality is a mixture of effect of additional tags and the ambient RFID channel. Hence, the setup had to be moved to different locations in the room till the ambient conditions produced significant false outages. For each set of heart rate measurements, at least 7000 individual tag reads were processed and the time between successive responses from the sensor tag was calculated. The reader setting used was 'MaxMiller' [54] mode with 'M4' encoding.

5.5 Results and Analysis

In this section, the effectiveness of the algorithm in improving beat interval determination is discussed. An example of the algorithm implementation through elimination of false outages is first shown. Then, beat classification accuracy for three different heart rate settings with the algorithm is demonstrated.

5.5.1 Beat Detection Improvement with the Algorithm

Fig. 5.5 demonstrates how the algorithm described in Section 5.3 works to improve the beat detection from RFID data. In this figure, the time from the previous reading of the sensor tag is on the y-axis and the x-axis displays the measurement time. On the graphs, the circles indicate the actual heart beats and crosses indicate the heart beats detected by the algorithm at that stage.

As stated in Section 5.4, the RFID tag is turned off for a period 110ms every time a heart beat is detected. Thus, setting a threshold at 110ms for time between successive tag reads should detect all transmitted heart beats. Therefore, in Fig. 5.5,

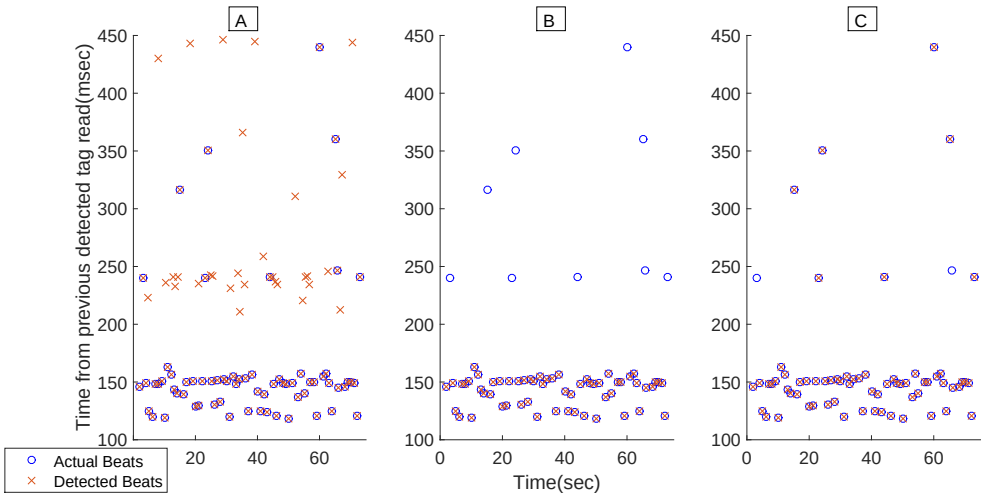

Figure 5.5: Comparison of real and detected beats: A)Setting a threshold at 110ms; B)After applying logistic regression and identifying high probability beats; C) After classifying low probability beats

the 'y-axis' starts at 100 ms so that the continuous tag reads are below this level. This scenario is presented in Fig. 5.5 A. Here, while all actual heart beats are detected (crosses inside circles), there are several false positives as well(standalone crosses). The algorithm is expected to identify and filter out these false positives.

The first 60 seconds of 60BPM heart rate data (about 7000 tag reads) is used to train the model. Fig. 5.5 B shows the result after the high probability beats are detected using the trained model. This step achieves two goals; it identifies beats on which the algorithm has a high level of confidence and subjects the ambiguous data points to further scrutiny. The true beats and the ambiguous data are cycled through regression analysis as described in Section 5.3.2. The result of this process is shown in Fig. 5.5 C. Here, all but two of the actual beats are correctly identified, the first of which was the second beat of the data set and did not have two previous beats for comparison. Such missed beats are accounted for with the process described in Section 5.3.3. It should be noted that the entire process only depends on past data and thus heart beat detection can be done in real-time.

Table 5.3: Heart beat detection and heart rate calculation improvement due to the algorithm

HR	F1 Score		Mean HR (BPM)			
(BPM)	No Algorithm	With Algorithm	No Algorithm	Error	With Algorithm	Error
45	0.86	0.97	79.76	77.2%	45.04	0.09%
60	0.81	0.98	105.75	76.3%	59.97	0.05%
120	0.91	0.98	144.94	20.8%	120.2	0.17%

Table 5.3 compares the performance of the algorithm with the case where beats are detected by setting a fixed threshold. The F1-score, as described in Eq. 5.4, is typically used to analyze the accuracy of data classification. Here, '*Precision*' is the fraction of detected beats that are real and '*Recall*' is the fraction of actual beats that are detected [101]. Thus an F1 score of 1 represents a case where there are no false positives or false negatives. The algorithm provides an improvement in detected heart beats over the threshold method for all heart rates tested. The F1 score of the 120 BPM data without the algorithm is comparatively higher than others in the same column. The 120BPM signal has twice as many heart beats as the 60 BPM signal in the same period; this higher number of actual heart beats improves the fraction of actual beats detected resulting in a higher F1 score.

$$F1_{score} = \frac{2 \times Precision \times Recall}{Precision + Recall} \tag{5.4}$$

Therefore, it can be said that the algorithm works to correctly classify the outages representing heart beats and eliminate false outages.

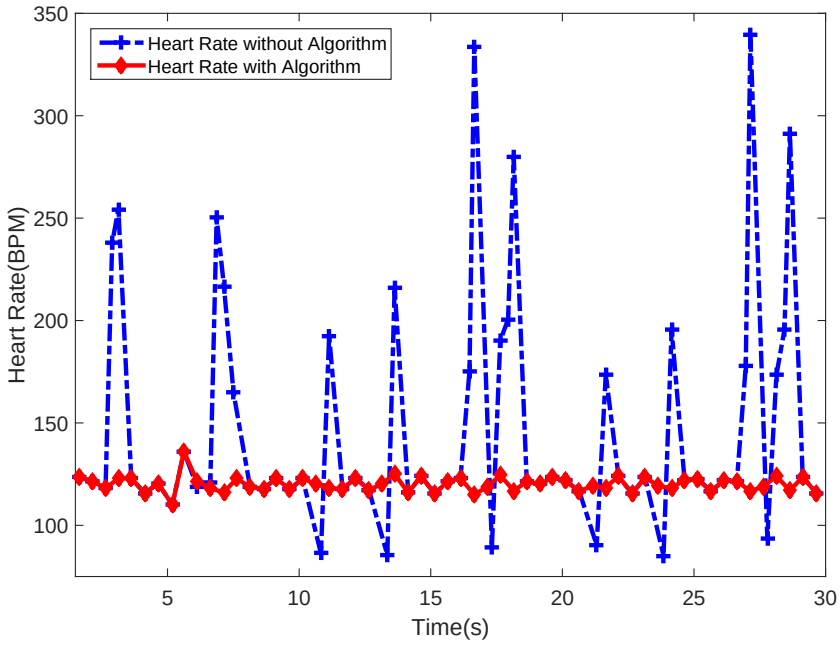

Figure 5.6: Calculated heart rate with and without using the algorithm for a sample of the 120BPM input

5.5.2 Heart Rate Calculation Improvement with the Algorithm

The calculated heart rate for a 120BPM input signal with and without the algorithm are compared in Fig. 5.6. Without the algorithm, the heart rate is unstable and most of the error is due to false beats. These additional beats reduce time between detected beats causing a spike in the calculated heart rate. There are also sudden drops in calculated heart rate for the graph without the algorithm. Here, the missed beats are not accounted for and this leads to a longer duration between detected heart beats thereby causing a lower calculated heart rate.

As can be seen in Fig. 5.6, large time jumps are absent for heart rate with the algorithm. As per Table 5.3, without the algorithm, the calculated heart rate is overestimated by as much as 77%. This is mainly because of false outages which cause spurious spikes in calculated heart rate. The proposed algorithm successfully

filters out these false outages to arrive at an accurate heart rate calculation.

5.6 Conclusions

The heart beat detection algorithm described above has several salient features. Firstly, training is not specific to a specific heart rate range. Once the parameters are extracted for a given protocol setting and outage duration, it can be run for any user in the same environment. The algorithm has the ability to account for errors arising from several sources including hardware glitches, reduced signal strength and presence of multiple tags in a close range. By removing the need for averaging, the algorithm allows for monitoring of heart rate variability. Finally, the algorithm paves the way for applications that allow for the use of multiple RFID tags for different applications at the same time in close vicinity of each other.

The RFID channel depends a lot on the reader settings. The effect of reader settings was shown in Fig. 3.7 where the number of tags read per second varied widely based on the reader settings deployed. Thus it should be noted that this algorithm may not always be required and the effects of noisy environments may be mitigated by using a more appropriate reader setting. However, for situations when there is an excess of false outages due to noise, this algorithm may be helpful.

6. System Enhancements and Applications

In Chapter 4, the hardware implementation of a wireless and battery-free RFID based heart rate monitor was discussed. This current chapter focuses on applications of that system, as well as further analysis for system improvement. Detection of typical heart rate variability and certain heart conditions are first discussed. An infant heart rate monitoring system is then described. Human heart rate data from the RFID heart rate monitoring system is collected and analyzed. Finally, uterine contraction monitoring with the RFID on/off system is further examined.

For all empirical tests conducted in this chapter, the Dense Reader mode [54] setting was used on the RFID reader as this setting was found to be very resilient to effects of additional tags at short distances while improving the tag read rate. A slower reader setting may be used for higher distances at the cost of data resolution.

6.1 Detection of ECG Variations

So far, the heart rate system analysis, has been initiated with a stable ECG signal from the simulator. In reality, the ECG signal varies, not only in terms of rate but also in terms of its shape and amplitude. Some of these rate variations signal health in a human, while others can signal dangerous situations. In either case, a cardiac monitor needs to determine the heart rate and its variability accurately to be viable in practical situations. In this section, heart rate monitoring in the presence of these variations is discussed.

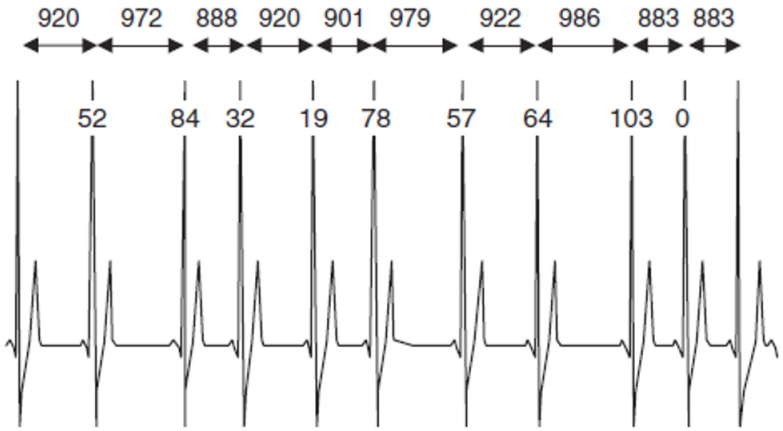

Figure 6.1: An example of heart rate variability with time differences between successive beats shown (units:ms)[2]

6.1.1 Heart Rate Variability

The time between successive heart beats is never constant regardless of how stable a person's heart rate. A typical example of time variation between 'R' waves [2] is shown in Fig. 6.1. Here, both the time between successive beats and the actual variation in these times are shown. Such natural variation in beat-to-beat or 'R-R' intervals is called heart rate variability (HRV).

While normal HRV is considered healthy, reduced HRV may be associated with deeper cardiac problems and a higher mortality risk even in the absence of other symptoms [2]. Hence, continuous monitoring of HRV is essential for identifying possible heart risks. Averaging over a few seconds (as shown in Section 4.4.4) removes the beat-to-beat variability information. Hence, averaging can only be used when long term trends heart rate are to be known. Accurate determination of 'R-R' is imperative to enable heart rate variability analysis. Some tests were thus done to ascertain the system's capability to monitor beat-to-beat variability in heart rate.

6.1.1.1 Test Setup and Data Collection

The system was placed about 3 feet from the RFID reader antenna. The ECG simulator was used to generate two different heart rates; 70 BPM and 110 BPM. For each heart rate, the variation of interval between 'R' waves was changed from 0% to 10% and then 20%. The output of the ECG amplifier was collected using National Instruments myDAQ to act as a reference. Actual 'R-R' intervals were calculated directly from the ECG signal which was sampled at 200 Hz. These intervals were compared with the intervals determined from the RFID on/off system. About 2 minutes of data was collected for each data set. The MATLAB script used to process and analyze this data is shown in Appendix B

6.1.1.2 Beat-to-Beat Variability Analysis

A comparison between actual and calculated 'R-R' intervals for the source 70 BPM signal is shown in Fig. 6.2. In the top plot, the source variation in 'R-R' intervals is set to be zero. As expected, the RFID calculated intervals closely match the actual ones. The slight variations can be explained due to the variations in tag read times. The middle plot shows the result when the 'R-R' varied from the mean by about 10%. Even in this case, the RFID results match the actual intervals. Similar results are seen for 20% variations as well. The data for these tests are summarized in Table 6.1. For each case the mean and standard deviation of the calculated 'R-R' intervals are exactly the same for the actual data and the RFID results. The mean error and the standard deviation of the error are both very small. In fact, most of the RFID 'R-R' intervals can be expected to be within 6 ms of the actual intervals. The correlation between the source and RFID intervals is shown in Fig. 6.3. The correlation coefficient [67] was calculated to be 0.9988 with a 95% confidence.

The heart rates calculated for the beat-intervals shown in Fig. 6.2 are shown in

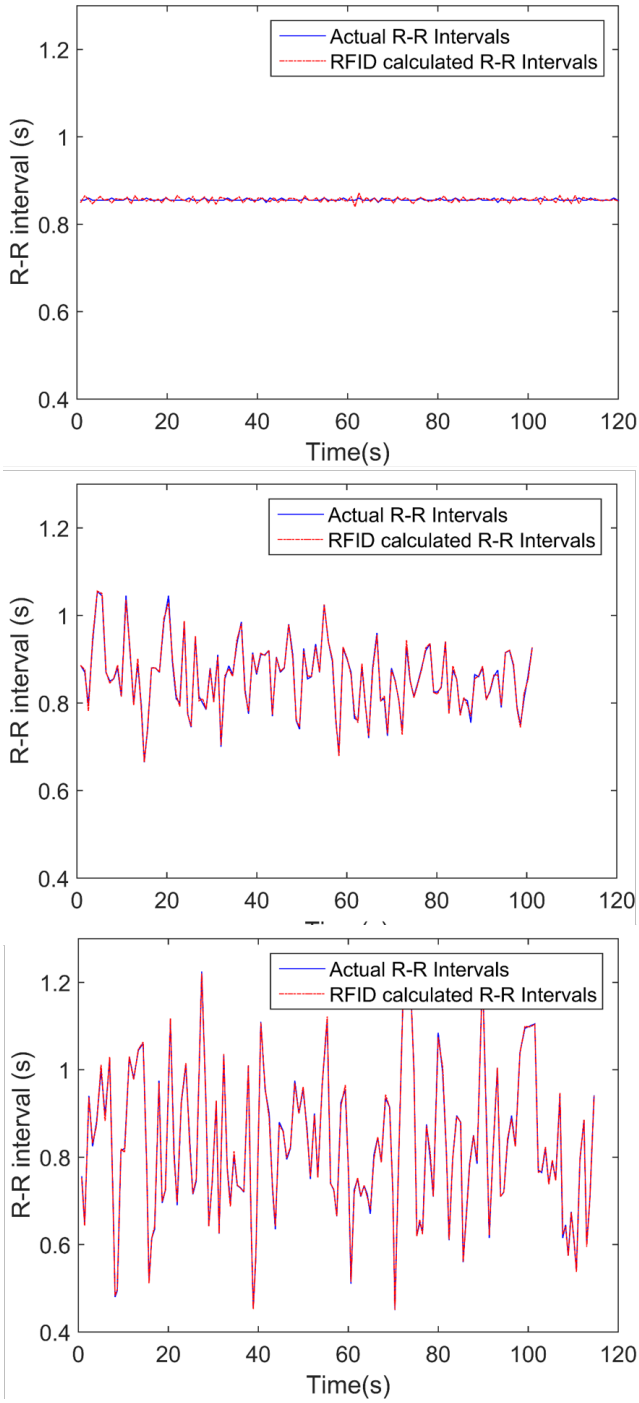

Figure 6.2: Comparison of actual and RFID R-R intervals for heart rate around 70 BPM with R-R variation: No variation (top), 10% variation (middle), 20% variation

Table 6.1: R-R interval determination accuracy for heart around 70 BPM

Parameter	R-R Variation		
—	0%	10%	20 %
Mean R-R(s)	0.856	0.858	0.813
STD R-R(s)	0.002	0.078	0.169
RFID mean R-R(s)	0.856	0.857	0.813
RFID STD R-R (s)	0.005	0.078	0.169
Mean error (s)	-9.66× 10^{-5}	-1.41× 10^{-4}	-7.6× 10^{-5}
STD Err (s)	0.005	0.006	0.006

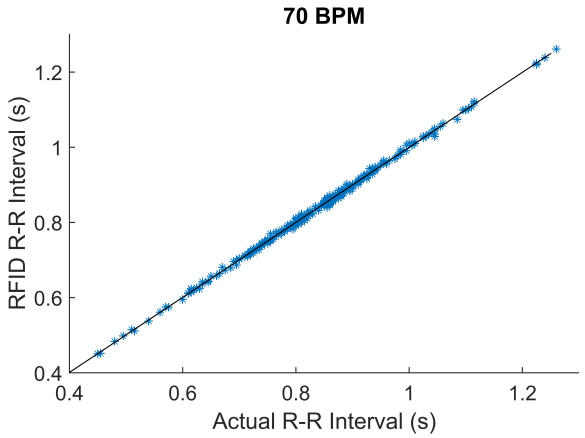

Figure 6.3: Correlation between actual and RFID determined R-R intervals for heart rate around 70 BPM

Fig. 6.4. The comparison between the actual and RFID calculated 'R-R' intervals for 20% variation in the 110 BPM source signal are shown in Fig. 6.5. The data for the 110 BPM tests are summarized in Table 6.2. The correlation coefficient between

the actual and RFID data was calculated to be 0.9973.

Table 6.2: R-R interval determination accuracy for heart around 110 BPM

Parameter	R-R Variation		
—	0%	10%	20 %
Mean R-R(s)	0.544	0.547	0.537
STD R-R(s)	0.002	0.057	0.125
RFID mean R-R(s)	0.544	0.547	0.536
RFID STD R-R (s)	0.006	0.057	0.125
Mean error (s)	-1.03$\times$ 10^{-4}	-1.06$\times$ 10^{-4}	-5.88$\times$ 10^{-5}
STD Err (s)	0.006	0.006	0.006

6.1.2 Arrythmia Detection

As discussed in Section 2.1.2.1, an arrythmia is a change from the normal sequence of ECG activity. Unlike the normal heart rate variability described in the previous section, arrhythmia can manifest as a sudden appearance or absence of beats or even drastic change in heart rate (rate arrythmias) or sudden changes in the regular shape of the ECG wave (shape arrythmias). Only rate arrythmias can be detected using the RFID on/off system as by relying on 'R' wave detection alone, shape information of the ECG signal is lost. In this section, some examples of rate arrythmia detection are discussed.

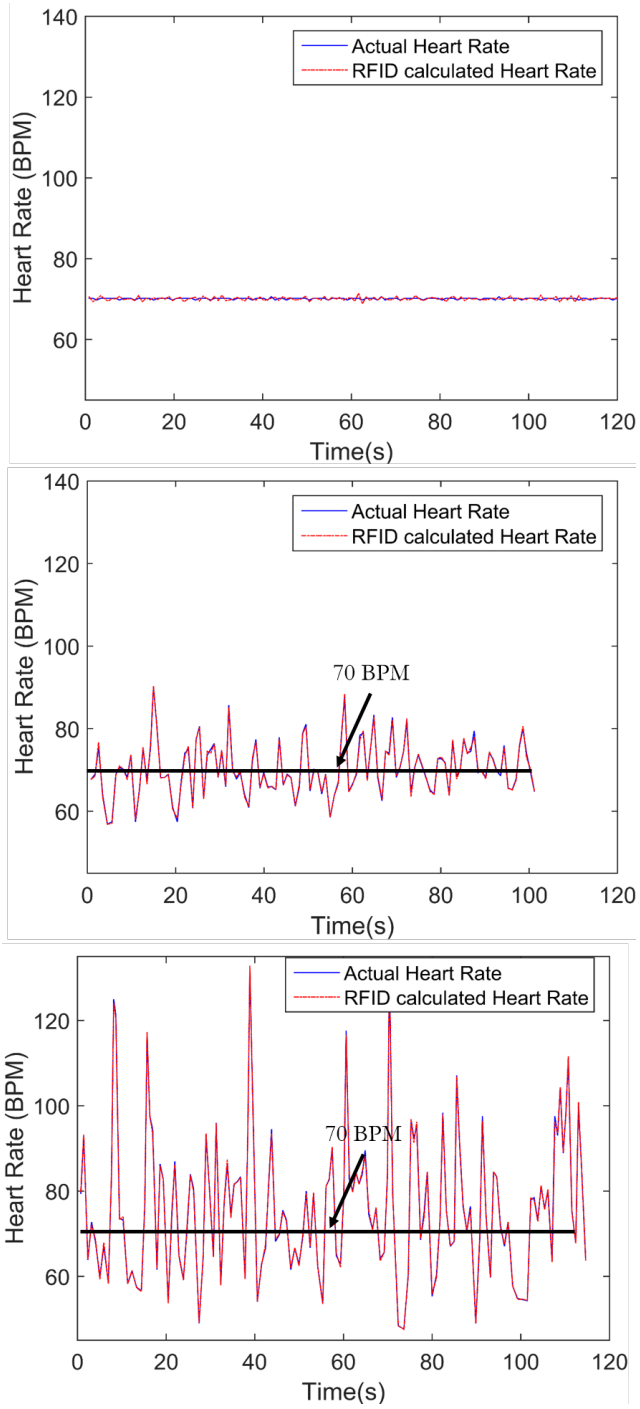

Figure 6.4: Comparison of actual and RFID heart rate for heart rate around 70 BPM with R-R variation: No variation (top), 10% variation (middle), 20% variation

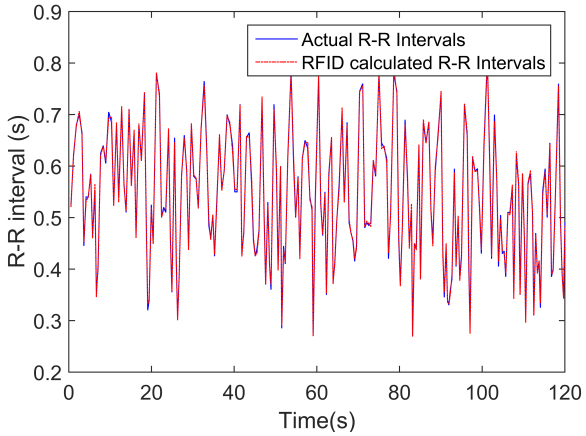

Figure 6.5: Comparison of actual and RFID R-R intervals for heart rate around 110 BPM with 20% R-R variation

6.1.2.1 Bradycardia and Tachycardia

The simplest forms of rate arrythmias are bradycardia and tachycardia. A sustained heart rate of less than 60 BPM in adults is classified as bradycardia whereas a sustained heart rate of over 100 BPM is called tachycardia [13]. Detection of these conditions is possible using the RFID on/off system. These conditions were simulated using the setup described in Section 6.1.1.1. The heart rate on the simulator was varied from 75 BPM to 45 BPM for bradycardia and from 75 BPM to 140 BPM for tachycardia. The results of these tests are shown in Figs. 6.6 and 6.7. In both cases, the RFID output closely followed the actual simulator generated heart rate.

6.1.2.2 Premature Contractions

Premature ventricular or atrial contractions could trigger another 'R' wave while interrupting the normal sinus rhythm. The bigeminy condition showed in Fig. 2.3, where heart beats appear in pairs, is caused due to premature contractions. Considerable research has been conducted to identify premature contractions from ECG

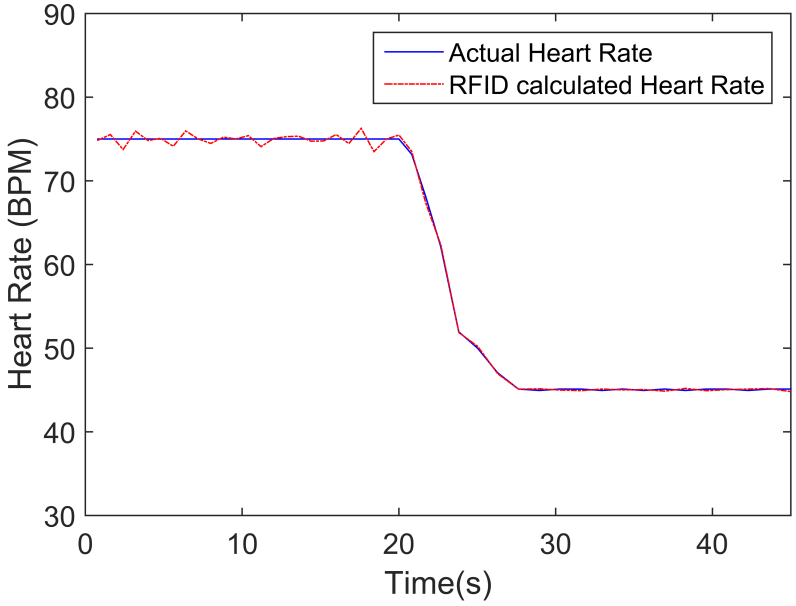

Figure 6.6: Bradycardia detection

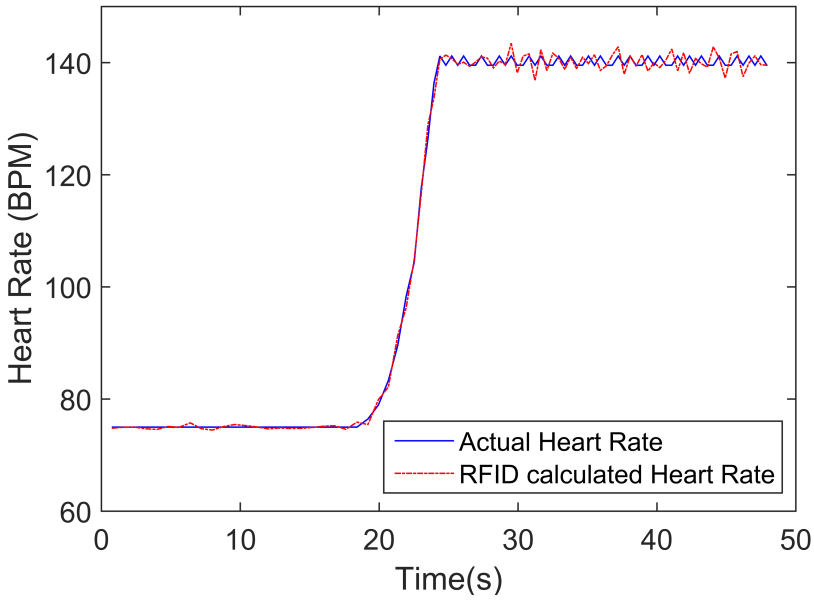

Figure 6.7: Tachycardia detection

signals using classification algorithms [40, 57, 89]. These algorithms use shape and timing features of ECG waves to detect premature cardiac contractions. The current work can only provide timing intervals between 'R' waves and no other shape features of the source ECG signal. Hence, the RFID on/off method in its current form is inadequate to detect premature heart contractions with absolute certainty. However, for most methods in literature, sudden irregularities in the timing of 'R-R' intervals are used as a prominent feature in identifying premature cardiac contractions. Thus, the RFID on/off method can be used as a basis for further detailed investigations. However, it is important to ascertain that the outage durations are short enough so that the sudden occurrence of such premature contractions are indeed detected by the RFID on/off system and not lost in the previous RFID outage.

Premature ventricular contractions (PVC) were simulated using the Laerdal SimBaby infant patient simulator (described in detail in the upcoming Section 6.2) which is capable of generating ECG signals with many cardiac conditions in addition to other infant health problems. The RFID system was connected to the ECG outputs of the simulator. The simulator was programmed to create PVCs The timing between the regular and premature contraction varies and is controlled by the simulator. The user is allowed to control the general heart rate and the frequency of occurrence of PVCs. The typical heart rate for the test was chosen to be 60BPM with a higher than 90% occurrence of PVCs. The amplified ECG of the simulator output is shown in Fig. 6.8 (top), note that the ECG waves are inverted such that the 'R' wave peaks towards 0 V. PVCs can be seen adjacent to four of the regular sinus beats. The corresponding time between RFID tag reads is shown in the bottom of Fig. 6.8. An RFID outage can be clearly seen for each ECG spike, whether it is a regular beat or a PVC.

The 'R-R' intervals for the premature contraction test described above for over one minute of monitoring is shown in Fig. 6.9. The 'R-R' interval largely oscillates

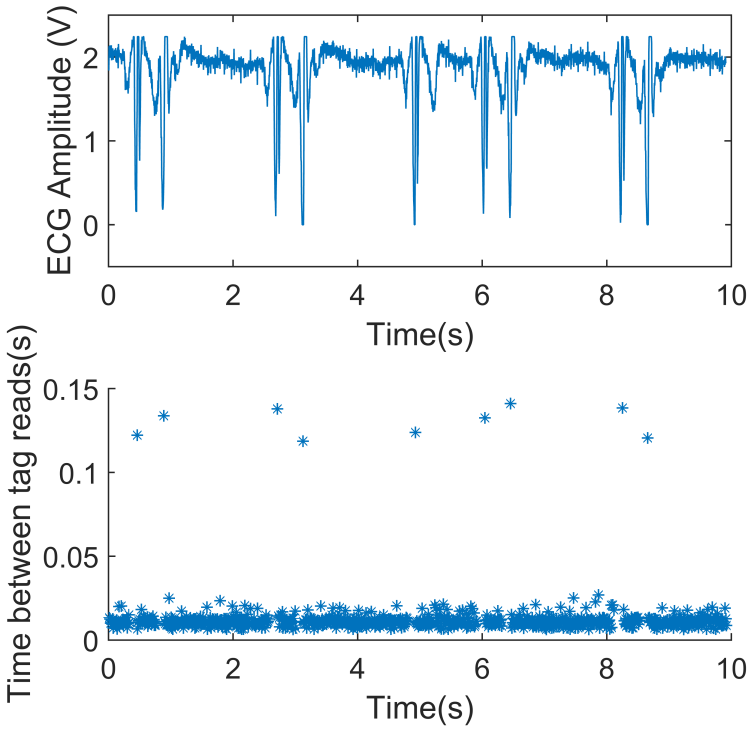

Figure 6.8: Detection of premature venticular contractions

between a low and a high value. The low value corresponds to a PVC and the higher value corresponds to regular sinus rhythms. There are three instances (around 20s, 34s and 48s) where the 'R-R' interval is relatively flat; these instances represent consecutive sinus beats without PVCs. The RFID calculated 'R-R' intervals follow the actual intervals closely, except for one instance close to about 45s. The RFID 'R-R' interval there is reduced because of a false triggering of the heart rate detection circuit caused by a noise spike. This spurious spike is shown in Fig. 6.10 with a black circle. The spike was caused due to the starting of a compressor close to the measurement setup. The system is, thus, not immune from such ambient noise sources.

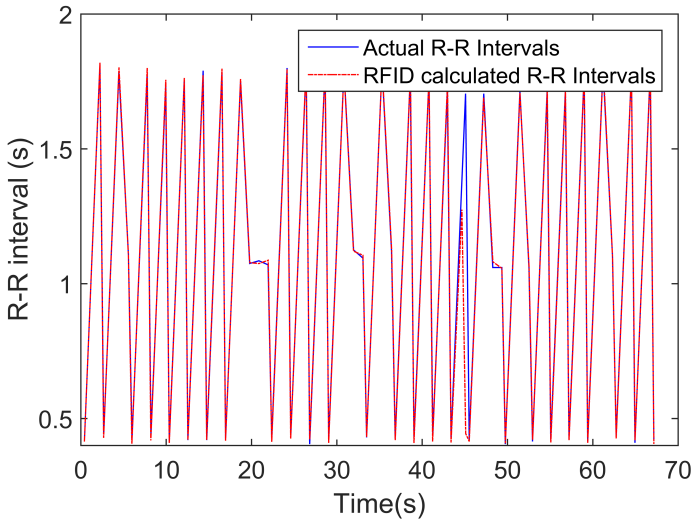

Figure 6.9: R-R intervals with premature ventricular contractions

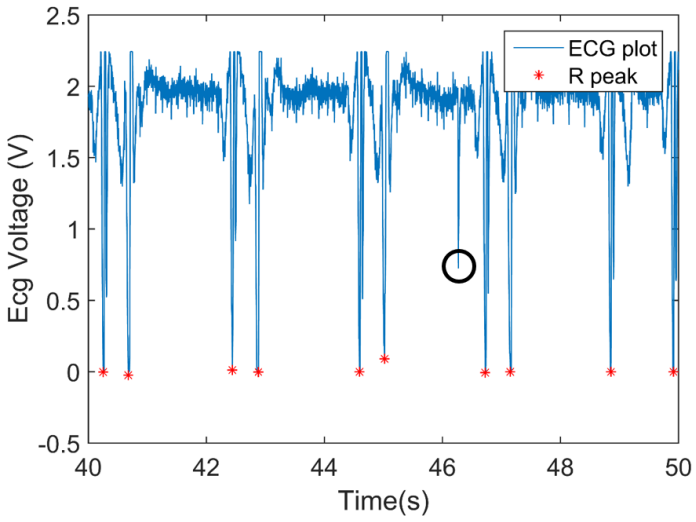

Figure 6.10: False trigger source for 'R' wave detection

6.1.3 Baseband Wander

An ECG wave typically wanders around a baseline and is not always stable. This wandering may be caused due to impedance changes in the electrode or slight move-

ments of the torso due to respiration. The frequency of this wander is usually below 0.5 Hz. [38]. An example of such wandering is shown in Fig. 6.11. This example was generated using the Tech Patient Cardio ECG simulator which has the capability of generating ECG waves that mimic the typical baseband wander in ECG signals.

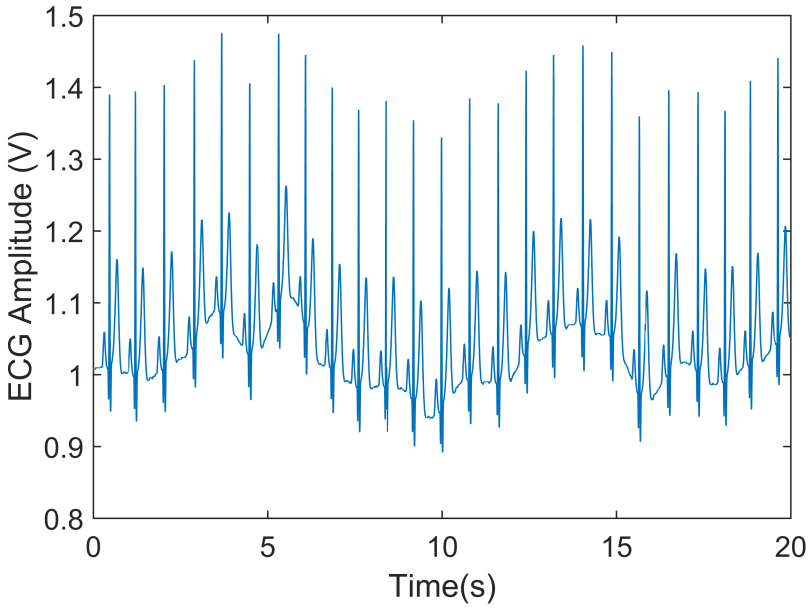

Figure 6.11: ECG baseline wander

If the baseband were to reduce drastically, it could potentially cause a reduction in the 'R' wave voltage such that it is not detected by the heart beat detection circuit. On the other hand, if the baseband were to rise, it could cause false triggering due to the detection of 'P' waves. The ECG amplifier discussed in Section 4.3 is expected to mitigate these issues caused by baseband wander due to filtering and biasing of inputs. The RFID heart rate monitoring output in the presence of baseline wander is compared to the actual heart rate in Fig. 6.12. For this figure, 5% variations in 'R-R' intervals around 75 BPM in addition to baseline wander in the source ECG

signal are used. Here again, the RFID output matches the actual signal very closely and the correlation coefficient was calculated to be 0.9943.

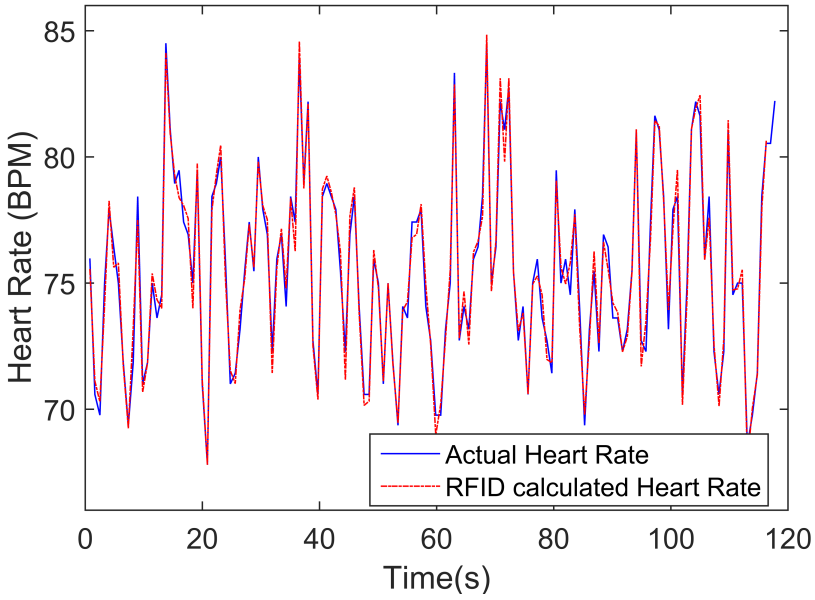

Figure 6.12: Comparison of actual and RFID detected R-R intervals in the presence of baseline wander

It can be concluded that teh RFID on/off system is capable of detecting typical beat-to-beat heart rate variability. Common rate arrythmias can also be detected using the system. The system is resilient in the presence of baseband wander.

6.2 Infant Cardiorespiratory Monitoring

Infants are a special group of people that might benefit tremendously from comfortable wearable monitoring devices. Studies have shown that continuous heart rate monitoring has led to an increase in patient survival rate especially in Neonatal Intensive Care Units (NICU) [30, 75]. By continuous monitoring of Electrocardiogram

(ECG) signals, critical conditions such as bradycardia and tachycardia in infants can be detected [82]. A detailed study on neonatal bradycardia is presented in [86]. For infants, bradycardia is defined as sustained heart rate below 80 BPM while awake and below 60 BPM while asleep [86]. If a cardiac condition like bradycardia is detected, it can be mitigated by external stimulation such as rubbing the baby [92]. Hence, alarm systems in addition to continuous monitoring are essential. A wireless and battery-free solution like the one discussed in this work is ideal for such continuous infant monitoring.

While the system described so far can be used to monitor an infant's cardiac activity, a complete infant monitoring system requires respiration monitoring as well. 'Apnea' is a critical condition where breathing stops for a period longer than 20 seconds or even a shorter duration accompanied with bradycardia [91]. In fact, apnea and bradycardia can often be related events. Cessation of breathing due to an apnea can reduce oxygen levels which in turn may induce a reflex slowing of the heart or bradycardia [79]. The American Academy of Pediatrics recommends home cardiorespiratory monitoring for infants that are at risk of apnea, bradycardia and hypoxemia or if they have other conditions that effect cardiac or breathing functions [91]. Hence, it is essential that cardiac monitoring happen in consonance with respiration monitoring for infants. For the benefits of the wireless and battery-free heart rate monitor to stay, the complementary respiration monitor should also have similar features. Hence, a respiration monitor that works on RFID technology and is suitable for continuous monitoring is required. The passive RFID respiration rate monitor described in Section 2.3.1.2 is well suited for this application.

A vision for an integrated RFID based infant monitor that combines heart and respiration monitoring is shown in Fig. 6.13.

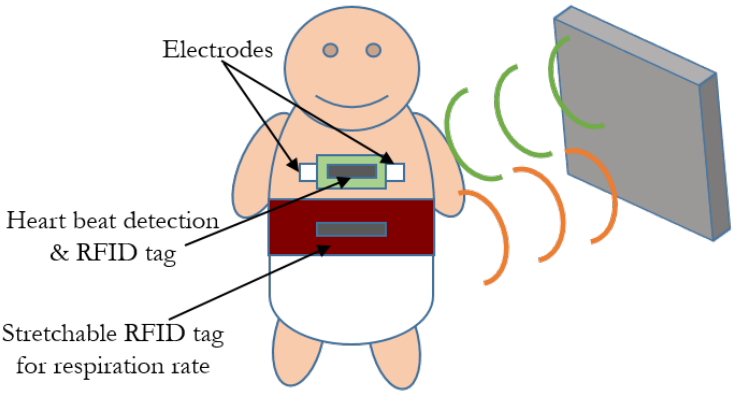

Figure 6.13: RFID based heart and respiration rate monitoring

6.2.1 Infant Monitor Test Setup

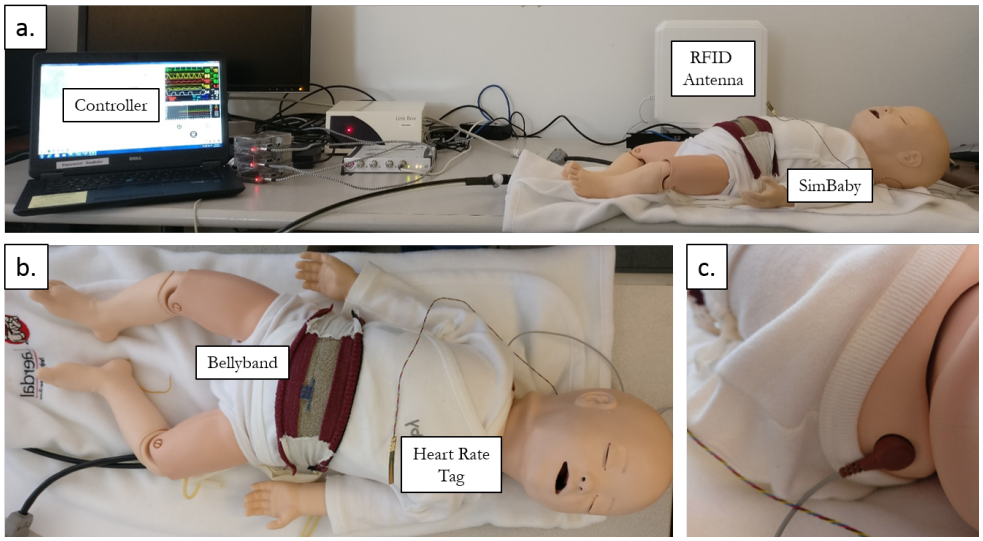

Figure 6.14: Setup for data collection: a. Complete Setup; b. SimBaby with fabric band and heart rate RFID tag; c. Contact for ECG signal

The goal of this exercise is to demonstrate the utility of the proposed RFID system

in monitoring critical cardiorespiratory conditions in infants. Hence, a SimBaby [66], which is a programmable infant mannequin is employed to get source data. The SimBaby is a life size model of an infant which is used to train medical practitioners for infant care. Using a connected computer, the mannequin's behavior and vital signs, which include its ECG signal, heart rate, respiratory activity, oxygen saturation and a host of other parameters, can be controlled. The ECG activity can be recorded by connecting electrodes to the right and left arm of the baby (shown in Fig. 6.14c). The SimBaby's abdomen rises and falls with every breath and hence its respiratory activity can be simulated by putting the RFID band on its abdomen. An image of the SimBaby with the fabric band and the heart rate monitoring system is shown in Fig. 6.14b. The overall data collection setup with the RFID antenna, SimBaby and the controller is shown in Fig. 6.14a.

The SimBaby control software was employed to simulate bradycardia and apnea. The performance of the heart rate monitor was first tested independently so that the performance degradation due to the presence of an additional respiration monitoring tag can be understood. To simulate bradycardia, the baby's heart rate was varied from 100 BPM to 75 BPM and then finally to 55 BPM. The actual heart rate was calculated by connecting a data acquisition module (National Instruments myDAQ) to the amplified ECG signal collected from the SimBaby. The RFID system error and correlation for heart rate measurement were calculated. The heart rate and respiration rate monitoring systems were then put together as shown in Fig. 6.14a and b. A scenario was programmed into the SimBaby, wherein the baby would be breathing for one minute and then stopped breathing for another minute to simulate apnea. For bradycardia, the baby's heart rate was set to decrease to 60 BPM after staying at 110 BPM for one minute. This scenario is illustrated in Fig. 6.15. The heart rate calculation error in the presence of the respiration rate tag was also studied.

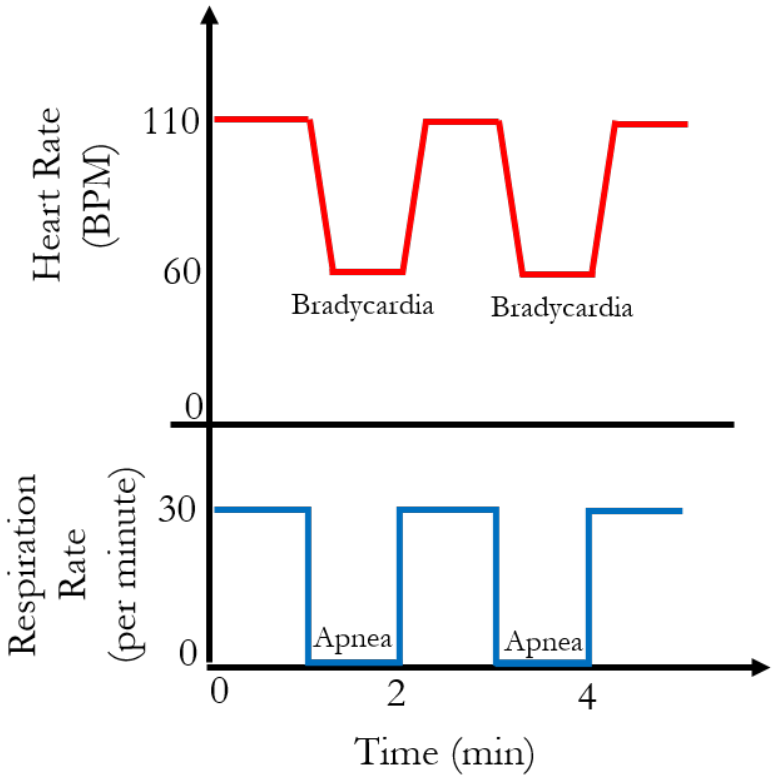

Figure 6.15: Bradycardia and apnea simulation scenario with the SimBaby

It should be noted that the development of the respiration rate monitor and the data analysis associated with it is not a part of this dissertation.

6.2.2 Infant Monitor Test Results

The first part of this section discusses the use of the RFID heart rate monitor with the infant simulator. The second part of the section investigates the heart rate monitor's performance in the presence of the respiration rate RFID tag.

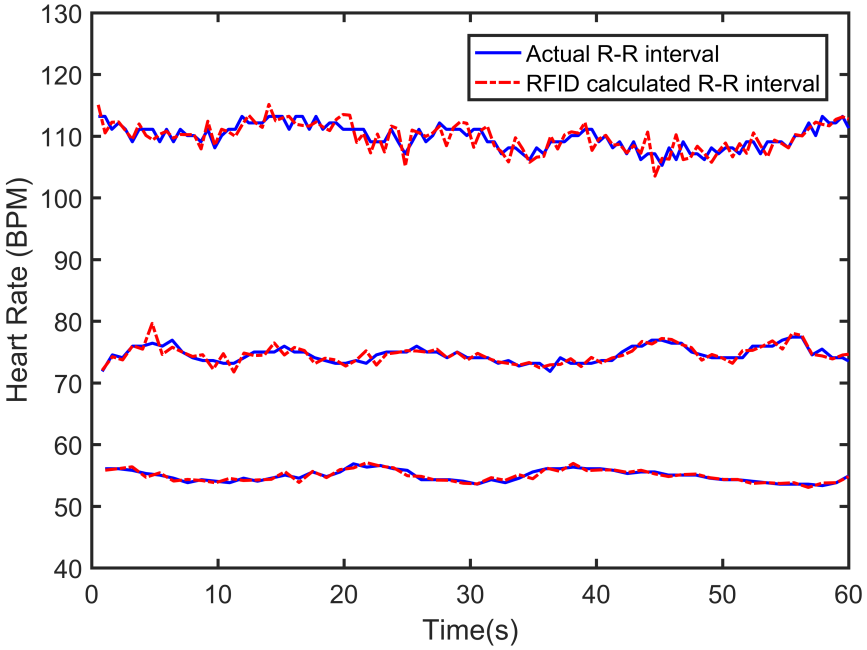

Figure 6.16: Comparison of actual and RFID calculated heart rates for ECG signals sourced from the SimBaby

6.2.2.1 Heart Rate Monitoring using SimBaby

The Fig. 6.16 shows the first 60 seconds of actual and calculated heart rates for three different heart rate settings; 110 BPM, 75 BPM and 55 BPM. It should be noted that the last two settings can be classified as bradycardia for an infant while awake and asleep respectively. For all three heart rate settings, the RFID calculated heart rate closely follows the actual heart rate. Table 6.3, compares the mean and standard deviation of actual and RFID calculated 'R-R' intervals. The mean error and the standard deviation of error are also calculated. The mean error is of the order of hundreds of microseconds and the standard deviation of error is less than 10 *ms* for all settings.

The SimBaby was also programmed to gradually transition from 110 BPM to 75 BPM to 55 BPM over 20 second intervals in a separate test. The actual and RFID

Table 6.3: R-R interval determination accuracy for three different heart rates

Parameter	Heart Rate Setting		
—	55 BPM	75 BPM	110 BPM
Mean R-R(s)	1.093	0.800	0.547
STD R-R(s)	0.017	0.014	0.009
RFID mean R-R(s)	1.093	0.800	0.547
RFID STD R-R (s)	0.018	0.016	0.012
Mean error (s)	-1.97× 10^{-4}	-1.12× 10^{-4}	-1.17× 10^{-4}
STD Err (s)	0.008	0.009	0.009

calculated heart rates for this test are shown in Fig. 6.17. The correlation between the two sets was calculated to be 0.9976.

The same test was performed after the addition of the respiration rate tag effectively adding noise to the heart rate tag channel. Their comparison is shown in the next section.

6.2.3 Heart Rate Monitoring with Respiration Rate Monitoring

The comparison of the error in RFID calculated 'R-R' intervals and its correlation with the actual intervals with and without the respiration rate tag are shown in Table 6.4. The performance does not deteriorate significantly after the respiration rate tag is added. The standard deviation of error increases from about 7 ms to 12 ms and this can be attributed to the time spent in reading the respiration rate tag which marginally increases the time between tag reads of the heart rate tag and causes some tag reads to be missed as discussed earlier. The correlation with the actual

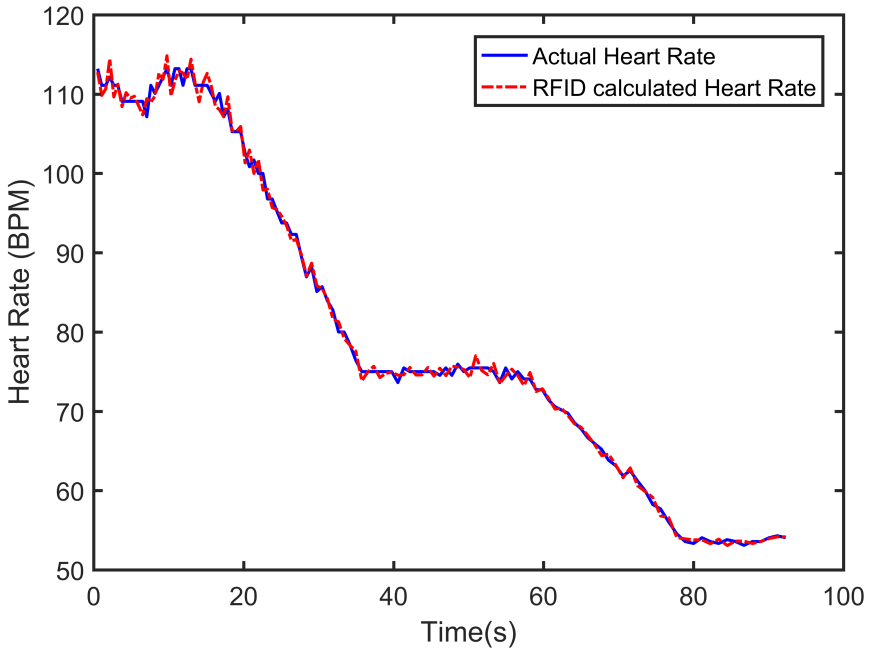

Figure 6.17: Comparison of actual and RFID calculated heart rates for bradycardia simulated using SimBaby

heart continues to remain very high even after the addition of the respiration rate tag which had nearly 55 % of the tag reads over the measurement period.

Table 6.4: Comparison of actual and RFID calculated 'R-R' intervals in the absence and presence of the respiration rate bellyband tag

Test	Mean Error (s)	Std Dev of Error (s)	Corr. Coeff.
Without Respiration Tag	-1.28×10^{-4}	0.007	0.9993
With Respiration Tag	-8.02×10^{-4}	0.012	0.9957

The Fig. 6.18 shows detection of bradycardia and apnea using the RFID based

heart and respiration rate monitors. The heart rate is held steady around 110 BPM for one minute and then bradycardia is simulated by dropping the heart rate to 60 BPM for the next minute. This cycle is repeated for a total period of five minutes. For respiration rate, the rate is held around 30 breaths per minute for a minute followed by the same period of no breathing activity. Periods of apnea and bradycardia are clearly visible in Fig. 6.18. The heart rate plot has a drop in heart rate at around 30 seconds due to a missed beat which may have been caused due to a sudden rise in baseline of the SimBaby ECG signal. Two spikes in heart rate can also be seen around 200 and 240 seconds. These were caused due to the the start of the SimBaby compressor which creates a spurious noise impulse that triggers the heart beat detection circuit thereby creating an outage.

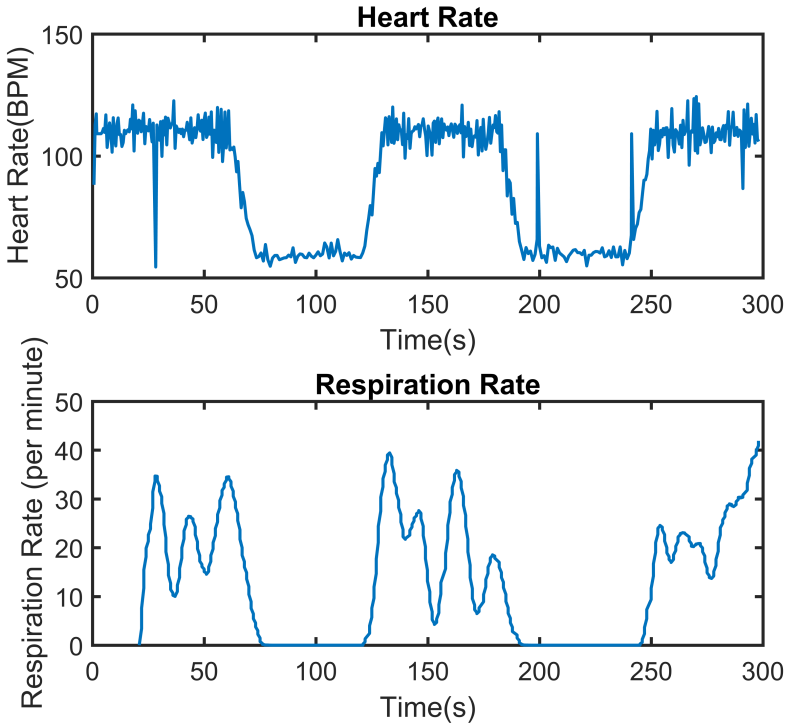

Figure 6.18: Detection of bradycardia and apnea using RFID tags

This section showed that the heart rate monitoring tag can be used in tandem with another tag to monitor critical conditions like bradycardia. The results obtained here open doors for combining the heart rate monitoring system with other sensors for continuous health monitoring.

6.3 Wearable Platform for Infant Cardiac Monitoring

The infant cardiorespiratory system discussed in the previous section included a wearable band for respiration monitoring. However, it lacked a wearable platform for heart rate monitoring. In this section, a wearable eco-system for infants that integrates a wearable onesie and a mobile user interface with the RFID heart rate monitoring system, is described.

6.3.1 System Block Diagram

A wearable heart rate monitoring onesie design and implementation is illustrated in Fig. 6.19. The wearable component of the system consists of a onesie integrated with two fabric electrodes and its interconnects for detecting the ECG pulse. A onesie is chosen because of its simplicity, design and mainly because it is the kind of clothing that is worn at most times by a baby. The electrodes consist of padded pieces of conductive fabric (TechniTex P180+B [116]). The two connectors on the onesie are attached to the inputs of the RFID heart rate monitoring circuit which was described in Chapter 4. The heart rate monitoring circuit includes the ECG amplifier, 'R' wave detection circuit and the power harvester in addition to a separate RFID tag (not shown in Fig. 6.19). An antenna connected to the RFID reader captures the RFID tag information, and then feeds the data into a processing unit. A Raspberry Pi 2 Model B is used as the data collection and processing unit. Heart rate is calculated in real-time on the processing unit. The calculated heart rate is then communicated

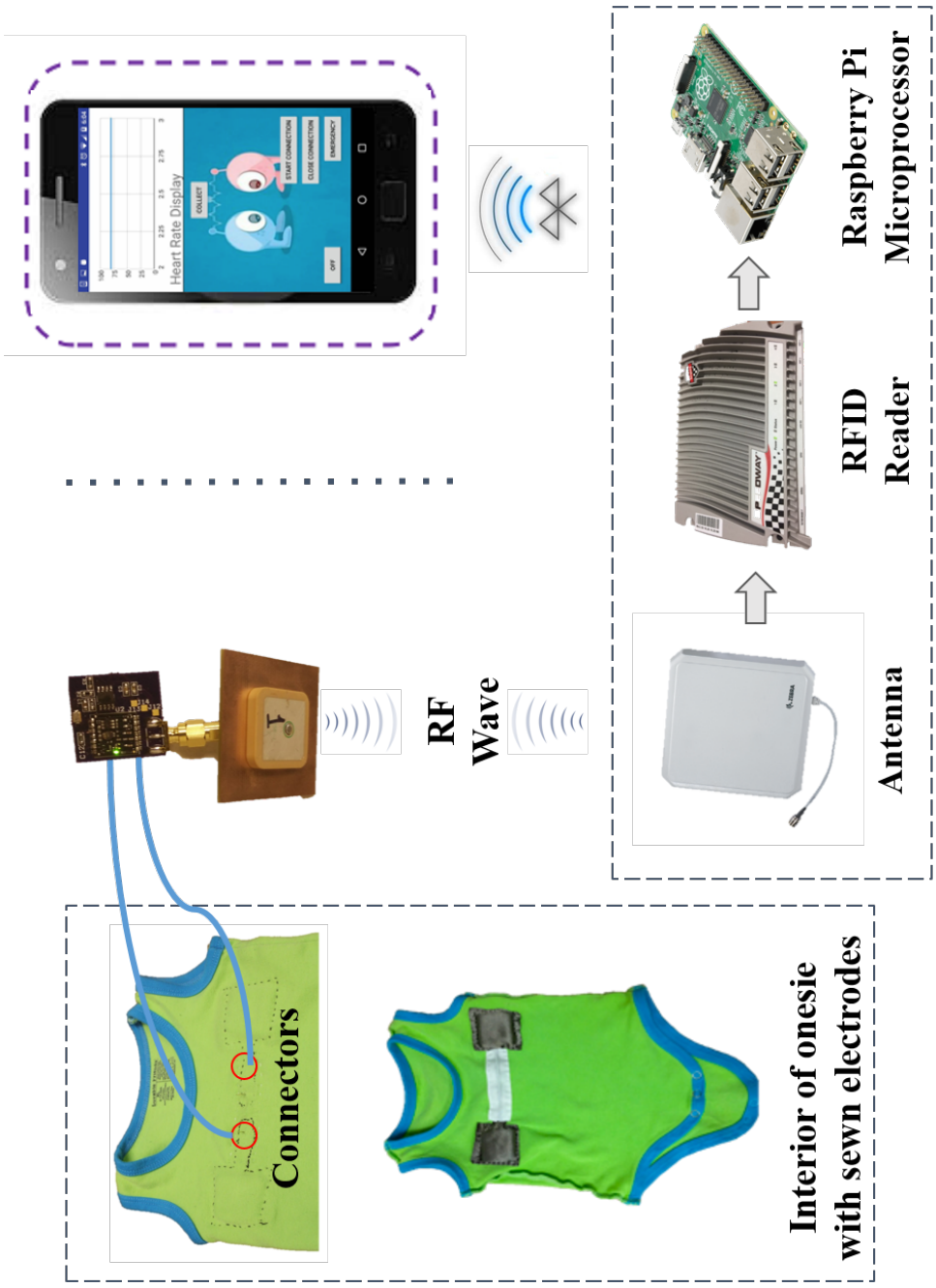

Figure 6.19: Wearable heart rate monitoring onesie: System architecture and design

via Bluetooth to a mobile app which allows the user to interpret the heart rate data. In this way, an end-to-end integrated solution for infant heart rate monitoring right

from sensing the ECG signal through to displaying of the calculated heart rate can be implemented. The main features of this system are described in the next section.

6.3.2 System Features

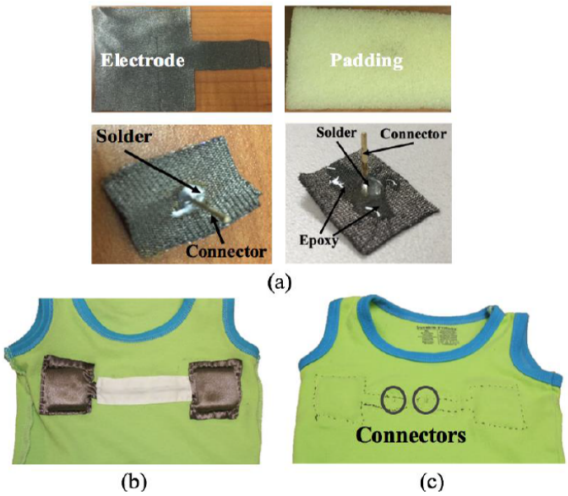

Figure 6.20: Baby onesie with electrodes and connectors:a) individual components used, b) interior of onesie with electrodes, c) front view of onesie with electrodes and connectors sewn

The wearable onesie has fabric electrodes which are not only more comfortable than sticky gel electrodes but are also reusable and can withstand several wash-cycles. The integration of these electrodes on the onesie is shown in Fig. 6.20. The RFID data is processed on the Raspberry Pi in real time and heart beat data is calculated by using averaging as described in Section 4.4.4. A local alarm system integrated with the processing unit is used as an emergency backup system to alert people nearby in case the babys heart rate is not in the normal range of 80 BPM to 180 BPM [82] or if there is a communication failure between any of the components of the system. The

Raspberry Pi also has a bluetooth connection module which can be used to connect to handheld mobile devices to transmit heart rate information. A mobile application was created to communicate not only the current heart rate but also raise alarms in case a critical heart condition is detected for the baby.

Additional details about system design and end-to-end performance can be found in [4].

6.4 Human Data

The results in the preceding sections were based on ECG signals obtained from simulators. It was seen that the RFID system heart rate output closely matched the actual heart rate generated by the simulators. As a final step in validating the system, system tests were done with human subjects. The results of these tests are discussed in this section.

6.4.1 Human Tests Setup

A pair of commercial dry gel electrodes (Kendall 230 Foam Electrodes) were placed on the human subjects' torso to acquire their ECG signal. The human ECG was amplified using the RFID system and its output was probed using a data acquisition (DAQ) module (NI myDAQ) at a sampling frequency of 200 Hz. The data acquired by the DAQ served as the reference signal for comparison. The remaining setup was similar to the one described in Section 6.1.1.1. Over two minutes of continuous data was collected from each individual subject. These tests were conducted after obtaining protocol approval from the Institutional Review Board (IRB) at Drexel University.

6.4.2 Human Tests Results

Fig. 6.21 shows an example of the ECG signal collected using the DAQ over 40 seconds. The ECG here is inverted again as the heart rate detection circuit triggers on negative edges. The detected 'R' peaks used for calculating actual 'R-R' intervals are also shown in this figure.

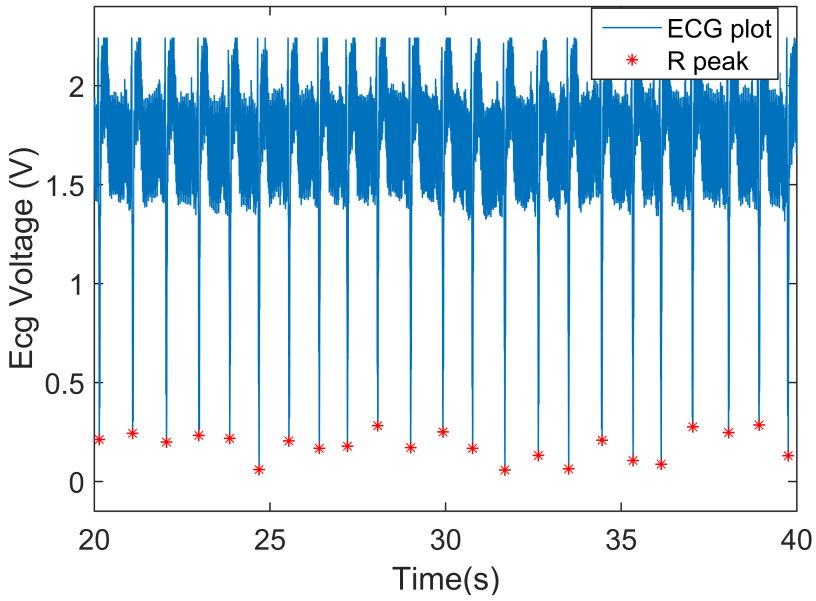

Figure 6.21: Representative ECG signal from a human subject with 'R' peaks marked

A comparison of actual 'R-R' intervals with the RFID determined 'R-R' intervals for one human subject is shown in Fig. 6.22 for over two minutes if data. The RFID calculated 'R-R' interval matches the real interval very closely. The same comparison with heart rate instead of beat intervals is shown in Fig. 6.23.

The data for all human tests are summarized in Table 6.5. For all human subjects the mean error in calculating 'R-R' intervals is smaller than 0.1 ms and a standard

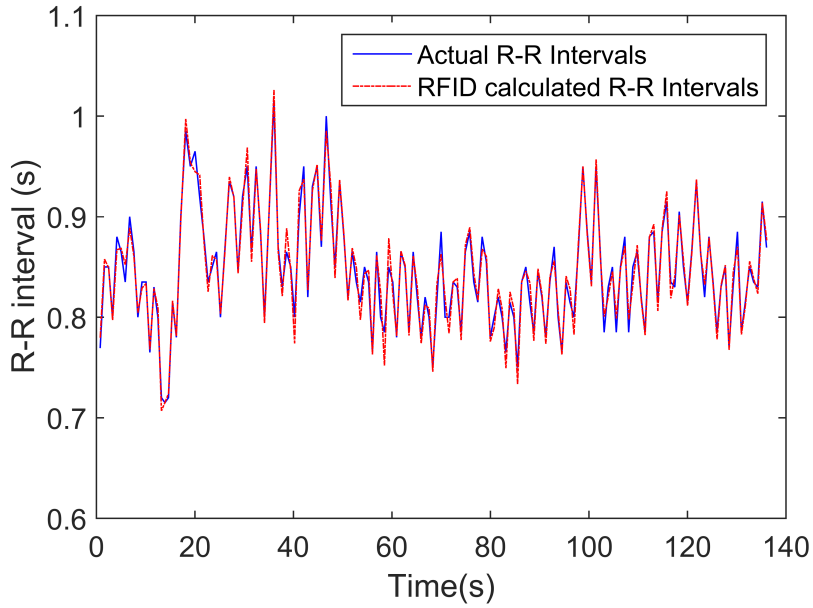

Figure 6.22: 'R-R' interval from human subject 1

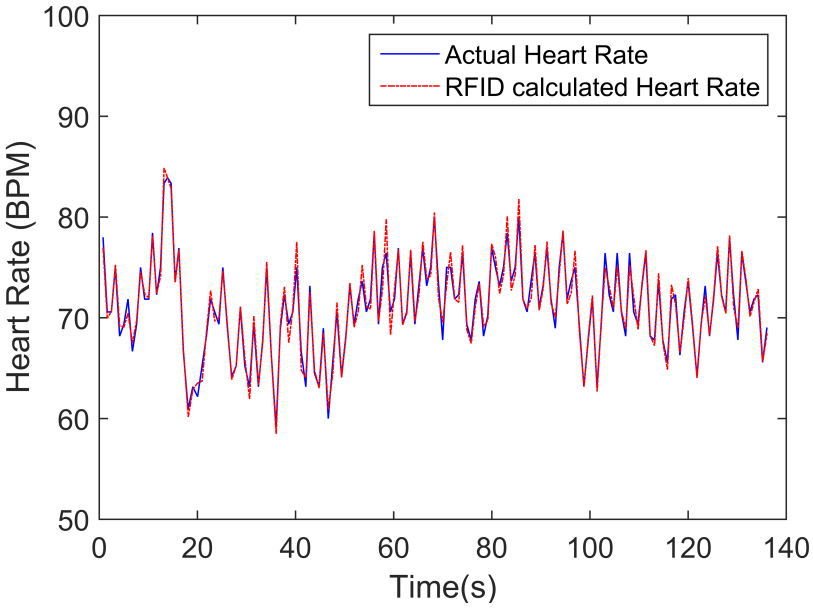

Figure 6.23: Heart rate from human subject 1

deviation of error less than 10 ms. Nearly 20 seconds of the data from the sample obtained from subject 3 had to be excluded because the subject had a violent bout of cough during measurement. The excluded period is shown within a dotted box in Fig. 6.24. It is interesting to observe that the 'R-R' interval reduced (heart rate increased) while the subject anticipated the coughing bout and once the episode was over, the 'R-R' interval steadily increased (heart rate decreased). For subject 4, one heart beat was missed due to a sudden shift in ECG baseline caused by subject movement. The error due to this missed beat is excluded from the results presented in Table 6.5 for subject 4.

Table 6.5: Comparison of actual and RFID calculated 'R-R' intervals for human tests

Subject	Actual Data (s)		RFID Data (s)		Error (s)		
	Mean	Std Dev	Mean	Std Dev	Mean	Std Dev	Corr. Coeff.
1	0.845	0.055	0.845	0.056	-1.79×10^{-4}	0.01	0.9835
2	0.824	0.049	0.824	0.05	-9.4×10^{-5}	0.006	0.9920
3[1]	0.773	0.135	0.773	0.124	-4.4×10^{-6}	0.009	0.9979
4[2]	0.739	0.041	0.740	0.041	-6.9×10^{-5}	0.006	0.9901
5	0.899	0.047	0.899	0.047	-8.0×10^{-5}	0.007	0.9877

Fig. 6.25 compares the actual and RFID calculated heart rate after the subject's heart rate was elevated immediately after doing some exercises. The subject was at rest while the data was collected. The data is for the same subject as in Fig. 6.23

[1]Almost twenty seconds of data excluded due to subject coughing
[2]Missed beat excluded

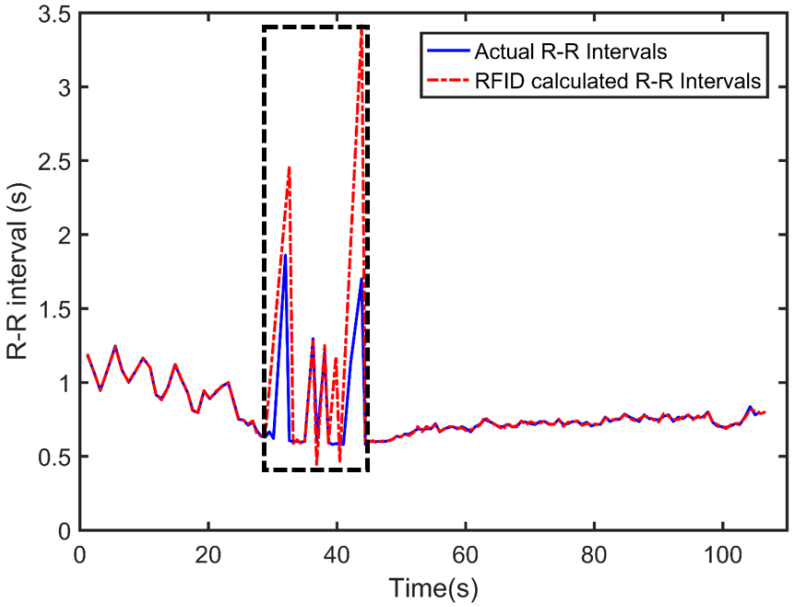

Figure 6.24: 'R-R' interval calculation error due to coughing

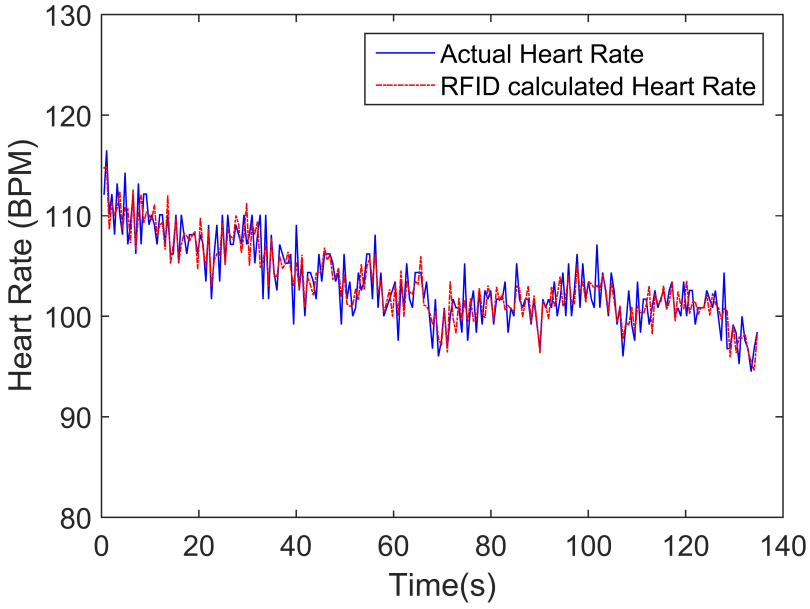

Figure 6.25: Heart rate after exercise from human subject 1

where the heart rate was around 75 BPM. For Fig. 6.25, the heart rate is much higher because of exertion due to exercise. It can be seen that the heart rate gradually lowers as the subject is resting from slightly higher than 110 BPM to less than 100 BPM. It can be seen that the RFID data does not match the actual data as well as it did in the previous results. The reason for the mismatch can be explained using Fig. 6.26. The amplitude of the ECG increased after the subject exercised and the recordings were out of scale for the DAQ. Hence, as can be seen in Fig. 6.26, the 'R' waves are clipped at 0 V. Thus, the actual 'R-R' interval from the ECG is not entirely accurate resulting in a slightly higher mismatch between the RFID and actual 'R-R' values. Even so, the correlation for 'R-R' intervals was calculated to be 0.9007. The DAQ range issue was fixed before testing other subjects.

This set of human tests prove that the RFID heart rate monitor can be used to monitor human heart rate in practical conditions. The correlation between the actual and RFID determined heart rate is very high.

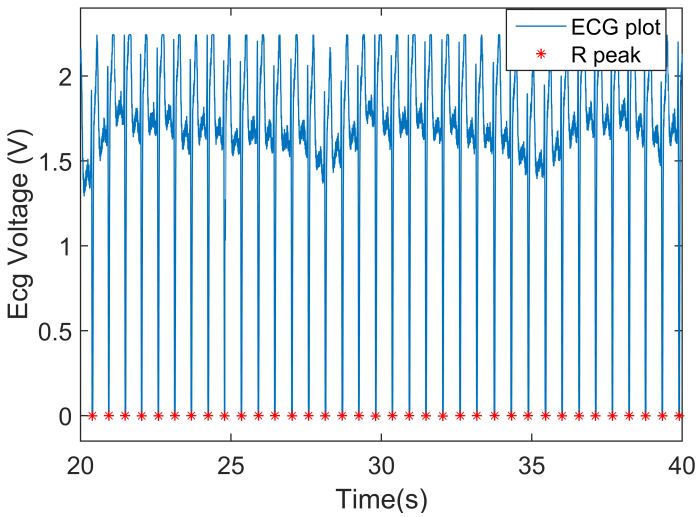

Figure 6.26: ECG after exercise from human subject 1

6.5 Uterine Contraction Monitoring

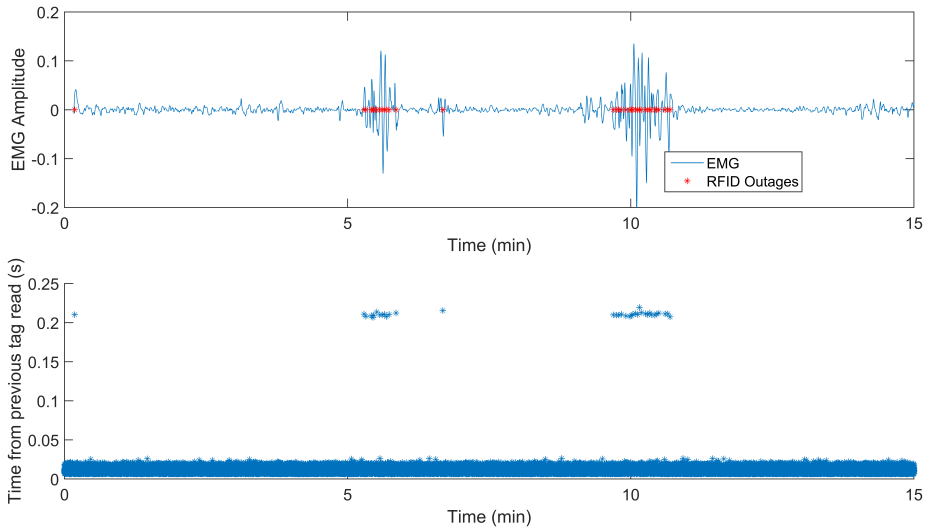

Figure 6.27: RFID outages with uterine contractions

Uterine contraction monitoring using the RFID on/off system was discussed in Section 3.4.2. The first 15 minutes of the EHG signal of Fig. 3.23 is shown in Fig. 6.27. As can be seen in this figure, uterine contractions are associated with large positive and negative going pulses. In Section 3.4.2, uterine contractions were detected by turning RFID tag off with every spike within a contraction EHG signal. The trigger points for these RFID outages are shown as red stars in Fig. 6.27. The bottom plot in the figure shows the time between RFID tag reads and large jumps in time between tag reads are clearly visible when uterine contractions happen in the top plot. Hence, unlike heart beat detection, uterine contractions were detected by groups of outages.

The bottom plot in Fig. 6.27 cannot be the final output of the RFID based uterine

contraction monitoring system. Just like 'heart rate' is the final output of the RFID cardiac mnonitoring system, parameters like duration and frequency of contractions should be outputted for uterine contraction monitoring system. The current standard method for displaying uterine contraction monitoring results are a tocodynamometer strip like the one shown in Fig. 2.5. An output that looks similar to the current standard would be more easily accepted and adapted by medical practitioners [88]. Hence, this section describes a method to present easily decipherable outputs for RFID based uterine contraction monitoring.

6.5.1 Uterine Contraction Plots from RFID Data

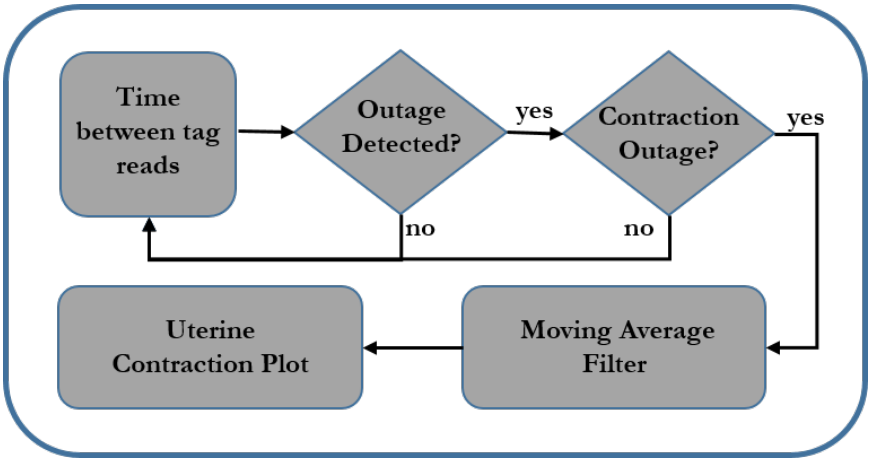

Figure 6.28: Algorithm to generate uterine contraction plots from RFID data

Fig. 6.28 shows the procedure followed to generate uterine contraction plots from RFID data. The output of the plot should be similar to a tocodynamometer strip so that uterine contraction frequency and durations can be easily deciphered from them. In order to achieve that result, time between RFID tag reads is calculated. Outages

are then separated from the continuous RFID data and the timestamps associated with these outages are recorded. These timestamps denote the location of EHG pulse edges. Time between outages are then calculated from these timestamps. These outages are then run through a false outage elimination routine. This routine looks at locations of neighboring outages and if an outage does not have other outages in close proximity, it is eliminated. The elimination routine relies on the principle that a standalone outage is caused due to a spurious pulse which does not correspond to a contraction. The RFID datastream is then recreated with continuous time intervals and each time is assigned a binary value based on presence or absence of an outage. This new datastream is then passed through a moving average filter to produce a smoothly varying output similar to a tocodynamometer strip. Two examples of this process are shown in the next section.

The MATLAB script used to implement this algorithm is shown in Appendix C.

6.5.2 Examples of Uterine Contraction Plots

The EHG source data in this section is again obtained from [7]. An RFID datastream is superimposed on this data as described in Section 3.4.2.

Fig. 6.29 (top) shows about eight minutes of EHG data for a woman in labor. Four contractions are easily visible in the data. The red stars indicate the trigger points for RFID outages. The time between tag reads are shown in the bottom of 6.29. Outages are visible in the bottom plot and can be easily separated from the rest of the data. In the false outage elimination step, standalone outages, like ones circled in the bottom plot are eliminated. Thereafter, the filtering process as described in the above section is completed and an output plot is generated. Fig. 6.30 shows a comparison of the plot generated from the RFID data with a tocodynamometer strip of that same data. It can be seen that both plots show four contractions at

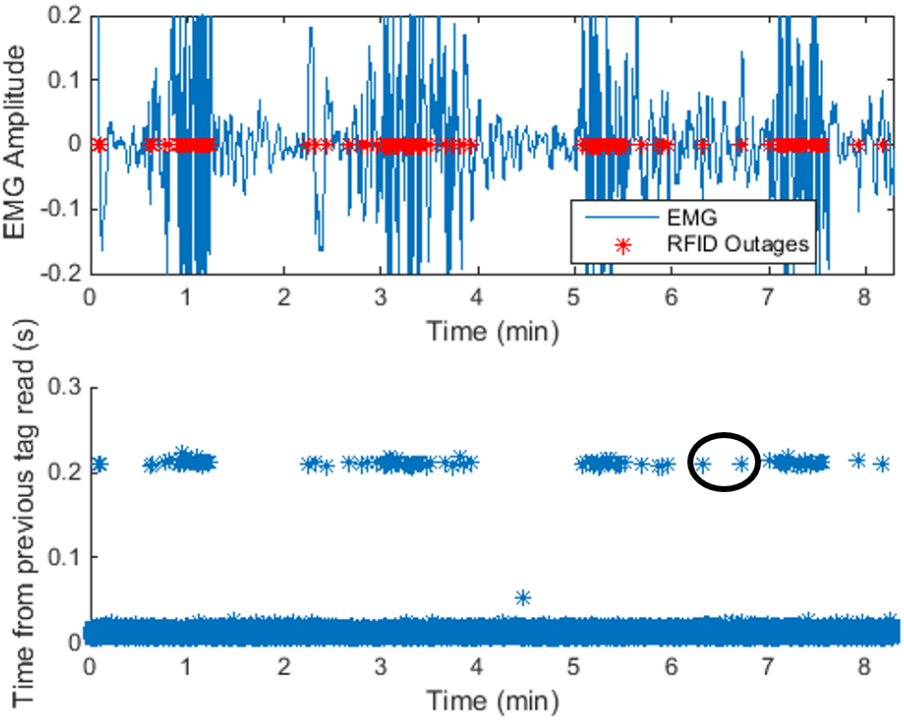

Figure 6.29: Comparison of RFID data outages with EHG data for a woman in labor

similar locations. The plots cannot be expected to be exactly identical because the source data for both are fundamentally different. The tocodynamometer relies on measuring the mechanical pressure during contractions while the RFID plot relies on the electrical signals obtained from the uterine muscles (EHG). The duration and frequencies of contraction can be obtained from the RFID data plot. One might argue that the RFID plot could be more accurate than the tocodynamometer strip as the former relies on the source electrical signals that trigger uterine contractions.

Fig. 6.31, shows a comparison of the tocodynamometer strip with its corresponding RFID output plot for a pregnant woman. The original EHG signal for this plot can be seen in Fig. 3.23. There are nine visible contractions on the tocodynamometer strip and all nine of those contractions are detected using the RFID method.

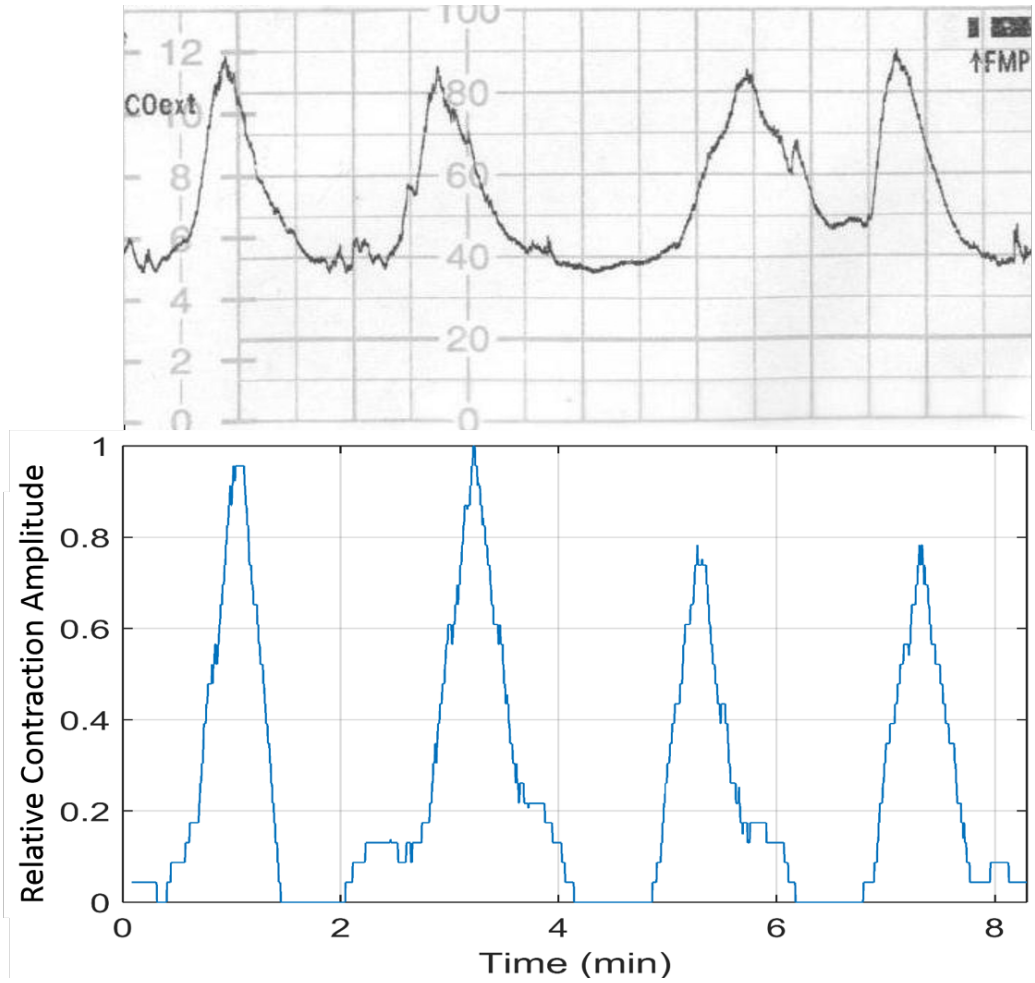

Figure 6.30: Tocodynamometer strip (top) and RFID output plot (bottom) for a woman in labor

As was mentioned earlier, the time between contractions is an important indicator of labor onset. Time between contractions or contraction intervals are determined by taking the difference between successive contractions. For the RFID data, the time of each contraction is chosen at the point at which a contraction peak is observed in Fig. 6.31. The source database contains annotations for the time at which the mother felt contractions. These annotations are used to compare the time between contractions as determined using the RFID method discussed in this work. This comparison is

shown in Table 6.6. As there are nine contractions visible in Fig. 6.31, there are eight contraction intervals. It is not expected that the compared contraction intervals be exactly the same as a contraction can start earlier than a mother starts feeling it [88]. However, the RFID detected contraction intervals are very close to the ones found from the database annotations.

Table 6.6: Comparison of annotated and RFID calculated uterine contraction intervals

	Time between contractions (s)	
Contraction Interval	Database Annotated	RFID Calculated
1-2	239	276
2-3	540	527
3-4	539	513
4-5	480	501
5-6	479	435
6-7	300	376
7-8	539	522
8-9	600	579

A novel and practical method of presenting uterine contraction data has been developed in this section. However, this method still needs to be validated by implementing hardware and collecting human data.

6.6 Conclusions

This chapter showed that beat-to-beat variability and some rate arrythmias can be detected using the proposed RFID heart rate monitoring system. It was shown that the heart rate system can be combined with another sensor to provide integrated continuous monitoring. The system was validated using human data. Finally, a method to present uterine contraction data using the RFID on/off system was also presented.

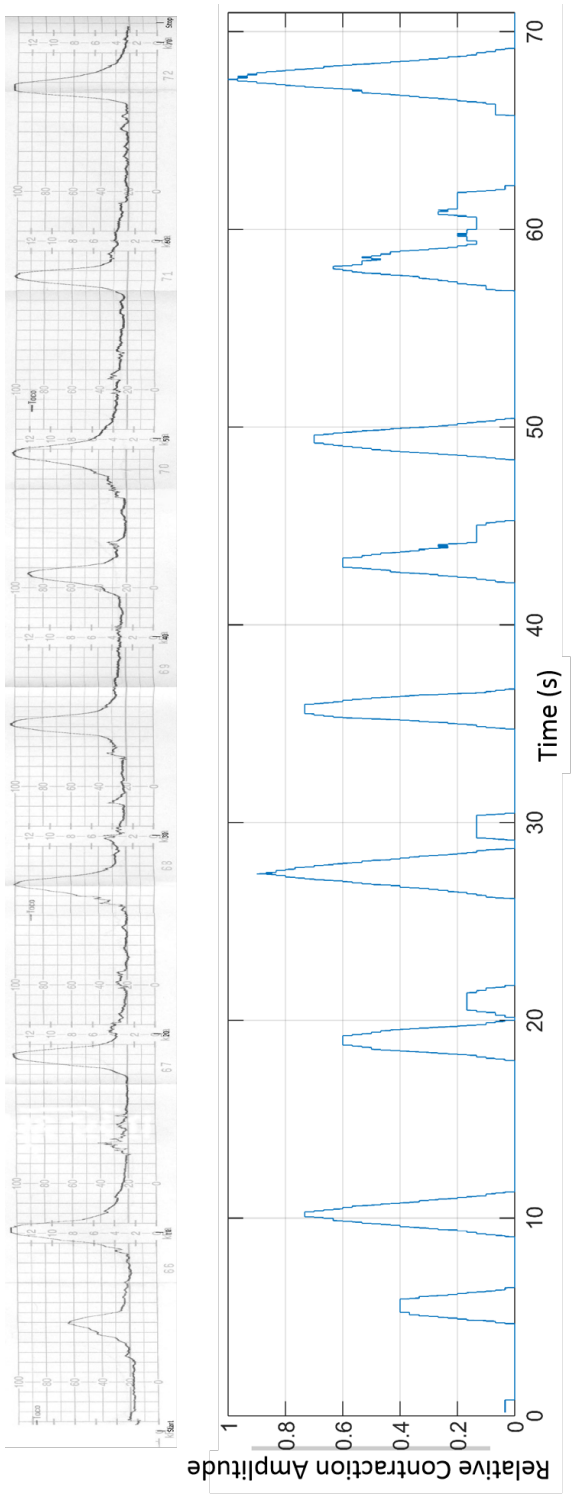

Figure 6.31: Tocodynamometer strip(top) and RFID output plot(bottom) for a pregnant woman

7. Conclusions and Future Work

7.1 Conclusions

Chapter 1 of this thesis introduced the fundamental research challenges in the future growth of wearable health monitoring devices. The chapter presented the conventional steps in designing a monitoring device; sensing, amplification, digitization and transmission. The idea that following these conventional steps poses barriers in improving the wearability of health monitoring devices was discussed. Hence, the requirement was highlighted for unconventional monitoring techniques that enable significant reduction in device power consumption and footprint by rethinking the conventional steps.

The second chapter discussed the state of the art in wireless health monitoring technologies. Types of bioelectric signals and basic differences in between them were discussed. Methods for detecting these biosignals which include electrodes and low power sensors were presented. The discussion then moved to a comparison of some existing and novel methods for wirelessly transmitting biosignal data. Some unconventional methods of biosignal detection that use perturbations in wireless RF signals were presented. Finally, the benefits of using passive RFID technology for biosignal data transmission were discussed along with some implementations of RFID health monitors from literature.

Chapter 3 started with a primer on the EPC C1G2 protocol for UHF RFIDs. The protocol description was followed by an analysis of protocol implications on tag read times. The novel concept of transmitting biosignal information by turning RFID tags on and off was then introduced. The chapter then presented an experimental analysis on time between tag reads as the RFID on/off system's resolution is dependent on tag

read intervals. Simulations were then completed to validate the use of the RFID on/off system for transmitting heart rate and uterine contraction information. Publicly available biosignal source data and empirically collected RFID timing data were used for the simulations. This exercise successfully demonstrated the possibility of using RFID outages to transmit biosignal data.

Hardware implementation for an RFID based heart rate monitor was discussed in the fourth chapter. The building blocks for implementing such a system include RFID tag, ECG amplifier, heart beat detection circuit and a power harvester. Low power components and circuit topologies were identified and designed for a hardware realization of the system .An innovative approach to detect heart beats and create RFID outage control pulses using an IC555 timer integrated circuit is discussed. A commercial power harvester (Powercast P2110) operating in the UHF RFID band was identified and integrated with the system. The Impinj Monza tag's range extension feature was re-purposed to provide the functionality to turn the tag on and off. A proof of concept system was integrated and tested for functionality. Transmission of heart rate data using the RFID on/off system hardware was demonstrated alonwith data analysis and discussion on the need for averaging, system range and the effect of additional tags. The system was improved by designing a low footprint patch antenna through simulations and experimental iterations. Additionally, the system was optimized using low-power and compact components for the ECG amplification and power harvesting circuits. A compact system that included circuits for power harvesting, ECG amplification and heart rate detection with a size of only a square inch was designed.

An algorithm to improve the detection of heart beats and eliminate false outages was presented in Chapter 5.

Chapter 6 highlighted the capabilities of the system with further enhancements

and applications. The chapter started with an experimental analysis on heart rate variability monitoring with the RFID on/off system. It further talked about detection of various rate arrythmias. The arrythmia discussion was followed by an implementation of an RFID based infant monitoring system using the developed technology. The results from heart rate monitoring completed on humans were then presented. Finally, uterine contraction monitoring was revisited and a technique to present uterine contraction data was shown.

In conclusion, this work presents several innovative contributions. The overarching contribution is an unconventional method of transmitting biosignal data by turning RFID tags on and off [126]. The versatility of the system is demonstrated by using heart rate and uterine contractions as the monitored biosignals. Significant work is shown in hardware implementation by choosing optimal components, devising novel methods for biosignal detection and reusing existing technology for new applications [124]. By using heart rate as an example the performance of the system in practical conditions for detection of real-world cardiac problems is explored and an algorithm is formulated to improve beat detection rate [125]. Combination with another RFID sensor to enable respiration monitoring is also discussed [127]. Finally, the work provides several research directions to help realize the full potential of this technology. However, the work stands to gain through research in several directions. Possible future areas of work related to this dissertation are described in the next section.

7.2 Future Work

The possible future research related to this thesis can be divided into three broad areas; overall RFID on/off technology, hardware improvements and data analysis. Several enhancements also encompass overlapping of the aforementioned research areas. These main research areas are illustrated in Fig. 7.1.

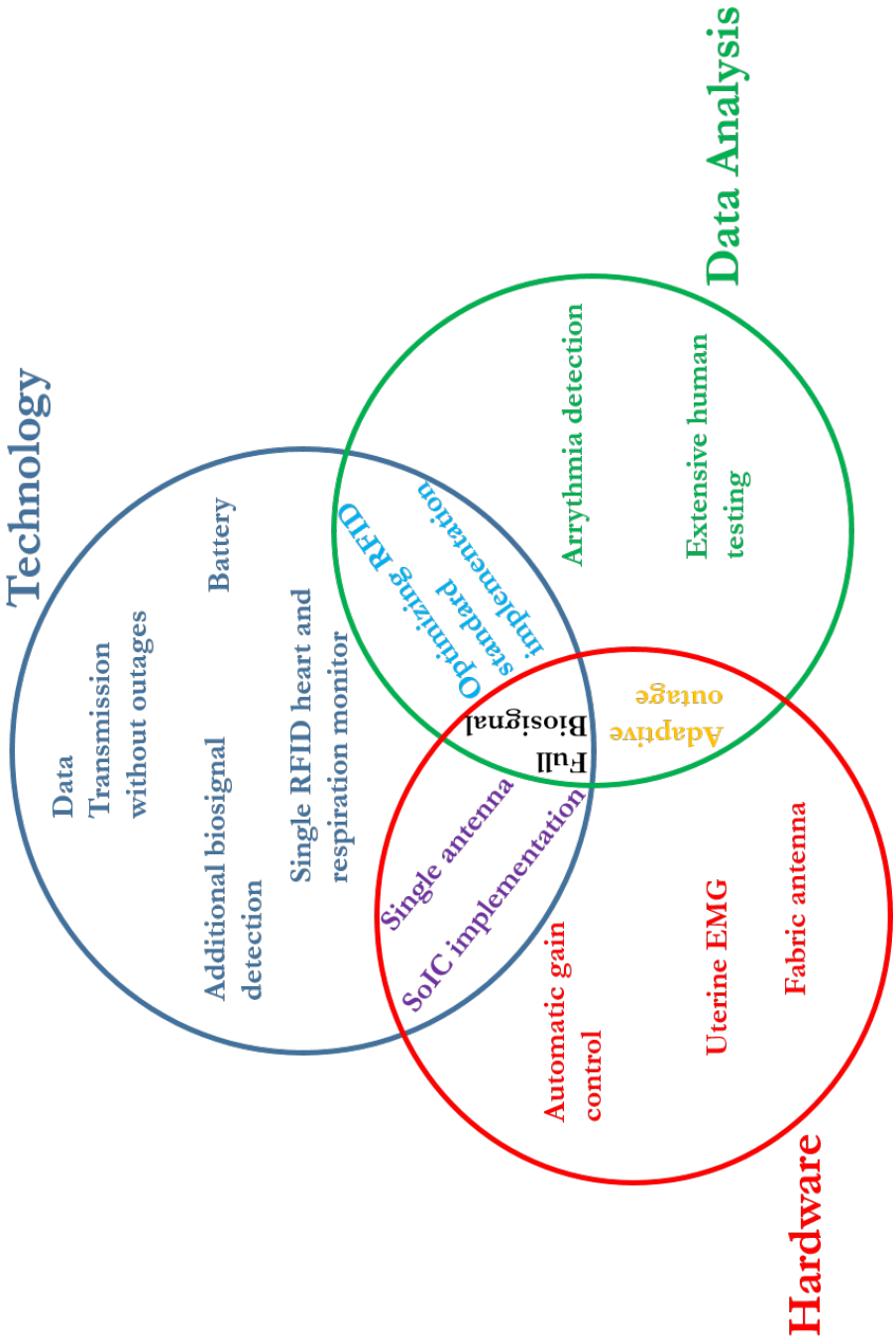

Figure 7.1: Area of future work

1. Technology

    - The main system advancement would be to eliminate the need for having outages. Removing outages allows for the RFID tag to never turn off and thereby remove the ambiguity caused by false outages. The elimination of outages can be achieved by flipping a bit on the RFID data message every time a biosignal feature is detected. This elimination is not possible with the current system as it would either require writing a bit of data for every RFID tag communication cycle which would increase power consumption. A better approach would be to integrate the heart beat detection with the RFID tag on a single chip that includes the bit flipping feature.
    - Respiration and heart rate monitoring applications discussed in Section 6.2 should be integrated and implemented with a single RFID tag.
    - This work explored heart rate and uterine contraction monitoring using the RFID on/off system, additional applications that monitor features of EMGs, EEGs, EOGs etc should be investigated.
    - One of the goals of this work was to create a battery-free monitor. However, there are applications where a small battery may not be a problem and could be used to detect many more biosignal features.

2. Hardware

    - A promising RFID based simulation for uterine contraction monitoring is discussed in this work. Thus, the next logical step would be design a hardware implementation for monitoring uterine contractions.
    - The power harvester antenna is the biggest single device of the system. Designing a fabric antenna would allow for seamless integration between the wearable platform and the system.

- Another hardware improvement would include an adaptive gain control circuit so that the system is able to accept varying biosignal voltage levels.

3. Technology and Hardware

   - The overall technology could also benefit from some hardware upgrades which include implementing a single antenna for power harvesting and the RFID tag.
   - The above goal is more achievable if a system on integrated chip (SoIC) is designed that includes the biosignal amplification, detection and RFID tag functions on a single chip. Such an implementation would provide enormous savings in power and size.

4. Data Analysis

   - More human testing needs to be done to validate the system among a wider population for the heart rate application. Human testing needs to be initiated for other applications like uterine contraction monitoring.
   - This work describes some preliminary work in arrythmia detection using the RFID on/off system. Extensive data analysis and algorithm development can be done to detect various kinds of arrythmia using this system.

5. Hardware and Data Analysis

   - Another research area is designing circuits for adaptive outage durations based on the data from the signal being monitored and environmental conditions.

6. Data Analysis and Technology

- More work needs to be done on selecting the correct protocol settings for a given application under ambient conditions so as to optimize for data resolution, latency and reliability.

7. Technology, Hardware and Data Analysis

   - The eventual goal is to transmit entire biosignals (like electrocardiograms) instead of just biosignal features (like heart rate). Integration into a SoIC could be the first step in this direction.

Bibliography

[1] Abracon, *915 MHz 25 x 25 x 4mm RFID(USA) patch antenna*, 2015, Revised 08.03.15.

[2] Juul Achten and Asker E Jeukendrup, *Heart rate monitoring*, Sports medicine **33** (2003), no. 7, 517–538.

[3] Fadel Adib, Hongzi Mao, Zachary Kabelac, Dina Katabi, and Robert C Miller, *Smart homes that monitor breathing and heart rate*, Proceedings of the 33rd Annual ACM Conference on Human Factors in Computing Systems, ACM, 2015, pp. 837–846.

[4] Sena Agezo, Yuxiang Zhang, Ziyu Ye, Somesh Chopra, Shrenik Vora, and Timothy Kurzweg, *Battery-free rfid heart rate monitoring system*, Proceedings of the conference on Wireless Health, ACM, 2016, p. 7.

[5] Jarmo Alametsä, Alpo Värri, Mikko Koivuluoma, and Laurentiu Barna, *The potential of emfi sensors in heart activity monitoring*, 2nd OpenECG Workshop Integration of the ECG into the EHR and Interoperability of ECG Device Systems, Berlin, Germany, Citeseer, 2004.

[6] Adrian Aleksandrowicz and Steffen Leonhardt, *Wireless and non-contact ecg measurement system–the Aachen SmartChair*, Acta Polytechnica **47** (2007), no. 4-5.

[7] Asgeir et al. Alexandersson, *The icelandic 16-electrode electrohysterogram database*, Scientific data **2** (2015).

[8] Ala Alwan et al., *Global status report on noncommunicable diseases 2010.*, World Health Organization, 2011.

[9] Analog Devices, *Ads129x low-power, 8-channel, 24-bit analog front-end for biopotential measurements*, 8 2015, Rev. K.

[10] Urs Anliker, Jamie A Ward, Paul Lukowicz, Gerhard Troster, Francois Dolveck, Michel Baer, Fatou Keita, Eran B Schenker, Fabrizio Catarsi, Luca Coluccini, et al., *Amon: a wearable multiparameter medical monitoring and alert system*, IEEE Transactions on information technology in Biomedicine **8** (2004), no. 4, 415–427.

[11] A Baba and MJ Burke, *Measurement of the electrical properties of ungelled ecg electrodes*, International journal of biology and biomedical engineering **2** (2008), no. 3, 89–97.

[12] Ju-Yeoul Baek, Jin-Hee An, Jong-Min Choi, Kwang-Suk Park, and Sang-Hoon Lee, *Flexible polymeric dry electrodes for the long-term monitoring of ecg*, Sensors and Actuators A: Physical **143** (2008), no. 2, 423–429.

[13] Minimol Balakrishnan, V Srinivasa Chakravarthy, and Soma Guhathakurta, *Simulation of cardiac arrhythmias using a 2d heterogeneous whole heart model*, Frontiers in physiology **6** (2015).

[14] C.A. Balanis, *Antenna theory: Analysis and design, 3rd ed (with cd)*, Wiley India Pvt. Limited, 2009.

[15] Constantine Balanis, *Modern antenna handbook*, Wiley, 2011.

[16] Michael Barr, *Introduction to pulse width modulation (pwm)*, `http://www.barrgroup.com/Embedded-Systems/How-To/PWM-Pulse-Width-Modulation`, Accessed: 2016-09-30.

[17] L Beckmann, C Neuhaus, G Medrano, N Jungbecker, M Walter, T Gries, and S Leonhardt, *Characterization of textile electrodes and conductors using standardized measurement setups*, Physiological measurement **31** (2010), no. 2, 233.

[18] J. S. Besnoff, T. Deyle, R. R. Harrison, and M. S. Reynolds, *Battery-free multichannel digital ecg biotelemetry using uhf rfid techniques*, RFID (RFID), 2013 IEEE International Conference on, April 2013, pp. 16–22.

[19] Dhaval Bhatt and Tarulata Chauhan, *A bluetooth enabled personal health monitoring system using android device*, (2014).

[20] Igor Bisio, Fabio Lavagetto, Mario Marchese, and Andrea Sciarrone, *A smartphone-centric platform for remote health monitoring of heart failure*, International Journal of Communication Systems **28** (2015), no. 11, 1753–1771.

[21] SA Bokhari, J-F Zurcher, Juan R Mosig, and Fred E Gardiol, *A small microstrip patch antenna with a convenient tuning option*, IEEE Transactions on Antennas and Propagation **44** (1996), no. 11, 1521–1528.

[22] Anup Kr Bordoloi, Pranjal Borah, Satyajib Bhattacharyya, and Nidhi S Bhattacharyya, *Planar patch antenna with 100-μm slit for size reduction and dual-band applications*, Microwave and Optical Technology Letters **56** (2014), no. 7, 1725–1726.

[23] Anup Kumar Bordoloi, *Microstrip patch antennas: some techniques of size reduction and tuning*, Ph.D. thesis, Tezpur University, 12 2013, http://hdl.handle.net/10603/100309.

[24] S. Bowbrick and A.N. Borg, *Ecg complete*, Churchill Livingstone, 2006.

[25] Y.W. Brans and W.W. Hay, *Physiological monitoring and instrument diagnosis in perinatal and neonatal medicine*, Cambridge University Press, 1995.

[26] Christoph Brüser, Kurt Stadlthanner, Andreas Brauers, and Steffen Leonhardt, *Applying machine learning to detect individual heart beats in ballistocardiograms*, 2010 Annual International Conference of the IEEE Engineering in Medicine and Biology, IEEE, 2010, pp. 1926–1929.

[27] Michael Buettner and David Wetherall, *An empirical study of uhf rfid performance*, Proceedings of the 14th ACM international conference on Mobile computing and networking, ACM, 2008, pp. 223–234.

[28] L. Catarinucci, R. Colella, and L. Tarricone, *A cost-effective uhf rfid tag for transmission of generic sensor data in wireless sensor networks*, IEEE Transactions on Microwave Theory and Techniques **57** (2009), no. 5, 1291–1296.

[29] CW Chang and JC Chiou, *Surface-mounted dry electrode and analog-front-end systems for physiological signal measurements*, Life Science Systems and Applications Workshop, 2009. LiSSA 2009. IEEE/NIH, IEEE, 2009, pp. 108–111.

[30] Wei Chen, *Neonatal monitoring technologies: Design for integrated solutions: Design for integrated solutions*, IGI Global, 2012.

[31] Yu M Chi and Gert Cauwenberghs, *Wireless non-contact eeg/ecg electrodes for body sensor networks*, Body Sensor Networks (BSN), 2010 International Conference on, IEEE, 2010, pp. 297–301.

[32] Yu Mike Chi, Tzyy-Ping Jung, and Gert Cauwenberghs, *Dry-contact and noncontact biopotential electrodes: methodological review*, IEEE reviews in biomedical engineering **3** (2010), 106–119.

[33] J. R. C. Chien and C. C. Tai, *A new wireless-type physiological signal measuring system using a pda and the bluetooth technology*, Industrial Technology, 2006. ICIT 2006. IEEE International Conference on, Dec 2006, pp. 3026–3031.

[34] Nicolás E Cortez, Jozué Vieira Filho, and Fabricio G Baptista, *Design and implementation of wireless sensor networks for impedance-based structural*

health monitoring using zigbee and global system for mobile communications, Journal of Intelligent Material Systems and Structures **26** (2015), no. 10, 1207–1218.

[35] R.F. Coughlin and F.F. Driscoll, *Operational amplifiers and linear integrated circuits*, Prentice-Hall, 1982.

[36] Custom Silicon Solutions, *Css 555 micropower timer*, 5 2009, Version 1.1.

[37] A. Dementyev and J. R. Smith, *A wearable uhf rfid-based eeg system*, RFID (RFID), 2013 IEEE International Conference on, April 2013, pp. 1–7.

[38] Usha Desai and C GurudasNayak, *Correction of baseline drift from the ecg by an efficient multiresolution analysis algorithm*, International Journal of Advanced Information Science and Technology (IJAIST) **31** (2014), no. 31, 5–9.

[39] Lukasz Dziuda, Franciszek Wojciech Skibniewski, Mariusz Krej, and Jaroslaw Lewandowski, *Monitoring respiration and cardiac activity using fiber bragg grating-based sensor*, Biomedical Engineering, IEEE Transactions on **59** (2012), no. 7, 1934–1942.

[40] Ataollah Ebrahimzadeh and Ali Khazaee, *Detection of premature ventricular contractions using {MLP} neural networks: A comparative study*, Measurement **43** (2010), no. 1, 103 – 112.

[41] Farsens, *Epc c1g2 compliant uhf rfid tag with power harvesting and spi communication for external low power sensors*, 4 2015, V05.

[42] N. Feinstein, K.L. Torgersen, J. Atterbury, Obstetric Association of Women's Health, and Neonatal Nurses, *Fetal heart monitoring: Principles and practices*, Kendall/Hunt Pub., 1993.

[43] Klaus Finkenzeller, *Rfid handbook: Fundamentals and applications in contactless smart cards, radio frequency identification and near-field communication*, John Wiley & Sons, 2010.

[44] GHCC, *Nicu baby*, `http://www.ghcc.com/admin/uploads/galleries/7/nicu_baby_2.jpg`, Accessed: 2016-05-10.

[45] A. L. Goldberger, L. A. N. Amaral, L. Glass, J. M. Hausdorff, P. Ch. Ivanov, R. G. Mark, J. E. Mietus, G. B. Moody, C.-K. Peng, and H. E. Stanley, *PhysioBank, PhysioToolkit, and PhysioNet: Components of a new research resource for complex physiologic signals*, Circulation **101** (2000 (June 13)), no. 23, e215–e220.

[46] Himani Goyal, *Understanding of ic555 timer and ic 555 timer tester*, International Journal of Inventive Engineering and Sciences (IJIES) **3** (2015), no. 2, 4–6.

[47] L. Grajales and I. V. Nicolaescu, *Wearable multisensor heart rate monitor*, Wearable and Implantable Body Sensor Networks, 2006. BSN 2006. International Workshop on, April 2006, pp. 4 pp.–157.

[48] Anna Gruetzmann, Stefan Hansen, and Jörg Müller, *Novel dry electrodes for ecg monitoring*, Physiological measurement **28** (2007), no. 11, 1375.

[49] Eran Hadar, Tal Biron-Shental, Oz Gavish, Oded Raban, and Yariv Yogev, *A comparison between electrical uterine monitor, tocodynamometer and intra uterine pressure catheter for uterine activity in labor*, The Journal of Maternal-Fetal & Neonatal Medicine **28** (2015), no. 12, 1367–1374.

[50] Gabi Haran, Michal Elbaz, Moshe D. Fejgin, and Tal Biron-Shental, *A comparison of surface acquired uterine electromyography and intrauterine pressure catheter to assess uterine activity*, American Journal of Obstetrics and Gynecology **206** (2012), no. 5, 412.e1 – 412.e5.

[51] HE Instruments, *Techpatient cardio version 3.2 operators manual*, 2011.

[52] David W Hosmer Jr, Stanley Lemeshow, and Rodney X Sturdivant, *Applied logistic regression*, vol. 398, John Wiley & Sons, 2013.

[53] Jay D. Iams, Roger B. Newman, Elizabeth A. Thom, Robert L. Goldenberg, Eberhard Mueller-Heubach, Atef Moawad, Baha M. Sibai, Steve N. Caritis, Menachem Miodovnik, Richard H. Paul, Mitchell P. Dombrowski, Gary Thurnau, and Donald McNellis, *Frequency of uterine contractions and the risk of spontaneous preterm delivery*, New England Journal of Medicine **346** (2002), no. 4, 250–255, PMID: 11807149.

[54] Impinj, *Optimizing tag throughput using readermode*, `https://support.impinj.com/hc/en-us/articles/202756368-Optimizing-Tag-Throughput-Using-ReaderMode`, Accessed: 2016-09-30.

[55] Impinj, *Impinj monza x-2k dura datasheet*, 2014, Rev. 1.51.

[56] Impinj, *Speedway readers*, 2015.

[57] Omer T Inan, Laurent Giovangrandi, and Gregory TA Kovacs, *Robust neural-network-based classification of premature ventricular contractions using wavelet transform and timing interval features*, IEEE Transactions on Biomedical Engineering **53** (2006), no. 12, 2507–2515.

[58] EPCglobal Inc., *Epc radio frequency identity protocol generation-2 uhf rfid*, 2013, ver. 2.

[59] Texas Instruments, *Msp430 ultra-low-power microcontrollers*, `http://www.ti.com/lsds/ti/microcontrollers_16-bit_32-bit/msp/overview.page?DCMP=MCU_other&HQS=msp430`, Accessed: 2016-10-5.

[60] Texas Instruments, *Ina 321: micropower, single-supply, cmos instrumentation amplifier*, 2006, original document from Burr Brown Products.

[61] Zhanpeng Jin, Joseph Oresko, Shimeng Huang, and Allen C Cheng, *Hearttogo: a personalized medicine technology for cardiovascular disease prevention and detection*, Life Science Systems and Applications Workshop, 2009. LiSSA 2009. IEEE/NIH, IEEE, 2009, pp. 80–83.

[62] Steven C Jocke, Jonathan F Bolus, Stuart N Wooters, AD Jurik, AC Weaver, TN Blalock, and BH Calhoun, *A 2.6-μw sub-threshold mixed-signal ecg soc*, 2009 Symposium on VLSI Circuits, IEEE, 2009, pp. 60–61.

[63] J. Jung and J. Lee, *Zigbee device access control and reliable data transmission in zigbee based health monitoring system*, Advanced Communication Technology, 2008. ICACT 2008. 10th International Conference on, vol. 1, Feb 2008, pp. 795–797.

[64] H. Kim, S. Kim, N. Van Helleputte, A. Artes, M. Konijnenburg, J. Huisken, C. Van Hoof, and R. F. Yazicioglu, *A configurable and low-power mixed signal soc for portable ecg monitoring applications*, IEEE Transactions on Biomedical Circuits and Systems **8** (2014), no. 2, 257–267.

[65] Thomas S Kosasa, FRANK K ABOU-SAYF, GAYLYN LI-MA, and RALPH W HALE, *Evaluation of the cost-effectiveness of home monitoring of uterine contractions*, Obstetrics & Gynecology **76** (1990), no. 1, 71S–75S.

[66] Laerdal, *Simbaby*, `http://www.laerdal.com/us/SimBaby`, Accessed: 2016-10-16.

[67] D.C. LeBlanc, *Statistics: Concepts and applications for science*, Statistics: Concepts and Applications for Science, no. v. 2, Jones and Bartlett, 2004.

[68] Peter Leijdekkers and Valérie Gay, *A self-test to detect a heart attack using a mobile phone and wearable sensors*, Computer-Based Medical Systems, 2008. CBMS'08. 21st IEEE International Symposium on, IEEE, 2008, pp. 93–98.

[69] Jim Lesurf, *Digital modulation: One bit at a time*, `http://www.st-andrews.ac.uk/~www_pa/Scots_Guide/RadCom/part19/page1.html`, Accessed: 2016-09-30.

[70] G.N. Levine, *Arrhythmias 101*, Jaypee Brothers,Medical Publishers Pvt. Limited, 2013.

[71] Chanjuan Li, Shiqiang Fu, Te Shao, and Hongmei Liu, *New design of low cost and easy tuning compact gps microstrip antenna.*, PIERS Proceedings, 2014.

[72] Chin-Teng Lin, Lun-De Liao, Yu-Hang Liu, I-Jan Wang, Bor-Shyh Lin, and Jyh-Yeong Chang, *Novel dry polymer foam electrodes for long-term eeg measurement*, IEEE Transactions on Biomedical Engineering **58** (2011), no. 5, 1200–1207.

[73] Torsten Linz, Lena Gourmelon, and Geert Langereis, *Contactless emg sensors embroidered onto textile*, 4th International Workshop on Wearable and Implantable Body Sensor Networks (BSN 2007), Springer, 2007, pp. 29–34.

[74] Torsten Linz, Christine Kallmayer, Rolf Aschenbrenner, and Herbert Reichl, *Fully untegrated ekg shirt based on embroidered electrical interconnections with conductive yarn and miniaturized flexible electronics*, Wearable and Implantable Body Sensor Networks, 2006. BSN 2006. International Workshop on, IEEE, 2006, pp. 4–pp.

[75] Jian Liu, Yan Wang, Yingying Chen, Jie Yang, Xu Chen, and Jerry Cheng, *Tracking vital signs during sleep leveraging off-the-shelf wifi*, Proceedings of the 16th ACM International Symposium on Mobile Ad Hoc Networking and Computing, ACM, 2015, pp. 267–276.

[76] TS Lugovaya, *Biometric human identification based on electrocardiogram*, Master's thesis, Faculty of Computing Technologies and Informatics, Electrotechnical University" LETI", Saint-Petersburg, Russian Federation (2005).

[77] Yu. A. Lyapina, S. B. Nazarov, V. N. Nikanorov, L. V. Posiseeva, and A. O. Nazarova, *The patterns of changes in the electrohysterogram amplitude characteristics in healthy pregnant women during the third trimester*, Human Physiology **37** (2011), no. 2, 213–216.

[78] Vaidotas Marozas, Andrius Petrenas, Saulius Daukantas, and Arunas Lukosevicius, *A comparison of conductive textile-based and silver/silver chloride gel electrodes in exercise electrocardiogram recordings*, Journal of electrocardiology **44** (2011), no. 2, 189–194.

[79] Richard J. Martin and Avroy A. Fanaroff, *Neonatal apnea, bradycardia, or desaturation: Does it matter?*, The Journal of Pediatrics **132** (1998), no. 5, 758 – 759.

[80] Robert Matthews, Neil J McDonald, Paul Hervieux, Peter J Turner, and Marty A Steindorf, *A wearable physiological sensor suite for unobtrusive*

monitoring of physiological and cognitive state, Engineering in Medicine and Biology Society, 2007. EMBS 2007. 29th Annual International Conference of the IEEE, IEEE, 2007, pp. 5276–5281.

[81] Earl McCune, *Practical digital wireless signals*, Cambridge University Press, 2010.

[82] Thomas K McInerny, Henry M Adam, Deborah E Campbell, and Deepak M Kamat, *American academy of pediatrics textbook of pediatric care*, Am Acad Pediatrics, 2008.

[83] N. Q. Mehmood and R. Culmone, *An ant+ protocol based health care system*, Advanced Information Networking and Applications Workshops (WAINA), 2015 IEEE 29th International Conference on, March 2015, pp. 193–198.

[84] Carey R Merritt, H Troy Nagle, and Edward Grant, *Fabric-based active electrode design and fabrication for health monitoring clothing*, IEEE Transactions on information technology in biomedicine **13** (2009), no. 2, 274–280.

[85] Microchip, *600 na, rail-to-rail input/output op amps*, 3 2013, Rev. D.

[86] Michelle S Miller, Kevin M Shannon, and Glenn T Wetzel, *Neonatal bradycardia*, Progress in Pediatric Cardiology **11** (2000), no. 1, 19 – 24.

[87] William Mongan, *Rfid control software*.

[88] Dr. Owen Montgomery, personal communication, 2016.

[89] Arief Adhi Nugroho, Nuryani Nuryani, Iwan Yahya, Artono Dwijo Sutomo, Bambang Haijito, and Anik Lestari, *Premature ventricular contraction detection using artificial neural network developed in android application*, Electric Vehicular Technology and Industrial, Mechanical, Electrical and Chemical Engineering (ICEVT & IMECE), 2015 Joint International Conference, IEEE, 2015, pp. 212–214.

[90] David Nunan, Gavin RH Sandercock, and David A Brodie, *A quantitative systematic review of normal values for short-term heart rate variability in healthy adults*, Pacing and Clinical Electrophysiology **33** (2010), no. 11, 1407–1417.

[91] American Academy of Pediatrics et al., *Apnea, sudden infant death syndrome, and home monitoring*, Pediatrics **111** (2003), no. 4, 914–7.

[92] Emory University Department of Pediatrics, *Apnea and bradycardia*, `http://www.pediatrics.emory.edu/divisions/neonatology/parent_info3.html`, Accessed: 2016-10-10.

[93] Stanislaw Osowski, Linh Tran Hoai, and Tomasz Markiewicz, *Support vector machine-based expert system for reliable heartbeat recognition*, IEEE transactions on biomedical engineering **51** (2004), no. 4, 582–589.

[94] A. Pantelopoulos and N. G. Bourbakis, *A survey on wearable sensor-based systems for health monitoring and prognosis*, IEEE Transactions on Systems, Man, and Cybernetics, Part C (Applications and Reviews) **40** (2010), no. 1, 1–12.

[95] R. Paradiso, G. Loriga, and N. Taccini, *A wearable health care system based on knitted integrated sensors*, IEEE Transactions on Information Technology in Biomedicine **9** (2005), no. 3, 337–344.

[96] Sungmee Park and S. Jayaraman, *Enhancing the quality of life through wearable technology*, IEEE Engineering in Medicine and Biology Magazine **22** (2003), no. 3, 41–48.

[97] D. Patron, W. Mongan, T. P. Kurzweg, A. Fontecchio, G. Dion, E. K. Anday, and K. R. Dandekar, *On the use of knitted antennas and inductively coupled rfid tags for wearable applications*, IEEE Transactions on Biomedical Circuits and Systems **PP** (2016), no. 99, 1–1.

[98] Matthai Philipose, Joshua R Smith, Bing Jiang, Alexander Mamishev, Sumit Roy, and Kishore Sundara-Rajan, *Battery-free wireless identification and sensing*, Pervasive Computing, IEEE **4** (2005), no. 1, 37–45.

[99] Taina Pola and Jukka Vanhala, *Textile electrodes in ecg measurement*, Intelligent Sensors, Sensor Networks and Information, 2007. ISSNIP 2007. 3rd International Conference on, IEEE, 2007, pp. 635–639.

[100] Powercast, *P2110b 915 MHz RF powerharvester receiver*, 7 2015, Rev. A.

[101] David Martin Powers, *Evaluation: from precision, recall and f-measure to roc, informedness, markedness and correlation*, (2011).

[102] Shashank Priya and Daniel J Inman, *Energy harvesting technologies*, vol. 21, Springer, 2009.

[103] Linda Rattfält, *Smartware electrodes for ecg measurements: Design, evaluation and signal processing*, (2013).

[104] RFMAX, *Circular polarity RFID panel antenna*.

[105] M. Shojaei-Baghini, R. K. Lal, and D. K. Sharma, *A low-power and compact analog cmos processing chip for portable ecg recorders*, 2005 IEEE Asian Solid-State Circuits Conference, Nov 2005, pp. 473–476.

[106] Silicon Labs, *Ultra low power, 64/32 kb, 10-bit adc mcu with integrated 240-960 mhz ezradiopro transceiver*, 2 2013, Rev. 1.3.

[107] Silicon Labs, *The only 0.8v/0.6 μA rail-to-rail op amp*, 2014, Rev. 1.

[108] James E Sinex, *Pulse oximetry: principles and limitations*, The American journal of emergency medicine **17** (1999), no. 1, 59–66.

[109] D.R. Smith, *Digital transmission systems*, Springer US, 2003.

[110] J.R. Smith, *Wirelessly powered sensor networks and computational rfid*, Springer New York, 2013.

[111] Phil Smith, *Comparing low-power wireless technologies*, 2011, Contributed By Convergence Promotions LLC.

[112] W. J. Smith and J. R. LaCourse, *Non-contact biopotential measurement from the human body using a low-impedance charge amplifier*, Bioengineering Conference, 2004. Proceedings of the IEEE 30th Annual Northeast, April 2004, pp. 31–32.

[113] H.A. Snellen, *Willem einthoven (1860–1927) father of electrocardiography: Life and work, ancestors and contemporaries*, Springer Netherlands, 2012.

[114] P. J. Soh, G. A. E. Vandenbosch, M. Mercuri, and D. M. M. P. Schreurs, *Wearable wireless health monitoring: Current developments, challenges, and future trends*, IEEE Microwave Magazine **16** (2015), no. 4, 55–70.

[115] Dick Stacey, *Tida-00329 test report*, Texas Instruments, 9 2014.

[116] Statex, *Shieldex technik-tex p180*, 10 2013, Rev. 7.

[117] Thomas J Sullivan, Stephen R Deiss, and Gert Cauwenberghs, *A low-noise, non-contact eeg/ecg sensor*, Biomedical Circuits and Systems Conference, 2007. BIOCAS 2007. IEEE, IEEE, 2007, pp. 154–157.

[118] Bahareh Taji, Shervin Shirmohammadi, Voicu Groza, and Izmail Batkin, *Impact of skin–electrode interface on electrocardiogram measurements using conductive textile electrodes*, IEEE Transactions on Instrumentation and Measurement **63** (2014), no. 6, 1412–1422.

[119] Texas Instruments, *Single-supply, micropower cmos operational amplifiers microamplifier series*, 1 1997, Revised 1/2005.

[120] Christoph Thuemmler, W Buchanan, and Vinoth Kumar, *Setting safety standards by designing a low-budget and compatible patient identification system based on passive rfid technology*, International journal of healthcare technology and management **8** (2007), no. 5, 571–583.

[121] T. H. Tsai, J. H. Hong, L. H. Wang, and S. Y. Lee, *Low-power analog integrated circuits for wireless ecg acquisition systems*, IEEE Transactions on Information Technology in Biomedicine **16** (2012), no. 5, 907–917.

[122] Akinori Ueno, Yasunao Akabane, Tsuyoshi Kato, Hiroshi Hoshino, Sachiyo Kataoka, and Yoji Ishiyama, *Capacitive sensing of electrocardiographic potential through cloth from the dorsal surface of the body in a supine position: a preliminary study*, Biomedical Engineering, IEEE Transactions on **54** (2007), no. 4, 759–766.

[123] E. Valchinov, A. Antoniou, K. Rotas, and N. Pallikarakis, *Wearable ecg system for health and sports monitoring*, Wireless Mobile Communication and Healthcare (Mobihealth), 2014 EAI 4th International Conference on, Nov 2014, pp. 63–66.

[124] Shrenik Vora, Kapil Dandekar, and Timothy Kurzweg, *Passive rfid tag based heart rate monitoring from an ecg signal*, 37th Annual International Conference of the IEEE Engineering in Medicine and Biology Society, PubMed, 2015, pp. 4403–4406.

[125] Shrenik Vora and Timothy Kurzweg, *Modified logistic regression algorithm for accurate determination of heart beats from noisy passive rfid tag data*, 2016 IEEE-EMBS International Conference on Biomedical and Health Informatics (BHI), IEEE, 2016, pp. 29–32.

[126] Shrenik Vora and Timothy Kurzweg, *Unconventional biosignal sensing with passive rfid tags*, The Bridge (IEEE Eta Kappa Nu) **112** (2016), no. 3, 25–29.

[127] Shrenik Vora, William Mongan, Kapil Dandekar, Adam Fontecchio, and Timothy Kurzweg, *Wireless heart and respiration monitoring for infants using passive rfid tags*, 2016 IEEE-EMBS International Conference on Biomedical and Health Informatics (BHI), IEEE, 2016.

[128] I. J. Wang, L. D. Liao, Y. T. Wang, C. Y. Chen, B. S. Lin, S. W. Lu, and C. T. Lin, *A wearable mobile electrocardiogram measurement device with novel dry polymer-based electrodes*, TENCON 2010 - 2010 IEEE Region 10 Conference, Nov 2010, pp. 379–384.

[129] N. Watthanawisuth, T. Lomas, A. Wisitsoraat, and A. Tuantranont, *Wireless wearable pulse oximeter for health monitoring using zigbee wireless sensor network*, Electrical Engineering/Electronics Computer Telecommunications and Information Technology (ECTI-CON), 2010 International Conference on, May 2010, pp. 575–579.

[130] J.G. Webster, *The measurement, instrumentation, and sensors: Handbook*, The electrical engineering handbook series, CRC Press, 1999.

[131] Wikipedia, the free encyclopedia, *Atrial fibrillation*, 2016, [Online; accessed October 14, 2016].

[132] ———, *Bigeminy*, 2016, [Online; accessed October 14, 2016].

[133] Nathanael Yoder, *peakfinder(x0, sel, thresh, extrema, includeendpoints, interpolate)*, `https://www.mathworks.com/matlabcentral/fileexchange/25500`, Accessed: 2016-09-30.

[134] Ya-Li Zheng, Xiao-Rong Ding, C. C. Y. Poon, B. P. L. Lo, Heye Zhang, Xiao-Lin Zhou, Guang-Zhong Yang, Ni Zhao, and Yuan-Ting Zhang, *Unobtrusive sensing and wearable devices for health informatics*, IEEE Transactions on Biomedical Engineering **61** (2014), no. 5, 1538–1554.

[135] Wei Zhou, Rong Song, Xiaoling Pan, Youjian Peng, Xiaoyu Qi, Juehao Peng, KS Hui, and KN Hui, *Fabrication and impedance measurement of novel metal dry bioelectrode*, Sensors and Actuators A: Physical **201** (2013), 127–133.

[136] ZigBee, *Zigbee alliance*, `http://www.zigbee.org/`, 2016, Accessed: 2016-09-30.

[137] Douglas P Zipes, *Clinical application of the electrocardiogram*, Journal of the American College of Cardiology **36** (2000), no. 6, 1746–1748.

[138] N. S. A. Zulkifli, F. K. Che Harun, and N. S. Azahar, *Xbee wireless sensor networks for heart rate monitoring in sport training*, Biomedical Engineering (ICoBE), 2012 International Conference on, Feb 2012, pp. 441–444.

Appendix A. Matlab Scripts for ECG and EHG Simulations

```
clc
close all
%This script takes ECG and RFID datastreams and then converts
%the ECG data to RFID on-off data.
% The script plots the original ECG data,
% the threshold trigger for turning
% RFID tags off and an RFID data stream with outages
%Load ECG data
load('rec_1m.mat')
time=0.002:0.002:10;
ecg=val(2,1:length(time));
% Load rfid sample data
load('rfid_on_data.mat')

threshold=80;
outage=0.1;

% Get RFID timestamps
[timestamps] = get_rfid_ts_ecg(ecg,time,threshold,outage,rel_ts,1);

%Get time between rfid responses and indexes of outages
[time_diffs,outage_idx] = get_rfid_outages(timestamps,outage);

%Get times where ECG signal was triggered
outage_idx_time=zeros(size(outage_idx));
for i=1:length(outage_idx)
    outage_idx_time(i)= ...
        find(abs(time-timestamps(outage_idx(i)))<0.001);
end

%Find R peak locations in ECG
[peakLoc]=peakfinder(ecg, 0.8, 80, 1, false, false);

%Find RFID and actual R-R differences
rfid_r_r=diff(timestamps(outage_idx));
actual_r_r=diff(time(peakLoc));
error=(rfid_r_r-actual_r_r)';

%Plot ECG and outages
figure
subplot(2,1,1)
plot(time,ecg/200);
xlabel('Time(s)')
ylabel('ECG Signal(mV)')

subplot(2,1,2)
```

```
scatter(timestamps(2:end),time_diffs,'*')
xlabel('Time(s)')
ylabel('Time Between Tag Reads (s)')

figure
plot(time,ecg/200);
hold on
plot(time,(80/200)*ones(size(time)),'k')
scatter(time(outage_idx_time),ecg(outage_idx_time)/200,'*r')
scatter(time(peakLoc),ecg(peakLoc)/200,'ob')
hold off
xlabel('Time(s)')
ylabel('ECG Signal(mV)')
legend('ECG Signal','Threshold','Detected Beat',...
    'R Wave','Location','best')

figure
plot(timestamps(outage_idx(2:end)),rfid_r_r)
hold on
plot(time(peakLoc(2:end)),actual_r_r,'r')
hold off
xlabel('Time(s)')
ylabel('R-R Interval (s)')
legend('RFID R-R','Actual R-R','Location','best')


%This script takes EMG and RFID datastreams and then
%converts the EMG data to RFID on-off data.
% The script plots the original EMG data,
% the edge trigger for turning
% RFID tags off and an RFID data stream with outages
clc
close all

%Get EMG data
[time,emg] = getfigdata('emg.fig');
close
% Load rfid sample data
load('rfid_on_data.mat')

threshold=0.03;
outage=0.2;

% Get RFID timestamps
rel_ts=rel_ts(rel_ts(:,1)<55);
rel_ts=[rel_ts ones(size(rel_ts))];
[timestamps] = get_rfid_ts_emg(emg,time,threshold,outage,rel_ts,1);

%Get time between rfid responses and indexes of outages
[time_diffs,outage_idx] = get_rfid_outages(timestamps,outage);

%Plot EMG and outages
```

```
subplot(2,1,1)
plot(time/60,emg);
xlim([0 max(time/60)])
ylim([-0.2 0.2])
hold on
scatter(timestamps(outage_idx)/60,...
    zeros(size(timestamps(outage_idx))),'*r')
legend('EMG','RFID Outages','Location','best')
xlabel('Time (min)')
ylabel('EMG Amplitude')
hold off
subplot(2,1,2)
scatter(timestamps(1:end-1)/60,time_diffs,'*')
xlim([0 max(time/60)])
xlabel('Time (min)')
ylabel('Time from previous tag read (s)')


function [timestamps] = get_rfid_ts_ecg(biosignal_data,time,...
    threshold,outage,rfid_sample_file,distance)
%This function takes digitized ECG data and returns rfid timestamps
% from an empirical rfid data stream
%biosignal_data: The biosignal ECG data
%time: Timestamps associated with biosignal data
%threshold: Threshold of detection
%outage: duration of outage
%rfid_sample_file: Source file for rfid data
%distance: Distance from reader at which data was collected

cross=zeros(size(biosignal_data));
cross(find(biosignal_data>threshold))=1;
prev_cross=0;
zero_count=0;
% Remove 1's from within the outage time
for i=1:length(cross)
    if prev_cross==0
        if cross(i)==1
            prev_cross=1;
            prev_time=time(i);
        end
    elseif prev_cross==1
        if time(i) <= (prev_time+outage)
            cross(i)=0;
        else
            prev_cross=0;
        end
    end
end

% Find timestamps of zero crossings
cross=abs(cross);
idx=find(cross==1)-1;
```

```
outage_time=time(idx);

% Find mean time between rfid responses
sample_rfid=get_rfid_point(rfid_sample_file,distance,10000);
avg_time=mean(sample_rfid)/1e3;
clear sample_rfid;

% Set up variables for creating a vector with rfid timestamps and
% run a for loop to populate timestamps
prev_outage=0;
on_time=0;
req_samples=0;
rfid_stream=zeros(size(time));
rfid_count=1;
idx=[idx,length(time)];
for i=1:length(idx)
    on_time=time(idx(i))-prev_outage;
    req_samples=floor(on_time/avg_time);
    rfid_stream(rfid_count:(rfid_count+req_samples-1))= ...
        get_rfid_point(rfid_sample_file,distance,req_samples)./1e3;
    rfid_count=rfid_count+req_samples-1;
    if sum(rfid_stream) < time(idx(i))
        while sum(rfid_stream) < time(idx(i))
            rfid_count=rfid_count+1;
            rfid_stream(rfid_count)= ...
                get_rfid_point(rfid_sample_file,distance,1)/1e3;
        end
    end
    while sum(rfid_stream) > time(idx(i))
        rfid_stream(rfid_count)=0;
        rfid_count=rfid_count-1;

    end
    rfid_count=rfid_count+1;
    rfid_stream(rfid_count)=outage+ ...
        get_rfid_point(rfid_sample_file,distance,1)/1e3;

    prev_outage=time(idx(i))+rfid_stream(rfid_count);
    rfid_count=rfid_count+1;
end
rfid_stream(rfid_stream==0)=[];
rfid_stream(end)=[];
timestamps=cumsum(rfid_stream);
end


function [timestamps] = get_rfid_ts_emg...
    (biosignal_data,time,threshold,outage,rfid_sample_file,distance)
%This function takes digitized emg data and returns rfid timestamps
% from an empirical rfid data stream
%biosignal_data: The biosignal EMG data
%time: Timestamps associated with biosignal data
```

```
%threshold: Threshold of detection
%outage: duration of outage
%rfid_sample_file: Source file for rfid data
%distance: Distance from reader at which data was collected

cross=zeros(size(biosignal_data));
cross(find(biosignal_data>threshold))=1;
cross(find(biosignal_data<(-1*threshold)))=-1;
prev_cross=0;
zero_count=0;
% Find alternating zero crossing points
for i=1:length(cross)
    if cross(i)==1
        if prev_cross==1
            cross(i)=0;
        end
        prev_cross=1;
        zero_count=0;
    elseif cross(i)==-1
        if prev_cross==-1
            cross(i)=0;
        end
        prev_cross=-1;
        zero_count=0;
    else
        %prev_cross=0;
        zero_count=zero_count+1;
       if zero_count>1000
            prev_cross=0;
       end
    end
end

% Find timestamps of zero crossings
cross=abs(cross);
idx=find(cross==1);
outage_time=time(idx);

% Find mean time between rfid responses
sample_rfid=get_rfid_point(rfid_sample_file,distance,10000);
avg_time=mean(sample_rfid)/1e3;
clear sample_rfid;

% Set up variables for creating a vector with rfid timestamps
% and run a for loop to populate timestamps
prev_outage=0;
on_time=0;
req_samples=0;
rfid_stream=zeros(size(time));
rfid_count=1;
idx=[idx,length(time)];
for i=1:length(idx)
```

```
    on_time=time(idx(i))-prev_outage;
    req_samples=floor(on_time/avg_time);
    rfid_stream(rfid_count:(rfid_count+req_samples-1))= ...
        get_rfid_point(rfid_sample_file,distance,req_samples)./1e3;
    rfid_count=rfid_count+req_samples-1;
    if sum(rfid_stream) < time(idx(i))
        while sum(rfid_stream) < time(idx(i))
            rfid_count=rfid_count+1;
            rfid_stream(rfid_count)= ...
                get_rfid_point(rfid_sample_file,distance,1)/1e3;
        end
    end
    while sum(rfid_stream) > time(idx(i))
        rfid_stream(rfid_count)=0;
        rfid_count=rfid_count-1;
    end
    rfid_count=rfid_count+1;
    rfid_stream(rfid_count)=outage+ ...
        get_rfid_point(rfid_sample_file,distance,1)/1e3;
    prev_outage=time(idx(i))+rfid_stream(rfid_count);
    rfid_count=rfid_count+1;
end
rfid_stream(rfid_stream==0)=[];
rfid_stream(end)=[];
timestamps=cumsum(rfid_stream);
end


function [ rfid_point ] = ...
    get_rfid_point(rfid_data_var,dist,no_of_points)
%This function returns a random rfid data time between
%reads from a database
%rfid_data_var is the two column database that has time between tag
%reads in column 1 and distance at which the data
%was collected in column 2
%no_of_points is the number of points required
rel_ts=rfid_data_var(rfid_data_var(:,2)==dist);
rel_ts=rel_ts(:,1);
rfid_point=randsample(rel_ts,no_of_points);


end


function [time_diffs,outage_idx] = ...
    get_rfid_outages(timestamps,threshold)
% This function returns the time between rfid tag responses
% and the indices of rfid outages as per a given threshold
% timestamps: rfid_timestamps in seconds
% threshold: rfid outage threshold
%timestamps=[0,timestamps];
time_diffs=diff(timestamps);
```

```
outage_idx=find(time_diffs>threshold);

end
```

Note: The function peakfinder [133] was obtained online.

Appendix B. Matlab Scripts for Comparison between Actual ECG Data and RFID Calculated HR

```
% This script takes extracts the epc codes and relative
% timestamps from a csv file and then asks user to select
% the sensor tag from all tags read. It then proceeds to
% plot the time between tag reads for that tag
% The script also takes in human data as collected
% using DAQ on Matlab and processes it to output time
% between tag reads
% User is prompted to specify a valid range for the ecg data

close all
clear all
clc

%Enter the RFID source filename
prompt='Enter RFID filename: ';
rfid_file=input(prompt);
if isempty(rfid_file)
          rfid_file = 'out.csv';
end
[epc96,rel_ts] = importRFIDcsv(rfid_file);

% Find unique RFID tags read and prompt user to select tag
rfid_tags=unique(epc96)
prompt='Enter Tag Index';
x=input(prompt);
if isempty(x)
          x = 1;
end

% Find timestamps for the sensor tag
cell_idx=strfind(epc96, rfid_tags{x});
idx=find(not(cellfun('isempty', cell_idx)));
rel_ts=rel_ts(idx)/1e6;

clear epc96 rfid_tags cell_idx prompt x rfid_file ;

% Find beat to beat interval from RFID data
rel_ts_diff=diff(rel_ts);
outage_idx=find(rel_ts_diff>0.1);
beat_times=rel_ts(outage_idx);
beat_intervals=diff(beat_times);



% Ask for actual ECG data
```

```
prompt='Enter ECG filename: ';
ecg_file=input(prompt)
if isempty(ecg_file)
          ecg_file = 'out.mat';
end
load(ecg_file)

% Prefilter ECG data
x=find(data>1.5);
ecg_start=x(1);
ecg_end=x(end);
data=data(ecg_start:ecg_end);
ts=ts(ecg_start:ecg_end);

% Find ECG R waves
[peakLoc]=peakfinder(data, 0.5, 1.2, -1);

% Show ECG data with identified R peaks
figure
plot(ts,data)
hold on
scatter(ts(peakLoc),data(peakLoc),'*r')
hold off
xlabel('Time(s)')
ylabel('Ecg Voltage (V)')
legend('ECG plot','R peak')

%Prompt user to specify start and end based on the ecg plot
prompt='Enter the start point of your data';
ecg_start=input(prompt)
prompt='Enter the start point of your data';
ecg_end=input(prompt)
close

% Find actual R-R intervals
ts=ts(peakLoc);
ts=ts(ts>ecg_start);
ts=ts(ts<ecg_end);
ts_diff=diff(ts);

% Plot R-R interval from RFID
figure
plot(beat_times(2:end)-beat_times(1),beat_intervals)
ylabel('R-R interval (s)')
xlabel('Time(s)')
title('RFID Output')

% Plot actual R-R intervals
figure
plot(ts(2:end)-ts(1),ts_diff)
ylabel('R-R interval (s)')
xlabel('Time(s)')
```

```
title('Actual Intervals')

% This section is used to plot adjusted R-R intervals after
% truncating appropriate data
%ts_diff=ts_diff(3:end-4);
%ts=ts(1:end-6);
figure
plot(ts(2:end)-ts(1),ts_diff,'-b')
hold on
plot(beat_times(3:end)-beat_times(2),...
    beat_intervals(2:end),'-.r')
hold off
ylabel('R-R interval (s)')
xlabel('Time(s)')
legend('Actual R-R Intervals',...
    'RFID calculated R-R Intervals')

figure
plot(ts(2:end)-ts(1),60./ts_diff,'-b')
hold on
plot(beat_times(3:end)-beat_times(2),...
    60./beat_intervals(2:end),'-.r')
hold off
ylabel('Heart Rate (BPM)')
xlabel('Time(s)')
legend('Actual Heart Rate','RFID calculated Heart Rate')


mean(ts_diff)
std(ts_diff)
mean(beat_intervals(2:end))
std(beat_intervals(2:end))
err=ts_diff-beat_intervals(2:end);
mean(err)
std(err)
corrcoef(ts_diff,beat_intervals(2:end))
```

Appendix C. Matlab Scripts for Generating Uterine Contraction Plots from RFID Data

```
clc
close all

%Get EMG data
[time,emg] = getfigdata('emg.fig');
close
% Load rfid sample data
load('rfid_on_data.mat')

threshold=0.03;
outage=0.2;

% Get RFID timestamps
rel_ts=rel_ts(rel_ts(:,1)<55);
rel_ts=[rel_ts ones(size(rel_ts))];
[timestamps] = get_rfid_ts_emg...
    (emg,time,threshold,outage,rel_ts,1);

%Get time between rfid responses and indexes of outages
[time_diffs,outage_idx] = get_rfid_outages...
    (timestamps,outage);

%Plot EMG and outages
subplot(2,1,1)
plot(time/60,emg);
xlim([0 max(time/60)])
ylim([-0.2 0.2])
hold on
scatter(timestamps(outage_idx)/60,...
    zeros(size(timestamps(outage_idx))),'*r')
legend('EMG','RFID Outages','Location','best')
xlabel('Time (min)')
ylabel('EMG Amplitude')
hold off
subplot(2,1,2)
scatter(timestamps(1:end-1)/60,time_diffs,'*')
xlim([0 max(time/60)])
xlabel('Time (min)')
ylabel('Time from previous tag read (s)')

%Find time between RFID outages
outage_times=timestamps(outage_idx);
outage_times_temp=[0 outage_times];
outage_time_diff=diff(outage_times_temp);
clear outage_times_temp
```

```
contraction_flag=zeros(size(outage_times));
contraction_flag(outage_time_diff<15)=501;
%Eliminate points that are not
%close to other contraction points
for i=1:(length(contraction_flag)-1)
    if contraction_flag(i)==0
        if abs((outage_times(i)-outage_times(i+1)))<15
            contraction_flag(i)=501;
        end
    end
end

%Plot non-contraction points, contraction points
%and eliminated points
figure
scatter(outage_times/60,outage_time_diff)
hold on
scatter(outage_times/60,contraction_flag,'*r')

%Match RFID datastream to sampling rate of actual data
out_vector=zeros(size(emg));
outage_times=outage_times(contraction_flag==501);
outage_times_new=outage_times*200;
outage_times_new=round(outage_times_new);
outage_times_new=outage_times_new/200;

%Find outages on actual timescale of original data
[~,~,idx]=intersect(outage_times_new,time);

%Add weight to recreate outages on original timescale
outage_count=20;
idx_temp=repmat(idx,1,outage_count);
idx_add=repmat(0:1:outage_count-1,length(idx),1);
idx=idx_temp+idx_add;
clear idx_temp idx_add
idx=idx(:);
out_vector(idx)=1;

%Filter to get smooth toco like output
window_size=15001;
movingAverage = conv(out_vector, ones...
    (window_size,1)/window_size, 'same');

%Plot toco like output
figure
plot(time/60,movingAverage./max(movingAverage))
xlim([0 max(time/60)])
xlabel('Time (min)')
ylabel('Normalized Amplitude')
grid on
```

Appendix D. Circuit Layouts

The layout of the final optimized board is presented in this Appendix. The board has four layers; top and bottom component layers have routing while the two inner layers are plane layers.

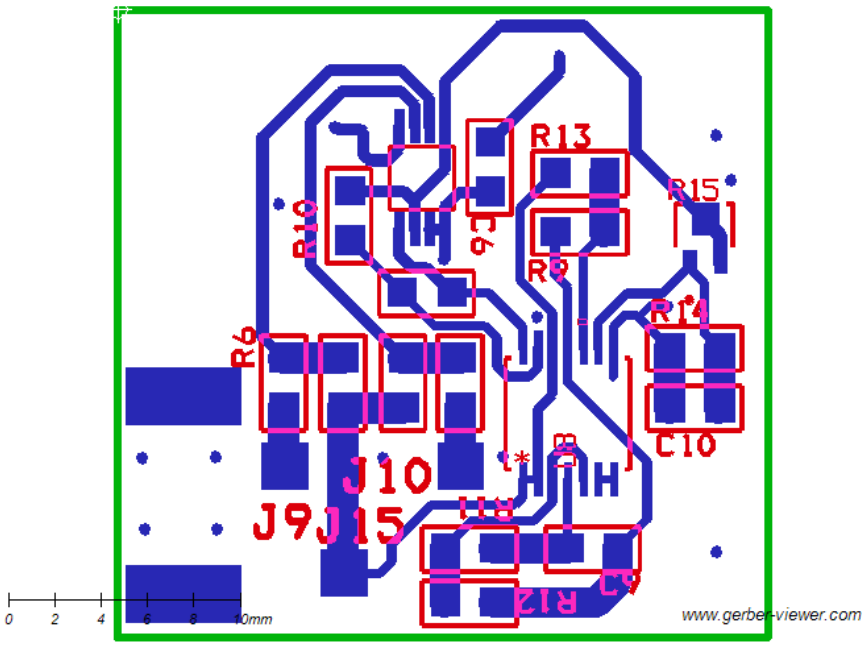

Figure D.1: Top routing layer

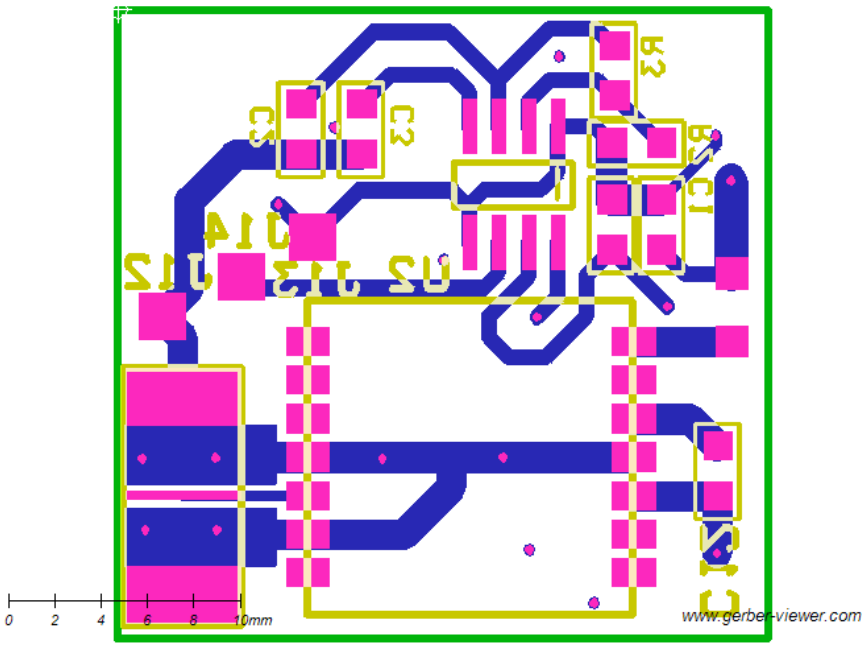

Figure D.2: Bottom routing layer

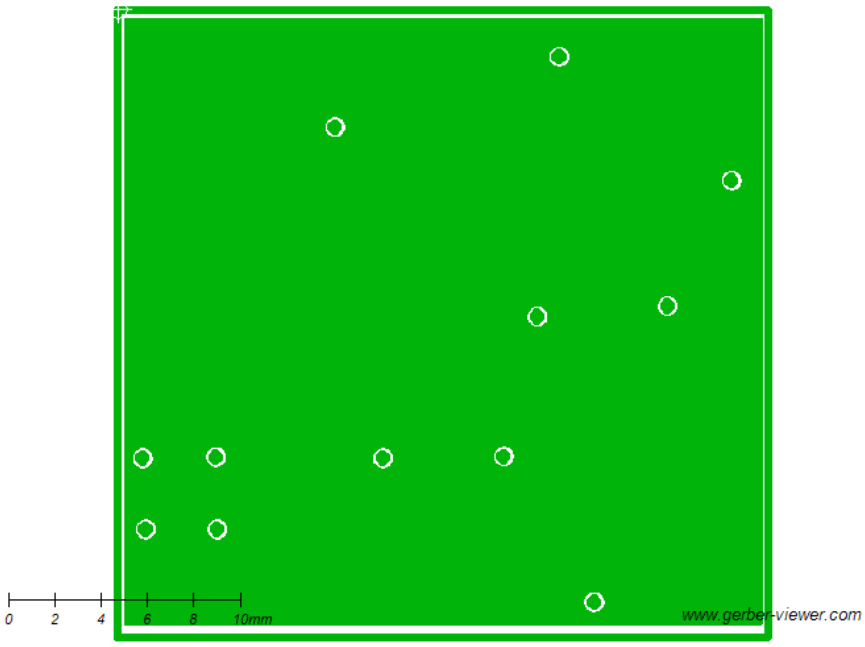

Figure D.3: Power plane

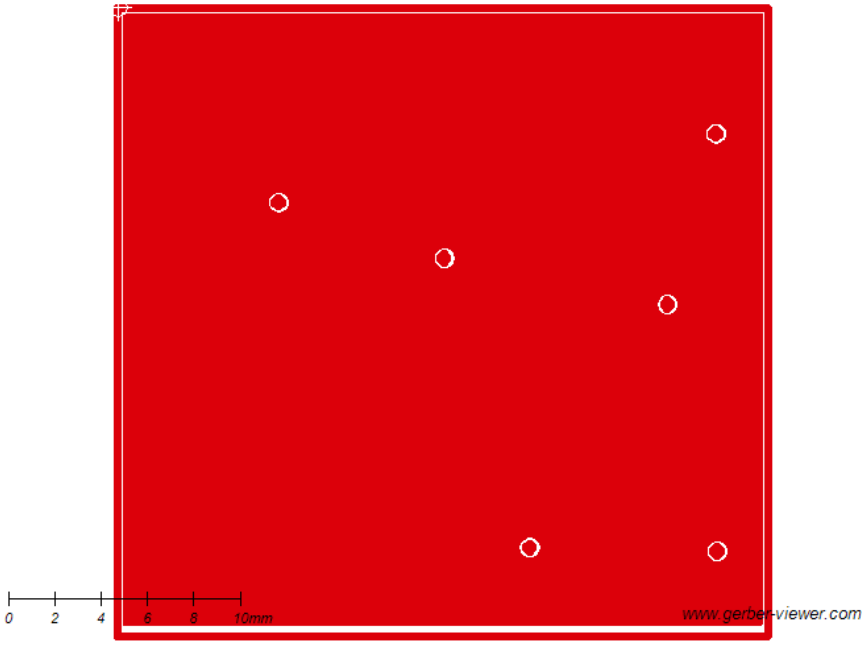

Figure D.4: Ground plane